FEDERAL UNIVERSITY OF UBERLÂNDIA
CENTRE OF EXACT SCIENCE AND TECHNOLOGY
MECHANICAL ENGINEERING POSTGRADUATE COURSE

DEVELOPMENT OF INSTRUMENTS FOR FLUID VELOCITY MEASUREMENT USING HEATED THERMISTORS

Dissertation Presented to Federal University of Uberlândia by

ISAAC NEWTON LIMA DA SILVA

for obtainment of the degree of
MASTER OF SCIENCE
in Mechanical Engineering

Line of Research: FLUID DYNAMICS AND HEAT TRANSFER

Examination Board:

Prof. Dr. Aristeu da Silveira Neto (supervisor)	UFU
Prof. Dr. Francisco P. Lépore Neto	UFU
Prof. Dr. Oscar Saul H. Mendoza	UFU
Dr. Reinaldo Lúcio Gomide	EMBRAPA

Uberlândia, 21st November, 1995.

Dedicated to Gerlúcia and Maria Clara.

ACKNOWLEDGEMENTS

I am very grateful to the following Professors for their helpful comments to this work: Milton Biage; Oscar S. H. Mendoza, Ernane A. A. Coelho, Francisco P. Lépore Neto.

I thank the Energy and Fluid Dynamics Laboratory assistant C. Nascimento and the undergraduate student P. Titara, for providing help in the construction of the test bench, and the Electronic Engineer P. Lopes, for making to order the acquisition board program to suit the research needs and for giving many valuable suggestions regarding the electronic circuits used in this work.

I acknowledge the financial support of the Conselho Nacional de Desenvolvimento Científico e Tecnológico, CNPq.

I am very indebted to the Empresa Brasileira de Pesquisa Agropecuária (EMBRAPA), for partially supporting this research with allocation of thermistors and other electronics components necessary to build the circuits, and, especially, to Dr. R. L. Gomide for presenting me the motivation for carrying out this study.

I greatly appreciate the help provided by Professor Marc Mulkens in reviewing the orthography of the manuscript.

Finally, I thank my supervisor, Professor Aristeu S. Neto, for giving me complete assistance during all stages of the dissertation work.

TABLE OF CONTENTS

Chapters	Page
1 - INTRODUCTION	1
1.1 - Working principles of the thermistor	2
1.2 - The heat pulse method	5
1.3 - The constant temperature method	9
1.4 - Laboratory and field applications	12
1.5 - Dissertation objectives	13
2 - THEORETICAL ASPECTS	15
2.1 - NTC thermistor mathematical model	15
2.2 - Thermistor step response	18
2.3 - Estimation of fluid velocity using the heat pulse method	24
2.4 - Estimation of fluid velocity using the constant temperature method	29
3 - DEVELOPMENT OF THE ANEMOMETERS	35
3.1 - The heat pulse circuit description	36
3.2 - The constant temperature circuit description	39
4 - EXPERIMENTAL APPARATUS AND PROCEDURES	42
4.1 - Thermistor description	42
4.2 - R-T Calibration system	44
4.3 - Electronic equipment	50
4.4 - Calibration to air speed	51

4.5 - Description of the data acquisition system..... 56

5 - RESULTS OF EXPERIMENTS AND DISCUSSIONS..... 63

5.1 - Performances of the thermistor anemometers. 63

5.2 - The heat pulse method results.................... 64

5.3 - The constant temperature method results...... 73

6 - APPLICATIONS.. 84

7 - CONCLUSIONS AND RECOMMENDATIONS............ 89

REFERENCES.. 93

APPENDIX A: A new four-constant fit for R-T characteristic of a thermistor................ 97

APPENDIX B: Linear interpolation by the least squares method..................... 99

APPENDIX C: Calibration sheets for calibrator's chambers D2 and D3.......... 101

APPENDIX D: Experimental uncertainties.................. 105

APPENDIX E: Pitot-tube operation.......................... 109

DEVELOPMENT OF INSTRUMENTS FOR FLUID VELOCITY MEASUREMENT USING HEATED THERMISTORS

ABSTRACT

In this work, two instruments for fluid velocity measurement are presented. The systems use heated commercial thermistors and two distinct techniques for heating the probes are used: the heat pulse and the constant temperature methods. Each of these corresponds to specific instruments. In the first method of operation, the probe's excitation is periodically switched between low-power and high-power. At low-power, the probe works in temperature sensing mode and at high-power, in velocity sensing mode. The thermal transient behaviour due to the cooling period after the application of a heat pulse is correlated to the fluid velocity around the thermistor. In the constant temperature principle, the probe temperature is maintained constant by varying the dissipated power through the thermistor, and the steady-state form of heat transfer is correlated to the fluid velocity. For each method, the employed theoretical model is described as well as the hardware used. The probes are previously calibrated in terms of the temperature variation, by means of a constant temperature bath, for determining their resistance-temperature curves and estimating thermal properties and time constants. After this, the probes are calibrated for air speed varying from 0.01 to 12 m/s, using a commercial calibrator. Suitability for Reynolds numbers up to 32,000 (based on the test section average width) is verified by a wind tunnel test. Analysis of instruments performance and limitations is also given. The automation of the data acquisition is performed using a Personal Computer and a programmable data acquisition board, so, in the first method, the heat pulse is under the control of a PC.

KEYWORDS: THERMISTORS, ANEMOMETRY, HEAT PULSE PRINCIPLE, CONSTANT TEMPERATURE PRINCIPLE, AUTOMATION OF ACQUISITION.

DESENVOLVIMENTO DE INSTRUMENTOS PARA MEDIÇÃO DE VELOCIDADE DE FLUIDOS USANDO TERMISTORES AQUECIDOS

RESUMO

Neste trabalho, dois instrumentos para medição de velocidade de fluidos são apresentados. Os sistemas usam termistores comerciais aquecidos por duas técnicas distintas: pulso de calor e manutenção da temperatura constante. Cada um deles corresponde a um instrumento específico. No primeiro método de operação, a excitação da sonda é periodicamente alternada entre baixa e alta potência. Em baixa potência, a sonda funciona em modo sensível à temperatura, e em alta potência, em modo sensível à velocidade. O transiente térmico, devido ao período de resfriamento, após a plicação de um pulso de calor, é correlacionado à velocidade do fluido na vizinhança do sensor. No princípio de temperatura constante, a temperatura do sensor é mantida constante variando-se a potência dissipada pelo thermistor, e o regime permanente de transferência de calor é correlacionado com a velocidade do fluido. Para cada método de aquecimento, são descritos o modelo matemático e o circuito eletrônico usados. As sondas são previamente calibradas em termos de variação de temperatura, por meio de um banho termostático, para a determinação das curvas de resistência-temperatura e estimação das constantes de tempo. Após isso, passa-se a calibração para velocidade de ar, esta variando de 0,01 a 12 m/s, usando-se um calibrador comercial. É verificada a aplicabilidade para números de Reynolds (baseado na largura média da seção de teste) até 32.000, por teste em túnel de vento. Análise das performances e limitações dos instrumentos é dada. A automação da aquisição de dados é realizada usando-se um computador pessoal e uma placa de aquisição programável, de modo que o pulso de calor, no primeiro método, pode ser controlado via PC.

PALAVRAS-CHAVE: TERMISTORES, ANEMOMETRIA, PRINCÍPIO DO PULSO DE CALOR, PRINCÍPIO DA TEMPERATURA CONSTANTE, AUTOMAÇÃO DA AQUISIÇÃO.

LIST OF FIGURES

Figure **Page**

Figure (1.1) The graphical output screen of the data acquisition program for a 2.54 mm-dia probe...... 7

Figure (1.2) The voltage output response for a 2.54 mm-dia probe.. 8

Figure (1.3) The temperature cycle for a 2.54 mm-dia probe.. 9

Figure (1.4) Characteristics of the constant temperature circuit response, power vs air velocity.... 10

Figure (1.5) Characteristics of the constant temperature circuit response, probe temperature vs air velocity........................... 11

Figure (2.1) Equivalent circuit model for a thermistor suggested by Kaliyugavaradan et al. (1993)............. 16

Figure (2.2) Comparison between manufacturer and laboratory R-T calibration data......................... 18

Figure (2.3) Thermistor sensitivity to temperature variations...................................... 23

Figure (2.4) Thermistor sensitivity to velocity variations... 23

Figure (2.5) Temperature decay behaviour thermistors, dimensionless temperature vs time (semi-logarithmic plot)................................ 28

Figure (2.6) Normalised temperature decay.............. 29

Figure (3.1) Diagram of the heat pulse circuit........... 36

Figure (3.2) Diagram of the constant temperature circuit... 40

Figure (4.1) Glass encapsulated probes.................. 43

Figure (4.2) Probe geometries and dimensions (not to scale)...................................... 43

Figure (4.3) Thermostatic bath utilised for thermistor R-T calibration.................................... 45

Figure (4.4) R-T calibration data for thermistor 1....... 46

Figure (4.5) Fitted calibration curves for thermistor 1. 47

Figure (4.6) Fitted calibration curves for thermistor 2. 48

Figure (4.7) Step response in water for thermistor 1... 49

Figure (4.8) Block diagram of model TSI 1125 Calibrator... 52

Figure (4.9) General view of probe calibrator model TSI 1125.. 52

Figure (4.10) Positioning the probes into the calibrator... 54

Figure (4.11) Detail of placement in chamber D2........ 55

Figure (4.12) Experimental apparatus for automating the acquisition of data... 57

Figure (4.13) Installation of the board in the computer 59

Figure (4.14) Rear wiring assembly of the board........ 60

Figure (4.15) Board block diagram, from CYRDAS 1600/1400 Series User's Guide............................. 61

Figure (4.16) The overview-level IPO diagram for program ONDA.. 62

Figure (5.1) Thermistor 2 Response in air following a 0.7 s heat pulse for air velocity varying from 0 to 15 m/s...................................... 65

Figure (5.2) Normalised temperature decay for thesmistor 1 and different air velocities, following a 2.0 s pulse.. 66

Figure (5.3) Effect of pulse duration on the slope of normalised temperature decay for thermistor 1 (V=7.60 m/s).................................... 67

Figure (5.4) Effect of pulse duration on the slope of normalised temperature decay for thermistor 2 (V=6.00 m/s).................................... 68

Figure (5.5) Temperature decay curve slope............ 69

Figure (5.6) Calibration curves for the 2.54 mm-dia probe at several fluid temperatures...................... 70

Figure (5.7) Calibration curve for thermistor 1, air velocity vs slope.. 71

Figure (5.8) Calibration curve for thermistor 2, air velocity vs slope.. 72

Figure (5.9) Constant temperature circuit output voltage for several air velocities and fluid temperatures - thermistor 2.................................. 73

Figure (5.10) P/ΔT response of the constant temperature circuit vs sqrt (velocity) for several fluid bulk temperatures - thermistor 2..................... 74

Figure (5.11) P/ΔT vs sqrt (velocity) at 299.82 K - thermistor 2.................................. 75

Figure (5.12) P/ΔT vs sqrt (velocity) at 303.15 K - thermistor 2.................................. 76

Figure (5.13) P/ΔT vs sqrt (velocity) at 306.48 K - thermistor 2.................................. 76

Figure (5.14) P/ΔT vs sqrt (velocity) at 309.82 K - thermistor 2.................................. 77

Figure (5.15) a' vs fluid temperature - thermistor 2... 78

Figure (5.16) b' vs fluid temperature - thermistor 2... 78

Figure (5.17) c' vs fluid temperature - thermistor 2... 79

Figure (5.18) Fitted calibration curve for constant temperature circuit at Tbulk=299.82 K - thermistor 2. 80

Figure (5.19) a' vs fluid temperature - thermistor 1... 81

Figure (5.20) b' vs fluid temperature - thermistor 1... 82

Figure (5.21) c' vs fluid temperature - thermistor 1... 82

Figure (6.1) Coordinate system for the wind tunnel.. 85

Figure (6.2) View of the Pitot tube installed in the wind tunnel.................................. 86

Figure (6.3) Air velocity profile in the wind tunnel (Re=32,000)................................ 87

Figure (C.1.a) Relation of pressure differential to air velocity, for the TSI calibrator (chamber D2)....... 102

Figure (C.1.b) Relation of pressure differential to air velocity, for the TSI calibrator (chamber D3)....... 103

Figure (E.1) Measurement of differential pressure by Pitot tube... 110

Figure (E.2) Inclined tube manometer..................... 111

LIST OF TABLES

Table **Page**

Table (C.1) - Calibrator's calibration sheets................ 101

Table (C.2) - Properties of dry air

at T=30 °C and P=1 atm.. 104

NOMENCLATURE

A, a, a' - regression parameters

A_S - surface area (m^2)

B, b, b' - regression parameters

C, c, c' - regression parameters

c - heat capacity (J/K)

c_p - specific heat (J/Kg K)

D - duct average width and well diameter (m)

d - leg diameter (m)

E - voltage (Volts)

fs - sampling frequency (Hz)

F_a - attenuation factor

g - acceleration due to gravity (m/s^2)

g_p - conductance ($Ohms^{-1}$)

h - mean convective heat transfer coefficient (W/m^2 K)

h_c - average thermal convective conductance (W/m^2 K)

I - current (A), intercept at X=0 of a line

I_T - sensitivity at constant temperature to temperature variations (K^{-1})

I_V - sensitivity at constant temperature to speed variations (s/m)

k_f - thermal conductivity of the fluid (W/m K)

L - characteristic length (m)

m - mass of thermistor (Kg)

M - Mach number (V/Vs)

Nu - Nusselt number (hL/K_f)

Nu_∞ - Nusselt number as velocity tends to zero.

P - dissipated electrical power (W)

Pr - Prandtl number (ν/α)

q_o - output quantity

q_i - input quantity

r - radial co-ordinate

r^2 - coefficient of correlation

r_s - resistance (Ohms)

Re - Reynolds number (VL/ν)

$R(T)$, R - thermistor resistance (Ohms)

R - dependent variable

R_s - sphere radius (m)

R_{tot} - total resistance (Ohms)

S - slope (s^{-1})

S_T - sensitivity at constant current to temperature variations (K^{-1})

S_V - sensitivity at constant current to speed variations (s/m)

T - temperature (K)

T_∞, T_{inf} - temperature of the fluid (K)

T_{bulk} - bulk temperature (K)

T_0 - initial temperature (K)

t - time (s), Student's t

thermistor 1 - 2.54 mm-dia probe

thermistor 2 - 1.52 mm-dia probe

V - air velocity (m/s)

Vs - speed of sound (m/s)

V_{ol} - volume of the bead (m^3)

w - frequency (Hz)

α - thermal diffusivity of the fluid (m^2/s)

ν - kinematic viscosity of the fluid (m^2/s)

ρ - density of the fluid (Kg/m^3)

ρ_w - density of the water (Kg/m^3)

τ - the time constant (s)

$\theta(R_s,t) = T-T_\infty$ - difference of temperature (K)

CHAPTER ONE

1 - INTRODUCTION

In engineering applications, it is often necessary to measure fluid flow velocities at low Reynolds numbers. Normally, this is done by measuring other parameters, such as pressure, volume or temperature, which are correlated to the fluid velocity.

Although widely employed, the Pitot and Prandtl tubes prove unsuitable for measurement at low velocities, since they operate by determining the difference between total and static pressures, and it is very difficult to quantify the associated differential pressure for low speeds, that is, the ratio $\Delta P/\Delta V<<1$ as the velocity tends to zero, as well as to adapt a manometric fluid to the liquid column manometer. Consequently, they are not applicable to velocities below 1 m/s, which corresponds to a difference between pressures of rate of 0.05 mm w.c. In addition, these instruments cause disturbances in the fluid flow, due to their large dimensions.

Hot-wire and hot-film anemometers also present inconveniences, since they are fragile and expensive.

For these reasons, thermistors are recently becoming very attractive for this application, mainly due to their great sensitivity to temperature variations, robustness and stability.

1.1 - Working principles of the thermistor

The thermistor is a ceramic thermo-electrical device which may be introduced into an electronic circuit as one of its elements. It is preferred as a temperature transducer in many applications because of its small size, robustness, low cost, low thermal mass and high sensitivity.

The principle of operation of the thermistor is an electrical resistance that is a highly non-linear function of its temperature. For a negative temperature coefficient (NTC) semiconductor, the electrical resistance R decreases exponentially as temperature rises.

When one permits electric current to pass through the thermistor, it suffers an internal Joule heating. If a large current produces heating, as a consequence of Ohm's law, then the increase in temperature causes a decrease in resistance (in case of a NTC thermistor). Thanks to this property, it is feasible to adapt the temperature transducer to sense fluid velocity.

This principle has been employed for the same purpose by Pinchak and Petras (1979), Chen at al. (1989) and Gomide (1990). Pinchak and Petras (1979) utilised self-heated thermistors for measurement of intragravel water flow through the spawning beds of salmon streams, where characteristic lines of calibration were obtained by plotting the data in terms of velocity bridge output voltage (high power mode of operation) vs temperature bridge output voltage (low power mode of operation). Thus, they used the same sensor to measure both velocity and temperature, considering the concept of dual bridge system that permits the thermistors to be operated in a time multiplexed configuration. They measured steady conditions of flow and temperature, but no general correlation between velocity and temperature was studied.

Chen et al. (1989) also used the technique of measuring pore velocities in packed beds. In that study, the authors reported characteristics of the steady-state and the transient forms of heat transfer used for measuring fluid flow. The fluid utilised was water.

Gomide (1990) used a single heated thermistor with periodic application of a heat pulse to detect variations in sap flow rate in the stem of woody plants. In his work, the transient response in the cooling phase was fitted by an exponential model of the heat transfer equation derived from the First Law of Thermodynamics. However, the changes in ambient temperature surrounding the plant stems affected the rate of heat transfer of the sensor, contributing as a source of problem.

Bailey et al. (1993) described and evaluated a thermal transient anemometer having a thermocouple periodically heated by an electrical pulse. The fluid utilised was air and the probe was modelled as an infinitely long homogeneous solid cylinder, according to the Carslaw and Jaeger (1959) solution. The great advantage of this procedure was that the probe responses indicated negligible effect of the fluid initial temperature on velocity measurements. It was also concluded that the experimental temperature decay curves were exponential and the slopes on a semi-logarithmic plot remained invariant with respect to pulse duration and decay time before repulsing.

An application of NTC probes in punctual water velocity measurements by means of heat transfer was presented by Sobrinho and Maciel (1994), where the measurements occurred under non-isothermal conditions. In order to calibrate that system for varying temperatures, each measurement began with readings of the fluid temperature. Afterwards, the probe was heated by application of a certain current and the voltage across the probe wires was read 10 seconds after the beginning of the application of the current. The adopted model used an empirical equation with parameters calculated depending on the fluid initial temperatures. This technique was based on a unique reading of the final temperature.

In the present study, NTC thermistors were used for fluid velocity measurement. They were installed in two different circuits: circuit 1, which worked with the heat pulse method and circuit 2, which maintained the probe temperature constant. Transient and steady-state forms of heat transfer from a thermistor to a fluid flow were considered. These methods are described in the next sections.

1.2 - THE HEAT PULSE METHOD

When an electrical current flows through a thermistor, energy is dissipated by means of heat. If the current is small, the heating is insignificant, and the probe voltage output is a function of the surrounding fluid temperature. If the current is high enough to generate heat, the thermistor output voltage is now a function of temperature and fluid velocity, since the heated probe loses heat by mainly by convection.

In the heat pulse method of operation, the probe's excitation was periodically switched between low-power, temperature sensing mode, and high-power, velocity sensing mode. The thermal transient behaviour during the cooling period after the application of the electrical pulse was correlated to the fluid velocity in the vicinity of the probe.

A typical response curve is shown in figure (1.1) taken with an automatic acquisition system, to be described later, at a sampling rate of 200 Hz for a pulse duration of 0.5 sec, followed by a cooling time of 5.0 sec. The figure axes are not quantified. However, the forms of the current pulses and output voltages correspondent to each phase of the brobe's excitation can be observed.

Figure (1.2) shows the voltage output in volts (with gains of 10.15 and 0.15 for the cooling and the heating phases, respectively) vs time. At an initial time, a constant current of 0.115 mA was delivered to the probe, and its temperature was approximately the fluid temperature, i.e., the system operated in low power.

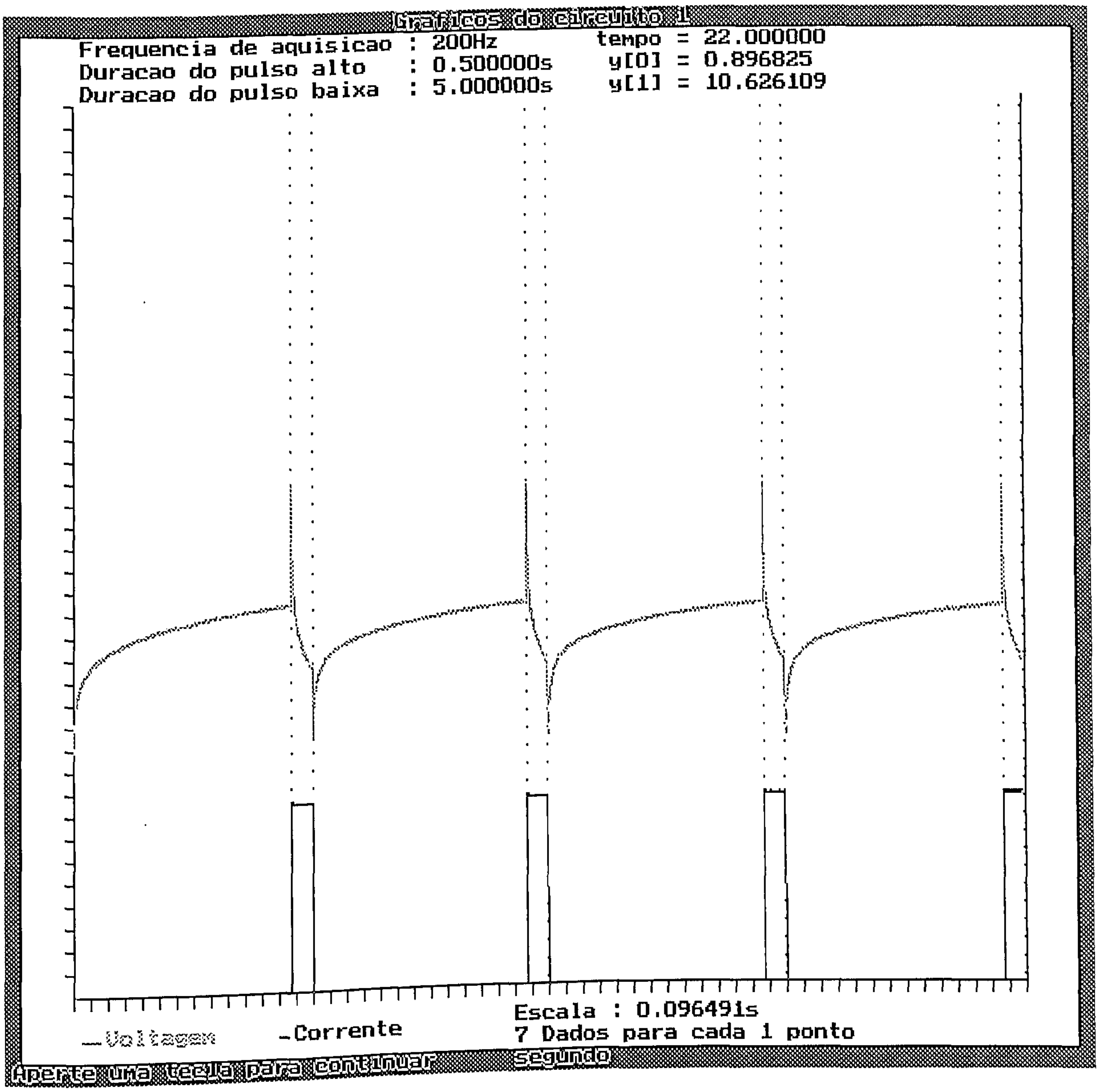

Figure (1.1) The graphical output screen of the data acquisition program for a 2.54 mm-dia probe.

The pulse phase used a constant current of about 10.9 mA, and caused the temperature of the thermistors to quickly increase to a magnitude (greater than the fluid local temperature) dependent upon its initial temperature. This is illustrated with a jump in the output voltage.

As the probe temperature continued to increase, its resistance decreased asymptotically to a minimum. Then, during the cooling phase, the probe resistance was at a minimum and the small current caused the voltage output to fall to a minimum. The temperature of the thermistor reduced to the ambient temperature. Figure (1.3) shows the probe temperature vs time.

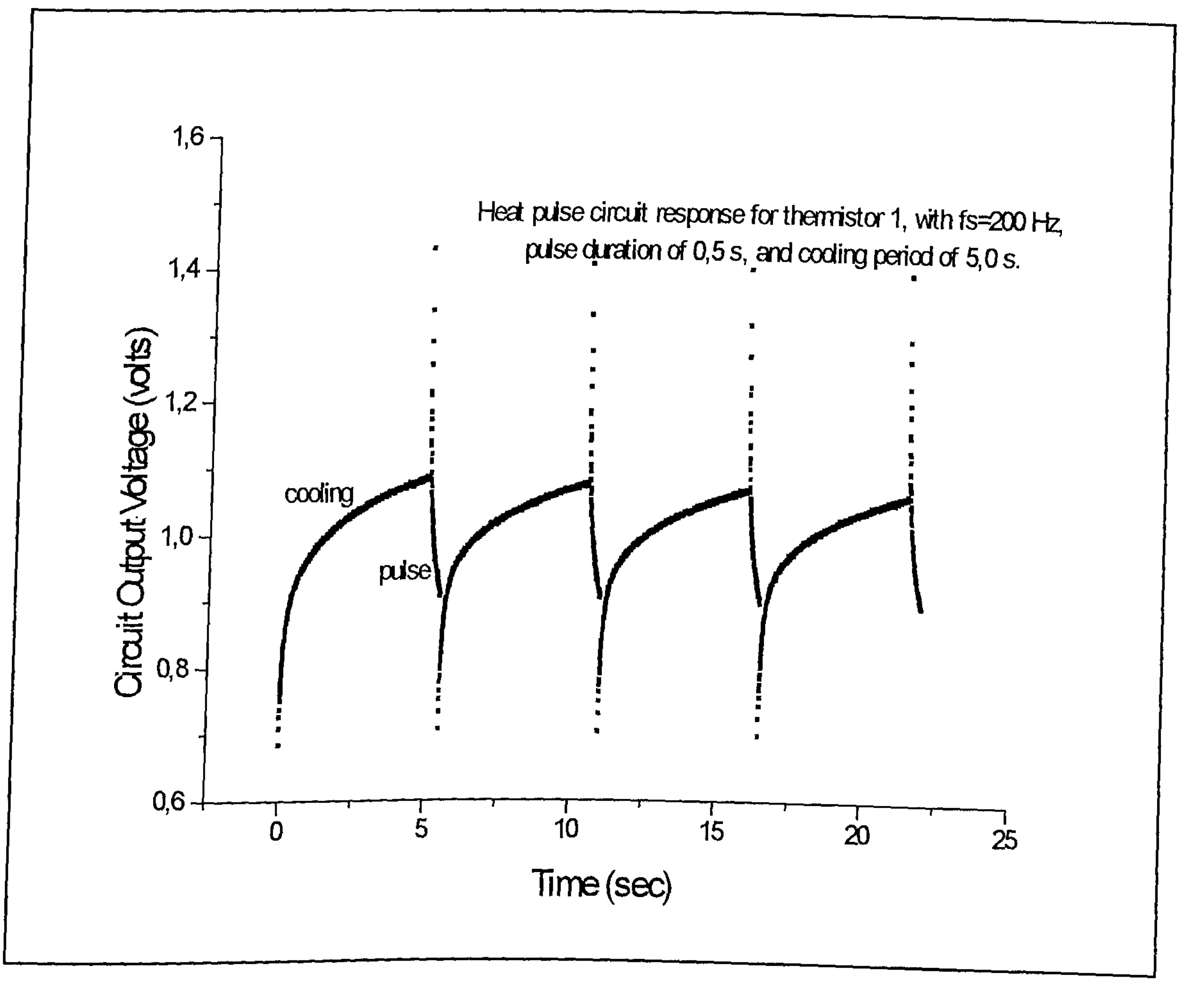

Figure (1.2) The voltage output response for a 2.54 mm-dia probe.

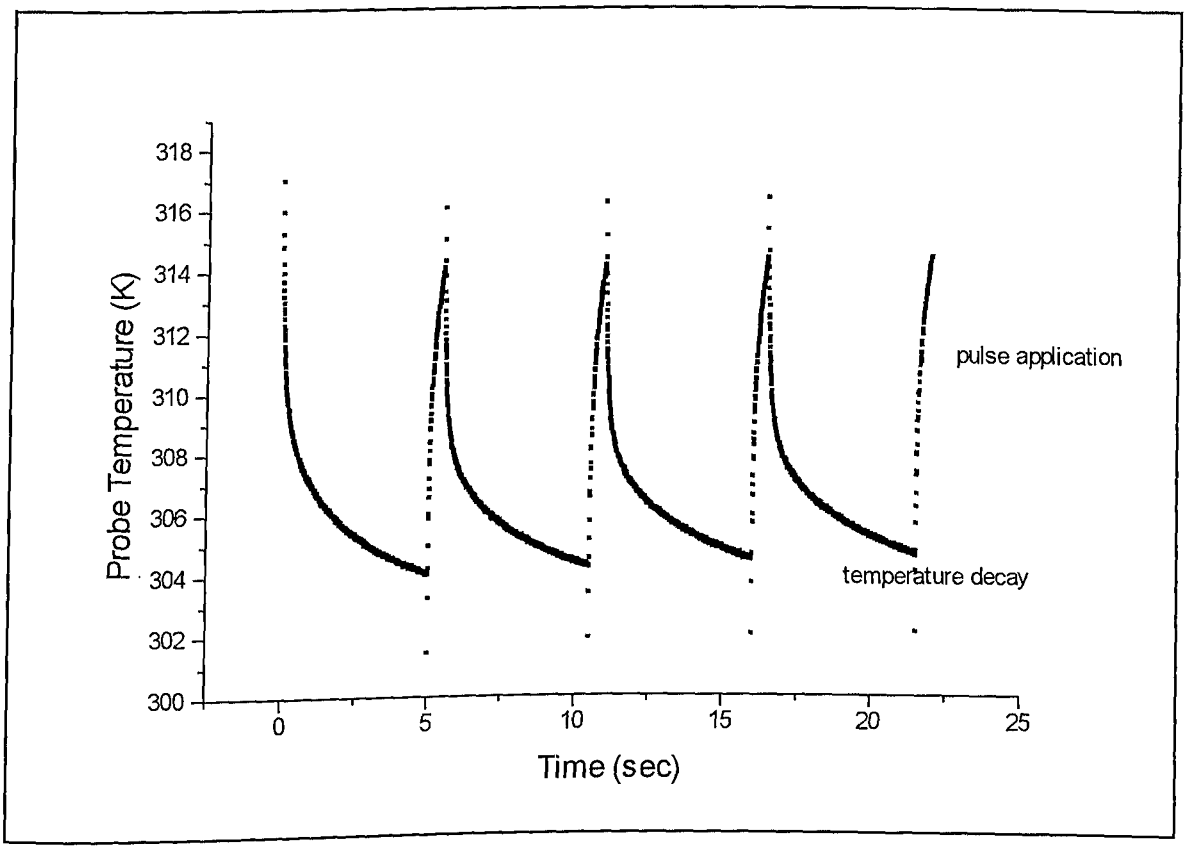

Figure (1.3) The temperature cycle for a 2.54 mm-dia probe.

1.3 - THE CONSTANT TEMPERATURE METHOD

The constant temperature method has often been used for measurement of steady velocities. In order to work accurately, the probe must be calibrated in the fluid in which it is to be used. Although the working fluid used in this study was air, the method can also be applied to other fluids.

In this principle of work, the probe temperature is maintained constant by varying the dissipated electrical power over the thermistor, see figures[1] (1.4) and (1.5). The circuit takes care of the establishment of the equilibrium power and then the steady-state heat transfer can be correlated to the fluid velocity.

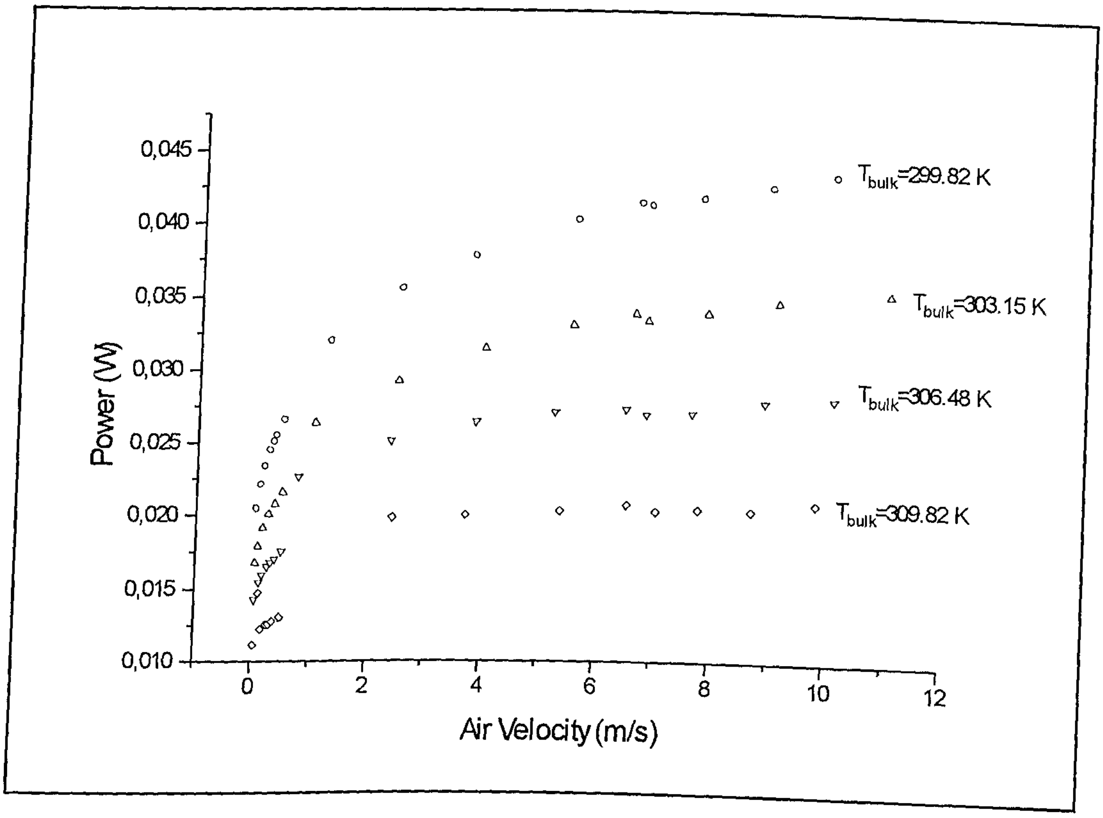

Figure (1.4) Characteristics of the constant temperature circuit response, power vs air velocity.

Figure (1.4) shows the air velocity and dissipated power correlation for different fluid bulk temperature. Figure (1.5) shows that the sensor temperature is maintained constant, independently of the fluid flow temperature, as it was expected.

[1] -These figures are examples of circuit responses, but are not correlated to results presented in chapter five.

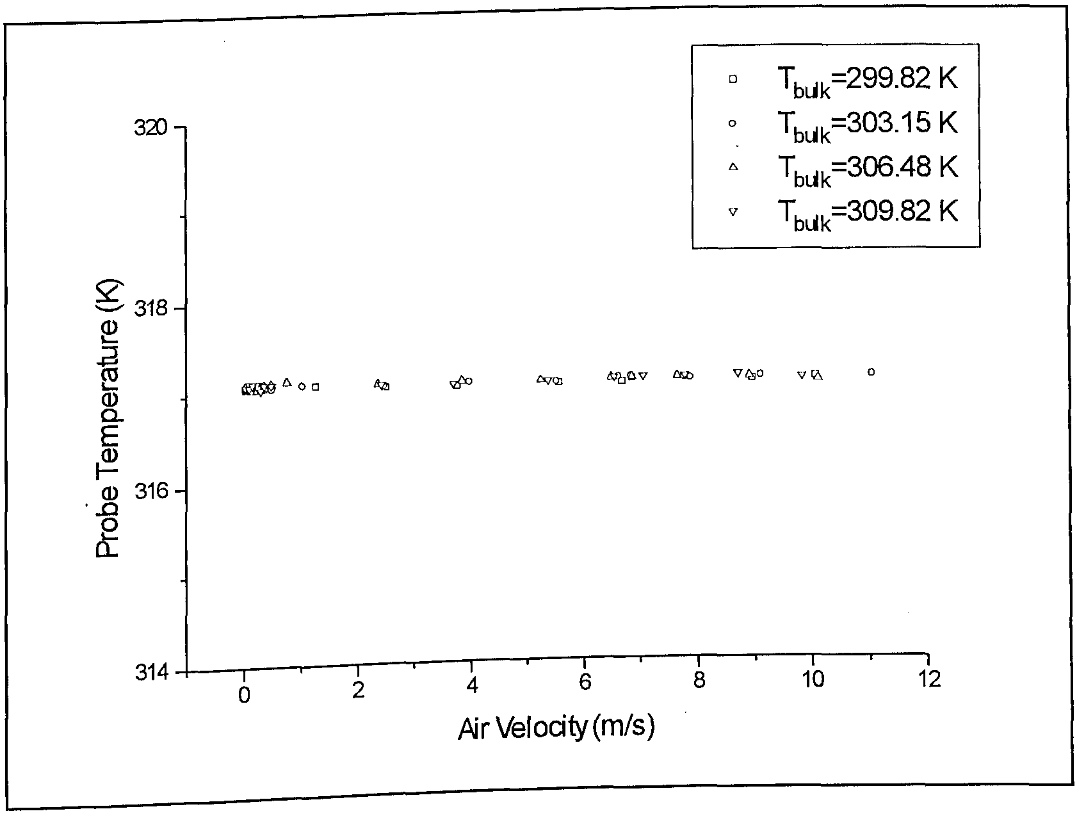

Figure (1.5) Characteristics of the constant temperature circuit response, probe temperature vs air velocity.

The sensor temperature must always be above the ambient temperature. This means that the ambient temperature determines the minimum temperature of sensor operation.

This mode of operation can be extended to measure both average and fluctuation components of velocity via an automatic bridge-balancing operation, however, in this study only average velocities are dealt with, although applications to Reynolds numbers up to 32,000 based on duct average width, i.e., turbulent flows, had been executed.

The equilibrium will arrive at any steady-flow velocity. The equilibrium power is a measure of velocity. Velocity fluctuations can be obtained depending on the attenuation factor of the system(defined by the time constant of the system and the frequency of interest), as well as on the amplifier gain.

A very significant limitation of any measurement system (particularly of this anemometer) is the circuit noise, because the minimum changes in the measured signals become bounded. The noise of the electronic circuit can be eliminated, in part, by proper grounding and cable shielding.

This problem is well stressed in Goldstein (1983) and the noise error contribution must be taken in account if one intends to apply the anemometer at high velocities, where high frequencies are present (normal in turbulent flow). Moreover, because of the shape of figure (1.4), very precise determination of power is necessary at high velocities. That will not be treated here.

1.4 - LABORATORY AND FIELD APPLICATIONS

The systems were analysed for the case of air since the majority of laboratory practical applications makes use of a gaseous medium as the working fluid. However, there is interest in the development of instruments using thermistors to make measurements of water flow within porous media. An example of an application is irrigation, for determining sap velocity in plants and, therefore, estimating transpiration.

Research with air was carried out at the Energy and Fluid Dynamics Laboratory/Federal University of Uberlândia, to introduce future studies in which the use of thermistors as anemometer would be necessary. There are proposals of using these sensors in natural, mixed and forced convection experiments. In the present work, suitability for Reynolds numbers up to 32,000 was verified by a wind tunnel test.

1.5 - DISSERTATION OBJECTIVES

The purpose of this study was to develop a comprehensive and applicable modelling procedure to be put to use with anemometers based on thermistors, as well as instruments that utilise these sensors associated with two forms of heating them.

The methods of heating the probes were: application of a heat pulse and maintenance of a constant temperature, where transient or steady-state heat transfer took place, respectively. Therefore, covering, in a general form, the usage of thermistors for anemometry. In order to achieve the main objective, the following steps had to be carried out:

a) Development of two sensors for flow velocity measurements, using small size thermistors, and two methods of control:

a.1) Development of a circuit that permitted to correlate the fluid velocity around the sensor with the thermal transient behaviour of the cooling period after a heat pulse generated by means of an application of an electrical pulse-Probe 1.

a.2) Development of a circuit that enable correlation of the fluid velocity around the sensor with voltage necessary to maintain the probe temperature constant-Probe 2.

b) Calibration of the probes using equipment existing at the laboratory.

c) Automation of the instrumentation system making use of a Personal Computer and a programmable data acquisition and process control board. The electrical pulse on the first instrument was put under control of a PC.

CHAPTER TWO

2 - THEORETICAL ASPECTS

2.1 - NTC THERMISTOR MATHEMATICAL MODEL

The NTC thermistor is a semiconductor whose electrical resistance varies with temperature, following an exponential expression:

$$R(T) = A\, e^{(B/T)} \qquad (2.1)$$

where A and B are regression parameters, and R(T) in Ohms is the resistance at an absolute temperature T. Parameter A represents the resistance value as the temperature tends to infinite, and B has dimension of absolute temperature K. Therefore, it is possible to determine the temperature knowing the voltage E through the probe, and the corresponding current I, since:

$$R(T) = E/I \quad (2.2)$$

Equation (2.1) obeys a two constant law, and is only an approximation derived from physical considerations. Recent new three and four constant curve fits for R-T characteristic of a thermistor are proposed in the literature, which provide a closer approximation than the conventional equation. Kaliyugavaradan et al. (1993) presented a four-constant equation derived assuming a two-terminal equivalent circuit as shown in figure (2.1):

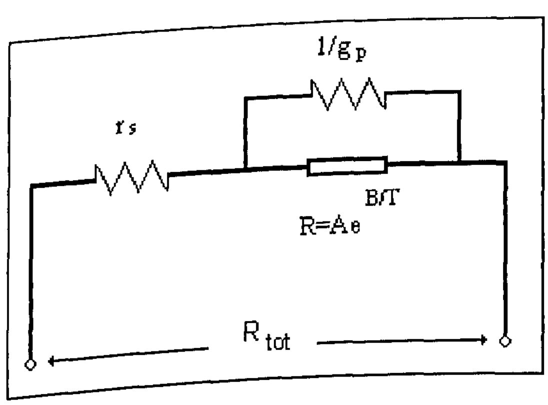

Figure (2.1) Equivalent circuit model for a thermistor suggested by Kaliyugavaradan et al. (1993)

In this model, the thermistor, represented by a temperature dependent resistance $Ae^{(B/T)}$, has a small conductance g_p across it and a low resistance r_s in serie with the parallel combination. For this model, that authors proposed the relation:

$$\frac{1}{(R_{tot} - r_s)} = g_p + (\frac{1}{A})\, e^{-B/T} \qquad (2.3)$$

where r_s and g_p are assumed constant in a certain range of temperature, and R_{tot} is the total resistance.

Although having a better fit and providing better accuracy, when compared to the conventional model, for the same temperature range, the use of the four constant model was not adopted in this work, since the method did not show convergence for the calibrated temperature range. Although the manufacturer's R-T data had not been used and uncertainties had been introduced by the R-T calibration system, the procedure was perfectly justified, since it was the only way to check the applicability of the model by laboratory experiments, see figure (2.2). Use of the manufacturer's R-T data would have resulted in greater uncertainty, since these had a very high tolerance: 24.9% at 80°C, according to the manufacturer.

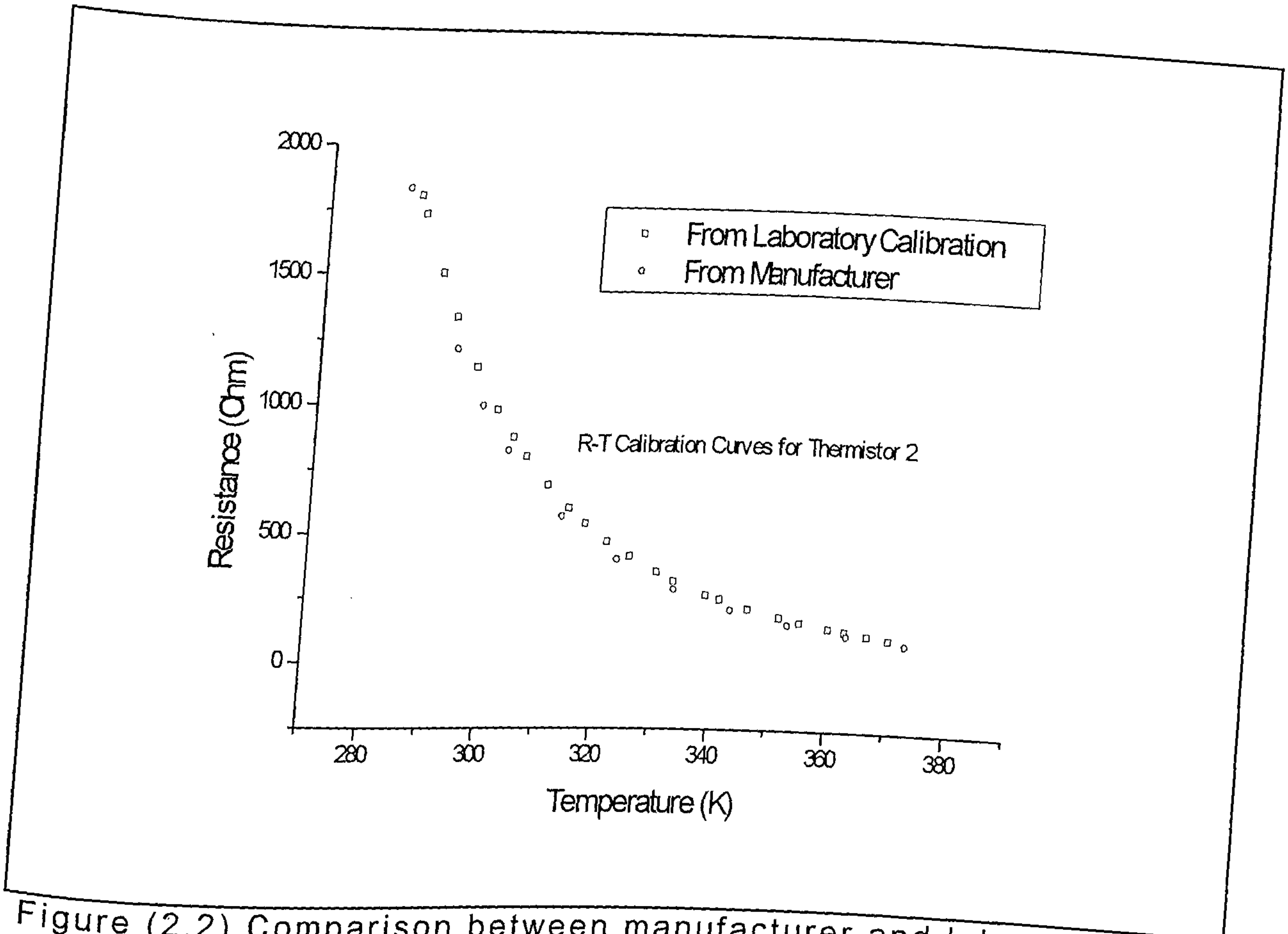

Figure (2.2) Comparison between manufacturer and laboratory R-T calibration data.

A computational routine used in an attempt to find the four parameters is presented in appendix A.

2.2 - THERMISTOR STEP RESPONSE

For this study, it is considered that the probes follow a first order response equation, given by:

$$a_1 \frac{dq_o}{dt} + a_0 q_o = b_0 q_i \tag{2.4}$$

where q_o - the output quantity

q_i - the input quantity

t - time

a_1, a_0, b_0 - physical parameters, assumed constants.

Therefore, the normalised response for this kind of instrument is given as (Jordan, 1983):

$$\frac{a_0}{b_0}\frac{q_o}{q_i} = 1 - \exp\left(-\frac{a_0}{a_1} t\right) \tag{2.5}$$

which can also be written as:

$$\frac{q_o(t)}{kq_i} = 1 - \exp(-t/\tau) \tag{2.6}$$

where τ (equal to a_1/a_0) is the time constant and k (equal to b_0/a_0) is the static sensitivity, also called gain factor, given in terms of the parameters of the differential equation (2.5) for a 1st order instrument.

In often used methods, a step has been applied to the instrument input and τ has been measured as the time to achieve

63.2 percent of the final output value (for instance Doebelin, 1976), since, from equation (2.6):

$$q_o \big|_{t=\tau} : q_o \big|_{t=\infty} = 1 - \frac{1}{e} \approx 0.632 \qquad (2.7)$$

The time constant τ was estimated for each probe, by plunging them into hot water, and monitoring their subsequent response. A comparison between the measured time constants and that from the manufacturer was done.

As treated by Morss (1988), the time constant is defined by the expression:

$$\tau = \frac{m \ c_p}{h \ A_s} \qquad (2.8)$$

where m - mass of thermistor

c_p - specific heat of the thermistor on water

h - mean heat transfer coefficient

A_s - wetted surface area.

It must be clear that τ is not a constant parameter for a given sensor, once it may decrease by decreasing m and c_p or increasing h. Also, h depends on the surrounding fluid and its velocity[1]. The approximate value for the time constant was estimated in water and the application of the probe in this

[1] After all, this effect is what we want to exploit.

research was in air, where the time constant is about 25 times that in water. This serves as an illustration of the limitations of thermistors for dynamic applications. A reduction in time constant is also a consequence of power dissipation, and produces a reduction in sensitivity to fluid temperature variations and an increase in sensitivity to speed variations, i.e., at high power the sensor tends to respond more rapidly to changes in velocity, but is less sensitive to temperature variations, as expressed by figures (2.3) and (2.4).

As a consequence of the time constant definition, the attenuation factor F_a for a frequency w of interest is derived by Morss (1988):

$$F_a = (1 + w^2\tau^2)^{-0.5} \tag{2.9}$$

Equation (2.9) represents a correction factor that can be used to diminish the limitations of thermistors to measure fluctuating temperature signal input.

The sensitivities to fluid temperature and speed variations have special importance on the characteristics of an instrument with heated thermistors. The sensitivity to a given variable is defined as the fractional rate of change in thermistor output voltage with respect to that variable, the other variable maintained fixed. Rasmussen (1962) presented expressions for temperature and speed sensitivities at constant current, (2.10) and (2.11), and temperature, (2.12) and (2.13), modes of operation:

$$S_T = \frac{1}{E}\frac{\partial E}{\partial T} \quad (2.10)$$

$$S_V = \frac{1}{E}\frac{\partial E}{\partial V} \quad (2.11)$$

$$I_T = \frac{1}{I}\frac{\partial I}{\partial T} \quad (2.12)$$

$$I_V = \frac{1}{I}\frac{\partial I}{\partial V} \quad (2.13)$$

where S_T and S_V are sensitivities at constant current to temperature and speed variations, respectively, and I_T and I_V are sensitivities at constant temperature to temperature and speed variations, respectively.

A graphical representation of S_T and I_V for the circuits used is shown in figures (2.3) and (2.4), respectively.

In figure (2.3) data from the heat pulse circuit was taken in account to plot the sensitivity to temperature variations of the 2.54 mm-dia thermistor in air at zero speed. It could be inferred from it that the sensitivity decreases as power across the

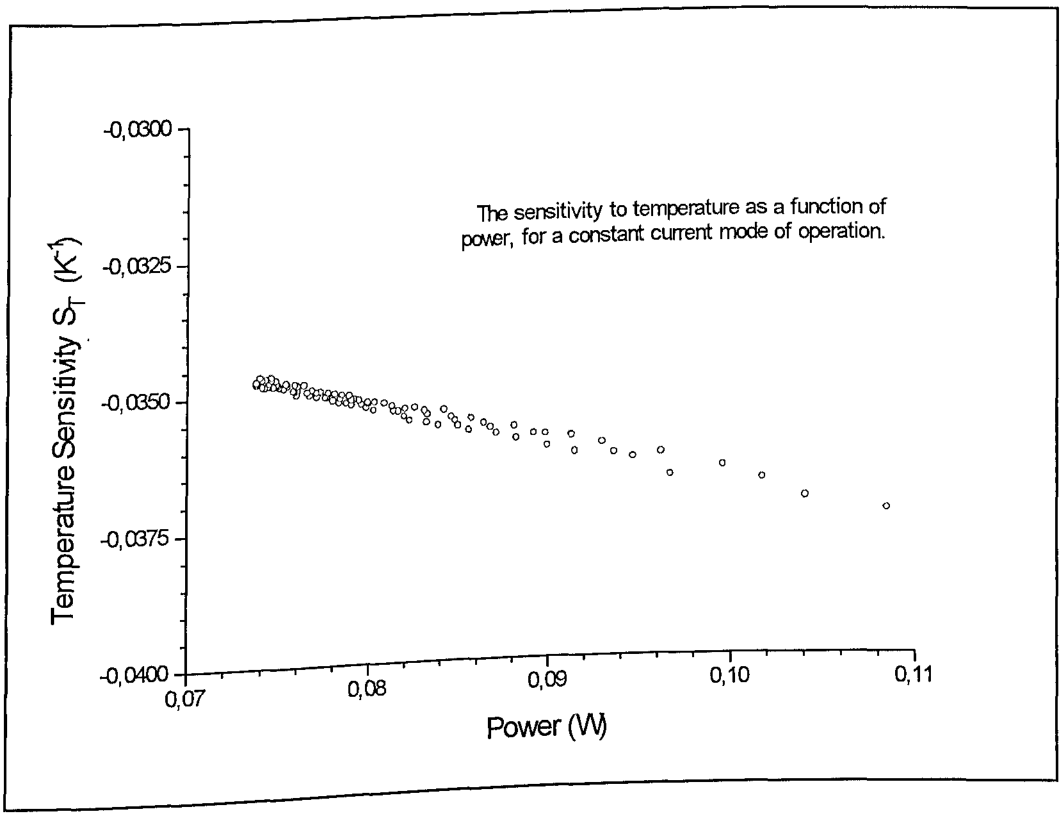

Figure (2.3) Thermistor sensitivity to temperature variations.

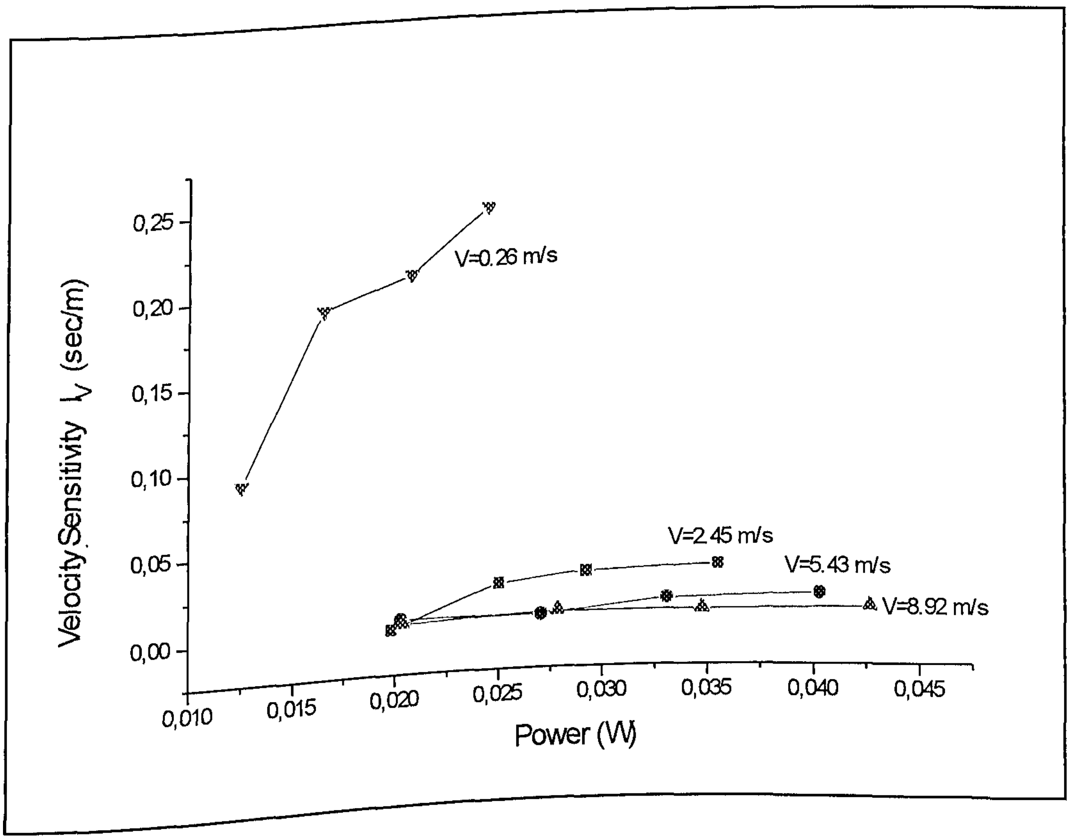

Figure (2.4) Thermistor sensitivity to velocity variations.

sensor increases. Data from a pulse period was utilised, e. g., for a constant current of 10.9 mA through the probe wires. For the low power period the temperature sensitivity was approximately -0.035 K^{-1}.

Figure (2.4) shows the velocity sensitivity of the 2.54 mm-dia thermistor obtained with the circuit of constant temperature. The family of curves shows that more power is necessary if a high speed range is to be measured, which may be a limitation of probe operation. Also, when the power dissipation is small, the circuit of constant temperature provides great sensitivities for both temperature and velocity variations, which may influence the correlation of the circuit output to the fluid velocity, if temperature variations occur.

2.3 - ESTIMATION OF FLUID VELOCITY USING THE HEAT PULSE METHOD

The problem of a sphere of radius R_s having uniform initial temperature T_0 is treated by Arpaci (1966) and Carslaw and Jeager (1959), for the case when it is plunged suddenly into a fluid at temperature T_∞. They assume a moderate convective heat transfer coefficient h, which implies $(T-T_\infty)\neq0$, and consequently:

$$k_f \frac{\partial \theta (R_s, t)}{\partial r} = h \theta (R_s, t) \qquad (2.14)$$

where $\theta(R_s,t) = T - T_\infty$

r - radial co-ordinate

k_f - thermal conductivity of the fluid

t - time

T - temperature of the sphere.

The problem can be simplified by assuming that the temperature within the sphere "bead" is uniform at any instant. It can be assumed that, at t=0 and bead temperature T_0, the system is submitted to an environmental temperature change so suddenly that can be approximated by a step. Assuming that the convective heat transfer coefficient h remains constant during the cooling period, and approximately equal to h_c (average thermal convective conductance), and that the environmental temperature T_∞ does not vary with time, then, in accordance with the above assumption, the energy balance for the bead over a small time interval dt is:

The change in internal energy = The heat transfer by convection

$$-\rho c V_{ol}\, dT = h_c A_s (T - T_\infty)\, dt \qquad (2.15)$$

where ρ - density of the fluid

c - heat capacity of the bead

V_{ol} - volume of the bead

A_S - surface area of the bead.

If T> T_∞, the minus signal indicates that the internal energy decreases as T increases. (2.15) can be written as:

$$\frac{dT}{T - T_\infty} = -\frac{h_c A_s}{\rho c V_{ol}} dt \tag{2.16}$$

integrating that equation from t=0 to t:

$$\int_{T_0}^{T} \frac{dT}{T - T_\infty} = -\frac{h_c A_s}{\rho c V_{ol}} \int_0^t dt \tag{2.17}$$

produces:

$$\ln \frac{T - T_\infty}{T_0 - T_\infty} = -\frac{h_c A_s}{\rho c V_{ol}} t + n \tag{2.18}$$

where n is the integration constant.

(2.18) can be rearranged as:

$$\frac{T - T_\infty}{T_0 - T_\infty} = n' \exp\left(-\frac{h_c A_s}{\rho c V_{ol}} t\right) \tag{2.19}$$

with n'=1, since $T=T_0$ at t=0.

Note in equation (2.19) that $(h_c A_s)/(\rho c V_{ol})$ is the inverse of the time constant of the probe in air, defined in (2.5) and (2.8). Consequently, higher method sensitivity can be achieved if small time constant thermistors are used (this will be seen in chapter five).

Equation (2.19) is an excellent approach to the problem of a rigid sphere in a fluid subject to steady flow and temperature fields.

If, however, the problem involves heat transfer from a sphere to a fluid subject now to unsteady flow and temperature fields, a perturbation method must be applied to derive the heat transfer equation The temperature field is decomposed into the undisturbed field and disturbed field due to the presence of the sphere, and its solution yields a history integral in the energy equation. That will not be treated in this work, but can be found in detail in Michaelides and Feng (1994), Stephenson (1975), Arpaci (1966) and Carslaw and Jaeger (1959).

The plot of figure (2.5) shows the dimensionless temperature decay vs time, as a result of application of equation (2.19) in experimental data.

If one disregards the initial decay period ($t<t_0$), as it does not obey the proposed theory, therefore, the slope, of the straight line obtained by this procedure has a direct relationship with the velocity, because h may be found from the knowledge of the Nu number, which is a function of the Re number, i.e., the velocity.

The other parameters are supposed to remain invariable over the employed bulk temperature range.

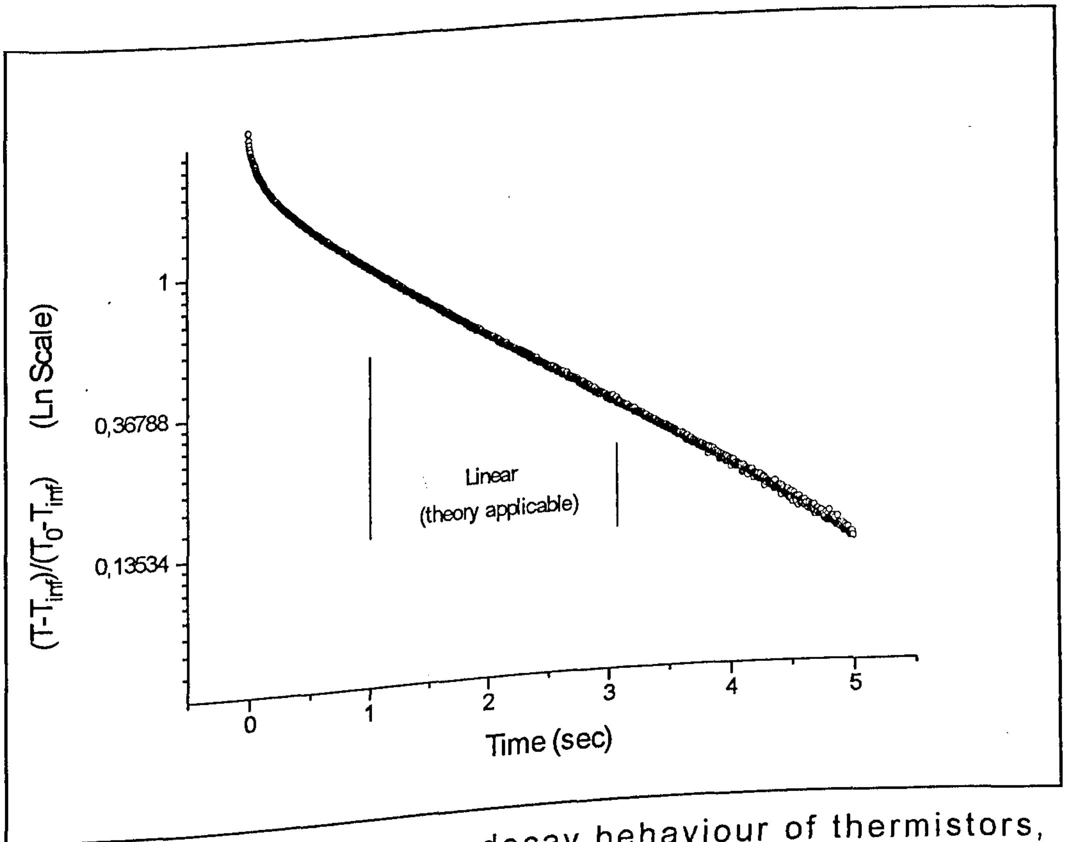

Figure (2.5) Temperature decay behaviour of thermistors, dimensionless temperature vs time (semi-logarithmic plot).

Figure (2.6) shows the dimensionless temperature decay on a semi-logarithmic plot immediately after the application of a heat pulse. The dimensionless temperature is normalised by a temperature T_0, at a selected initial time t_0 which eliminates the period of transition. The slope of this curve can be found following a procedure to be described in Appendix B, and is utilised to construct the calibration curves for the heat pulse circuit. It was found that the velocity was well fitted by a second degree polynomial in the slope, $V=P_2(S)$, see chapter five.

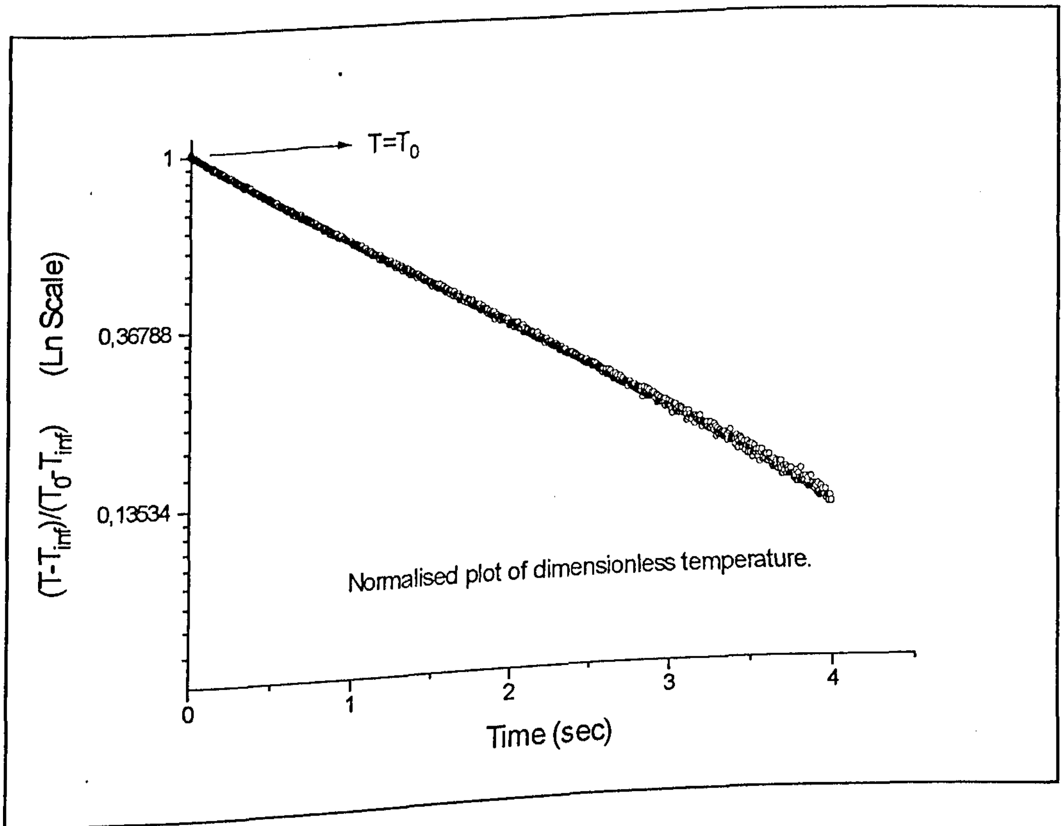

Figure (2.6) Normalised temperature decay.

2.4 - ESTIMATION OF FLUID VELOCITY USING THE CONSTANT TEMPERATURE METHOD

This section describes the use of NTC thermistors maintained at a constant temperature for air velocity measurement.

In order to derive an expression that represents the behaviour of the thermistor when submitted to a constant temperature, it is assumed that its shape is perfectly spherical and its internal temperature is uniform at all times and the same as the temperature of the surface in contact with the moving fluid. Then, if the effect of radiation can be neglected, the heat transfer equation for the thermistor within a fluid at temperature T_∞ is:

$$P = h_c A_s (T - T_\infty) \tag{2.20}$$

where P - dissipated electrical power = $R(T)I^2$

h_c - convective heat transfer coefficient

A_s - surface area

T - probe temperature

T_∞ - environmental temperature

R(T) - thermistor resistance

I - current across the probe.

In velocity measurement, the principal interest is the dependence between flow velocity and the probe overheating. For a given range of velocities and fluid density, h=h(V) (and $h \approx h_c$, as already mentioned) is a function of fluid velocity and has the general form (Doebelin, 1976):

$$h = a + b\sqrt{V} \tag{2.21}$$

where a and b are determined by fitting the experimental data within a given range of velocity.

According to Carslaw and Jaeger (1959), this equation was first proposed in 1914 by King, and is called King's law. (2.21) can also be deduced from observation of the Nusselt number defined for a sphere:

$$Nu = Nu_\infty + C \; Pr^n \, Re^m \qquad (2.22)$$

where
- Nu - Nusselt number (hL/K_f)
- Nu_∞ - Nusselt number as V tends to zero.
- C - correlation coefficient
- Pr - Prandtl number (ν/α)
- Re - Reynolds number (VL/ν)
- L - characteristic length
- kf - thermal conductivity of the fluid
- m - Reynolds number parameter
- n - Prandtl number parameter
- ν - kinematic viscosity of the fluid
- α - thermal diffusivity of the fluid.

The empirical parameter m=0.5 was reported by numerous investigators, according to Yovanovich (1988).

As the real phenomenon is rather complex, other relations similar to equation (2.21) that correlate the fluid velocity to the probe heating have been found experimentally by many researchers. A comparable formula was proposed by Kung et al. in 1987, according to Sobrinho and Maciel (1994):

$$\frac{1}{\Delta T} = a + b V^n \qquad (2.23)$$

where a, b and n were determined by fitting the experimental data within a given range of velocity, and ΔT is the difference between probe and fluid temperatures.

Also according to the same authors, Grahn (1968) proposed an equation given by:

$$h = a + b \ln (V) \qquad (2.24)$$

Sobrinho and Maciel (1994) used, for a given temperature of the fluid T_∞, an equation:

$$\Delta T = T - T_\infty = a + b \ln(V) \qquad (2.25)$$

where T is the temperature of the heated probe.

In the present work, it was found, from observation of experimental data for a given fluid temperature T_∞, that the convective heat transfer coefficient h was well fitted by a second degree polynomial in $\sqrt{V}$:

$$h = a + b\sqrt{V} + c V \qquad (2.26)$$

where a, b and c were determined by fitting the experimental data within a given range of velocity.

The velocity can be expressed as a function of circuit output voltage and fluid temperature, by substituting (2.26) in (2.20):

$$V = \left[\frac{-b' + \sqrt{b'^2 - 4c'\left(a' - \frac{P}{(T - T_\infty)}\right)}}{2c'} \right] \tag{2.27}$$

which can be written as:

$$V = \left[\frac{-b' + \sqrt{b'^2 - 4c'\left(a' - \frac{E^2}{R(T - T_\infty)}\right)}}{2c'} \right] \tag{2.28}$$

where a', b' and c' are obtained by multiplying the initial parameters a, b and c by the probe geometrical characteristic A_s. The possibility of a minus sign before the square root term in (2.27) and (2.28) was not considered, as it did not correspond to the physical reality observed.

Although dealing with steady-state, it is often needed to measure velocities at different fluid temperatures, and these parameters were observed to have a dependence correlation with fluid initial temperature. In this work, an empirical polynomial model of degree two in T_∞ was adopted:

$$a' = a_1 + a_2 T_\infty + a_3 T_\infty^2 \tag{2.29}$$

where a_1, a_2 and a_3 were regression parameters. Analogous formulae were used for b' and c'.

CHAPTER THREE

3 - DEVELOPMENT OF THE ANEMOMETERS

During this research, two basic electronic circuits to operate the thermistors were designed, built and tested: the heat pulse and constant temperature circuits. As the tests called for corrections of the circuits, initial assembly was done on a solderless prototyping board. The circuits will be described in this chapter. Evaluation, as well as suggestions of improvement, will be done in later chapters.

3.1 - THE HEAT PULSE CIRCUIT DESCRIPTION

The circuit used to study the transient behaviour of thermistors in anemometric applications was constructed using: an input voltage regulator, a constant current source, a differential amplifier, an amplifier gain control and an inversor block, as shown in the diagram of figure (3.1):

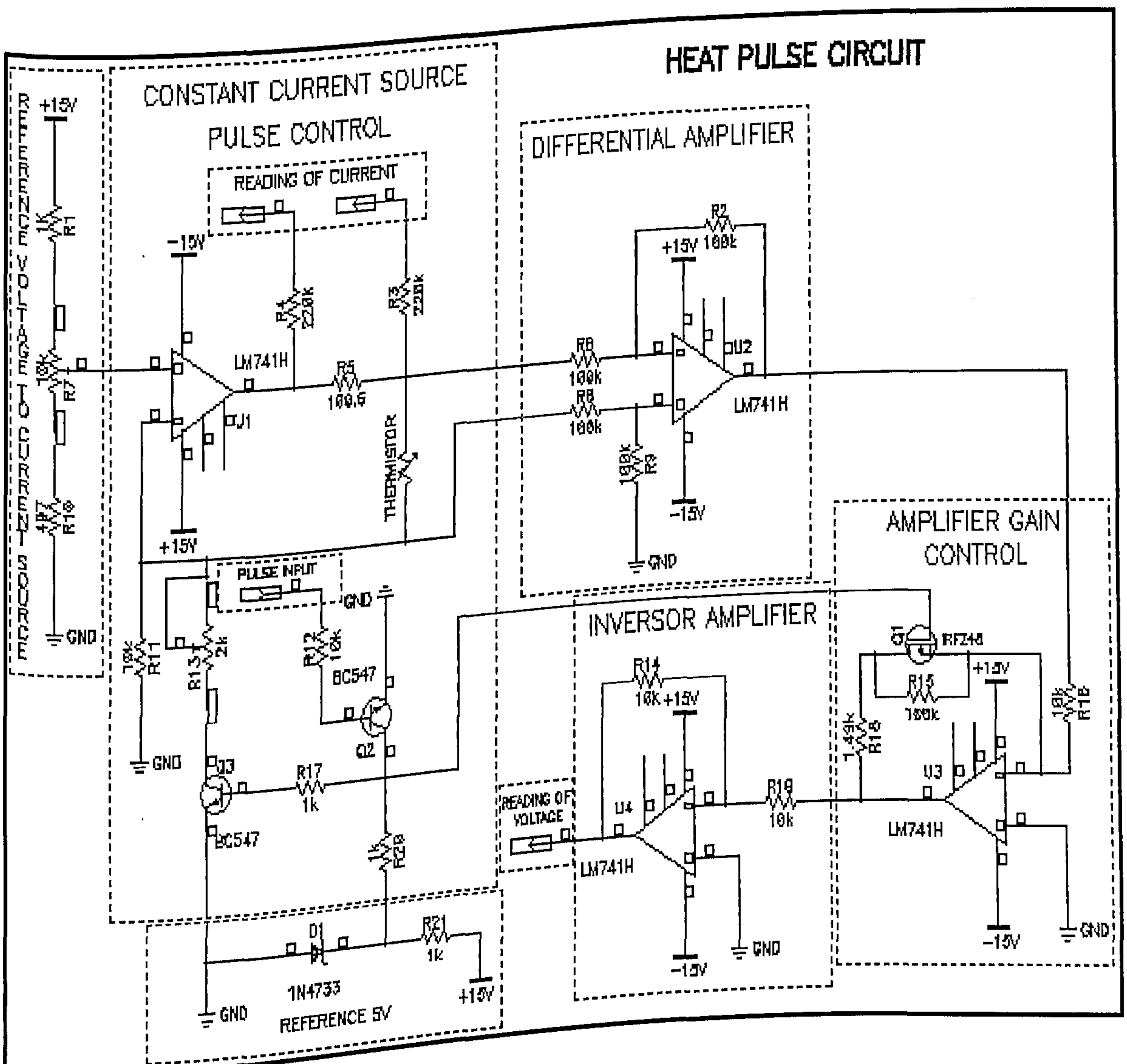

Figure (3.1) Diagram of the heat pulse circuit.

The input voltage was regulated by a voltage divider, and fixed to a value that corresponded to the current source block requirement (1V). The constant current source operation was established by the ratio of its operational amplifier voltage input and the equivalent feedback resistance, determined by the two feedback resistances R11 and R13, which provided two levels of current, according to the mode of thermistor performance (heating or cooling phases).

For instance, when the pulse input from the computer was set in logic "0" the transistor Q2 (BC547) was not conducting and the reference voltage (5V) was delivered to the base of Q3 (BC547) and the gate of Q1 (MOSFET IRFZ48), switching them on. The circuit was then operating in the heating phase, and the equivalent feedback resistance was calculated by the parallel group of R11 and R13. R13 was, then, regulated for the current source block supplying a constant current of about 10.9 mA to the sensor. Also, the resistance R15, in the amplifier gain control block, was put in short-circuit and the operational amplifier gain became 0.15.

On the other hand, when the pulse input was set in logic "1" the transistor Q2 was saturated, and Q3 and Q1 was turned off. The circuit was operating in the cooling phase, and the equivalent resistance, in the constant current source, was equal to R11. A constant current of 0.115 mA was supplied to the thermistor. The amplifier gain control again changed the circuit gain to 10.15.

The current was known indirectly by reading the voltage over R5 (with an established value of 100.6 Ohms). R3 and R4 were base resistances and were required by the A/D board for operating in differential mode.

A differential amplifier, after the current source block was responsible for furnishing an output voltage equal to the difference between the signals applied to its inputs (in the case, the sensor wire voltages between amplifier pins 2 and 3), multiplied by a gain (selected as 1, for the case). As its function was similar to a voltmeter's, an ideal operation would not affect the thermistor current level, i.e., it would not allow current trough it. However, this was not verified in practice, and a slight discrepancy between the calculated and actual resistances was observed. The procedure adopted to correct this discrepancy will be dealt with in the next chapter.

The amplifier gain control was composed of an operational amplifier with the gain resistances controlled by the pulse input signal. Its output was inverted in relation with the input signal.

The inversor amplifier had exclusively the purpose of inverting the signal coming from the precedent block. No gain existed in this block and its output voltage was read by the A/D board.

All operational amplifiers used in this circuit were LM741H, with symmetrical feeding of ±15V.

3.2 - THE CONSTANT TEMPERATURE CIRCUIT DESCRIPTION

The applied constant temperature circuit, as shown in figure (3.2), was essentially a bridge circuit that operated by adjusting the power through the sensor to keep its temperature (that is its resistance) constant. The unbalanced bridge produced an umbalanced voltage, which was applied to the input of a high-gain amplifier, that supplyed the bridge feedback voltage. As the power over the thermistor resistance R increased, its temperature and thus its resistance conducted the bridge back to the equilibrium. This feedback system maintained the desired probe temperature for every velocity.

Supposing that the bridge was initially unbalanced (which was the actual form of operation of this circuit, since the probe was always transferring heat to fluid in its vicinity, even when the fluid is at a zero velocity), due to changes in fluid velocity for instance, then the difference of voltage applied to the operational amplifier LM741H, by virtue of thermistor resistance and temperature changes, would cause the electric tension that fed the bridge to be automatically adjusted to restore the original value.

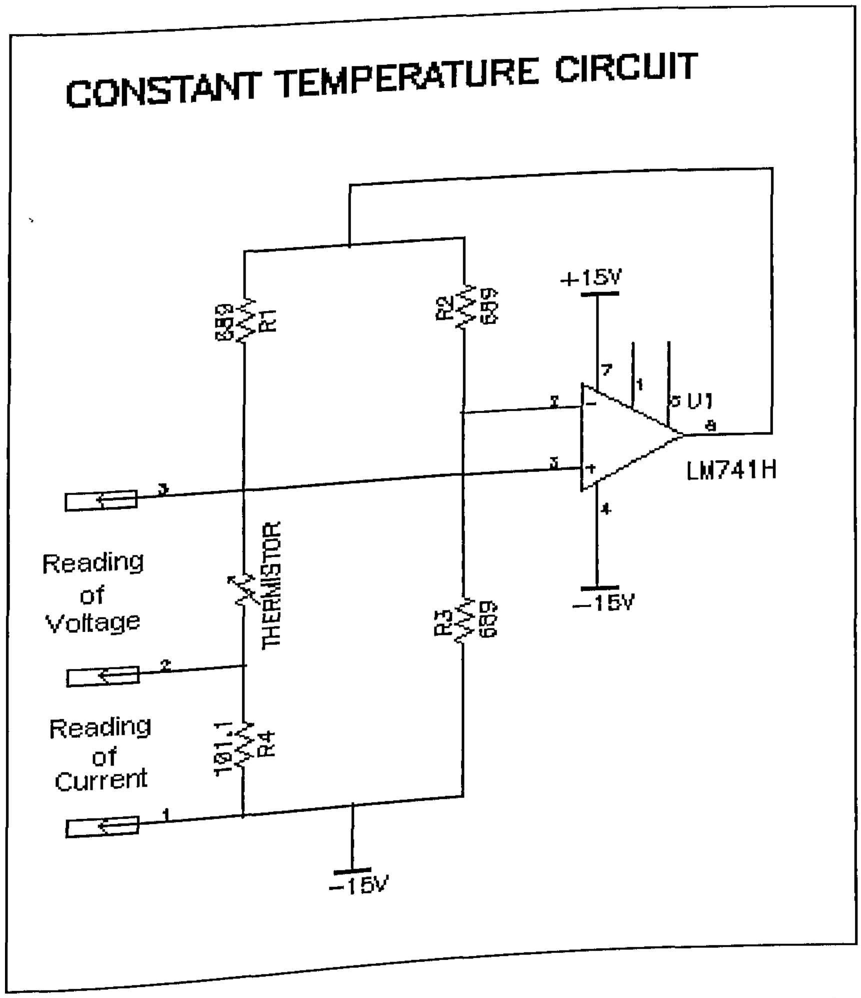

Figure (3.2) Diagram of the constant temperature circuit.

The resistances R1, R2 and R3 were chosen according to the selected temperature of operation. The same value was used for all of them, which provided the best operational condition to the circuit. The probe resistance R was theoretically maintained equal to (R3-R4) that corresponded to a fixed temperature. R4 was of 100 Ohms and had no function on the circuit other than enabling current measurement.

The values of 375, 496, 696 and 1000 Ohms were tested in the circuit, but 696 Ohms was chosen as it corresponded to a temperature of operation above the utilised fluid temperature, without overheating the probe.

The probe wire voltage (or current or power), adjusted to restore the bridge balance, corresponded to a specific velocity V on a calibration procedure at a constant fluid temperature. Once calibrated, the anemometer could be used to measure fluid velocity by means of reading the output voltage and getting the corresponding velocity from a calibration curve, like figure (1.4).

As the calibration assumed the environmental temperature to be kept constant during that procedure, a calibration taking a range of temperature in account was tried, as will be described in chapter four.

In the circuit of figure (3.2), the operational amplifier was fed asymmetrically with 0-30V. This was necessary in order to amplify the range of tension supplied to the bridge to a value of 0~30V (instead of 0~15V, for symetric feeding), on the contrary, the amplifier saturation could be attained for velocities lower than that of the range in study.

CHAPTER FOUR

4 - EXPERIMENTAL APPARATUS AND PROCEDURE

4.1 - THERMISTOR DESCRIPTION

This study was carried out using 2.54 and 1.524 mm diameter glass encapsulated thermistors, supplied by Fenwal Electronics, models 121-102EAJ-Q01 and 120-102EAJ-Q01, respectively. From now on, they will be called thermistor 1 and thermistor 2, respectively. Details of probe geometries and dimensions are shown in figures (4.1) and (4.2):

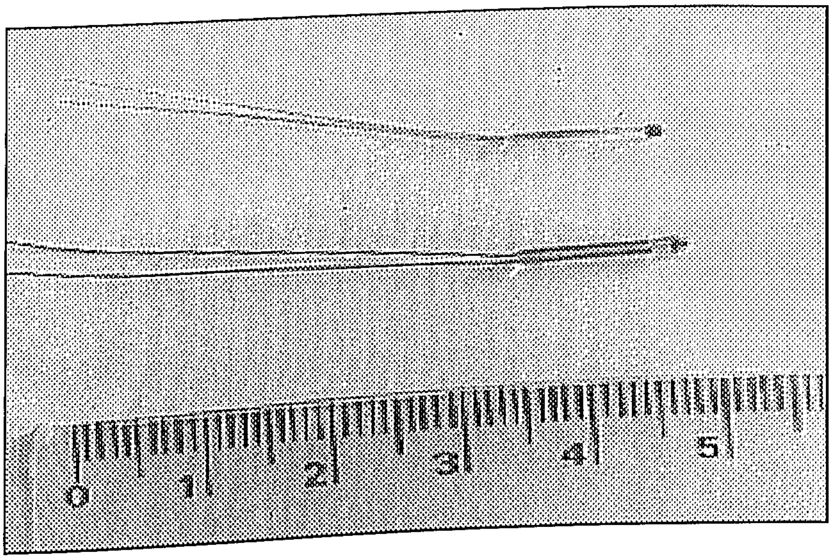

Figure (4.1) Glass encapsulated probes.

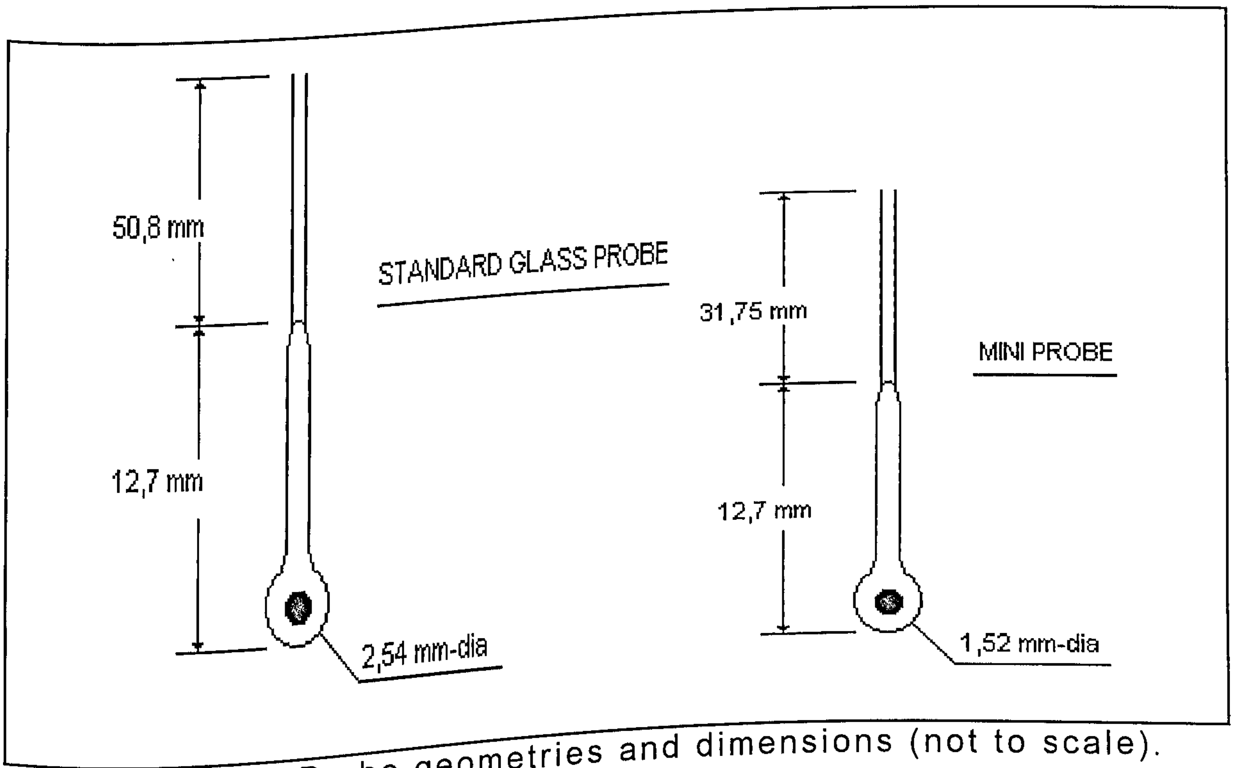

Figure (4.2) Probe geometries and dimensions (not to scale).

4.2 - R-T CALIBRATION SYSTEM

Prior to utilisation of thermistors in laboratory tests, calibration procedures were conducted in order to obtain their resistance-temperature characteristic curves, as well as to evaluate their time constants.

The two regression constants of the NTC characteristic curves were obtained with help of a mercury-in-glass thermometer, with 0.1 °C of resolution, and a thermostatic bath with capacity of 16l , filled with distilled water. The bath, as shown in figure (4.3), permitted a temperature increment of 1.0 °C, presenting a refined control, which allowed good precision on the procedure. The probe calibrations were done in two different manners: (1) Installed in the heat pulse circuit, and the power set in the low mode, therefore registering temperature variations, and (2) Out of any circuit. A slight discrepancy was observed between these two results, for values of temperature near the lower and upper ranges of calibration. This fact was already commented in the previous chapter. Consequently, the resistance calculated from the R-T data acquired with the sensor installed in the heat pulse circuit was slightly different when compared with the data obtained by reading directly the probe resistance with multimeters of 41/2 digits accurate to 0.1 Ohms.

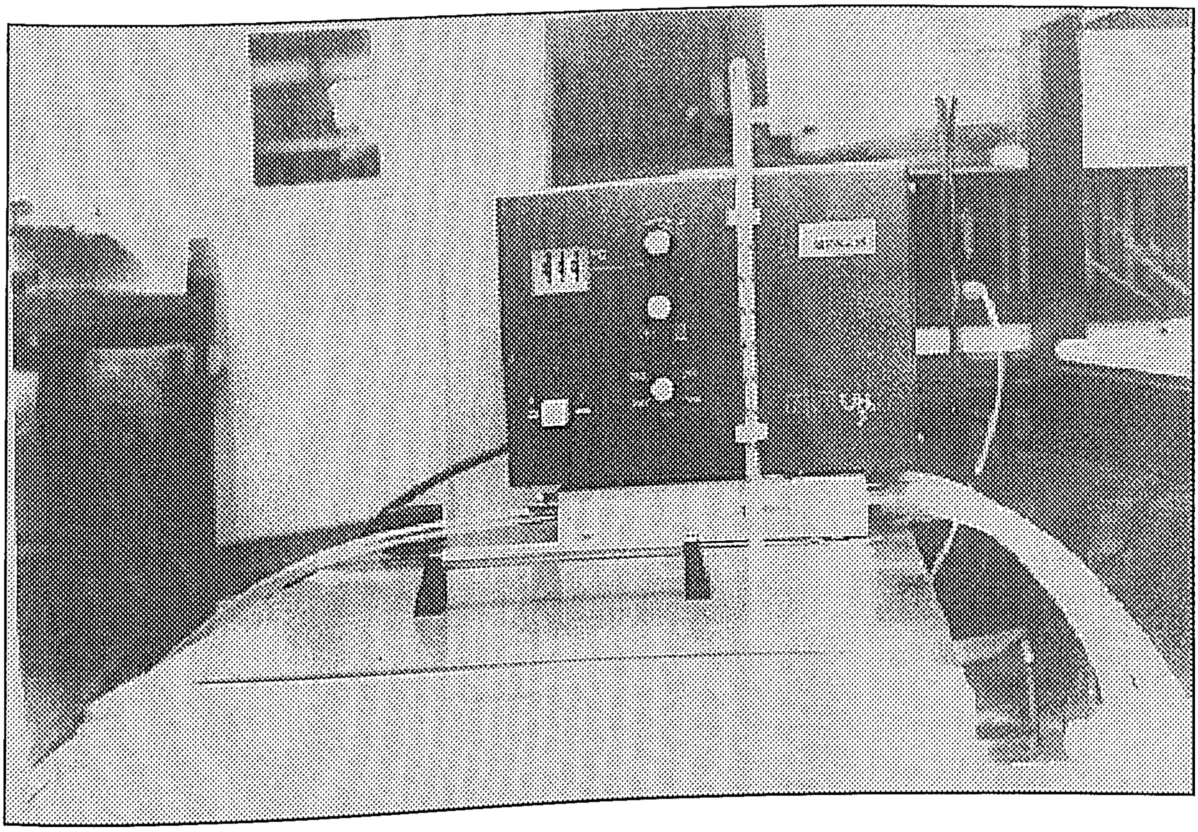

Figure (4.3) Thermostatic bath utilised for thermistor R-T calibration.

In the heat pulse circuit, the probe resistances were obtained indirectly by reading the voltage across the thermistor wires and knowing the applied current over it.

A correction for the observed problem had to be done for both sensors, although the theoretical circuit gain resulted in acceptable values for the range of probe utilisation (25~40°C). The trends were similar for both probes. The discrepancy on the calibration curves can be seen in figure (4.4).

By examination of the difference between the resistance calculated with the theoretical circuit gain and the actual resistance, a polynomial fit of degree two was done, which

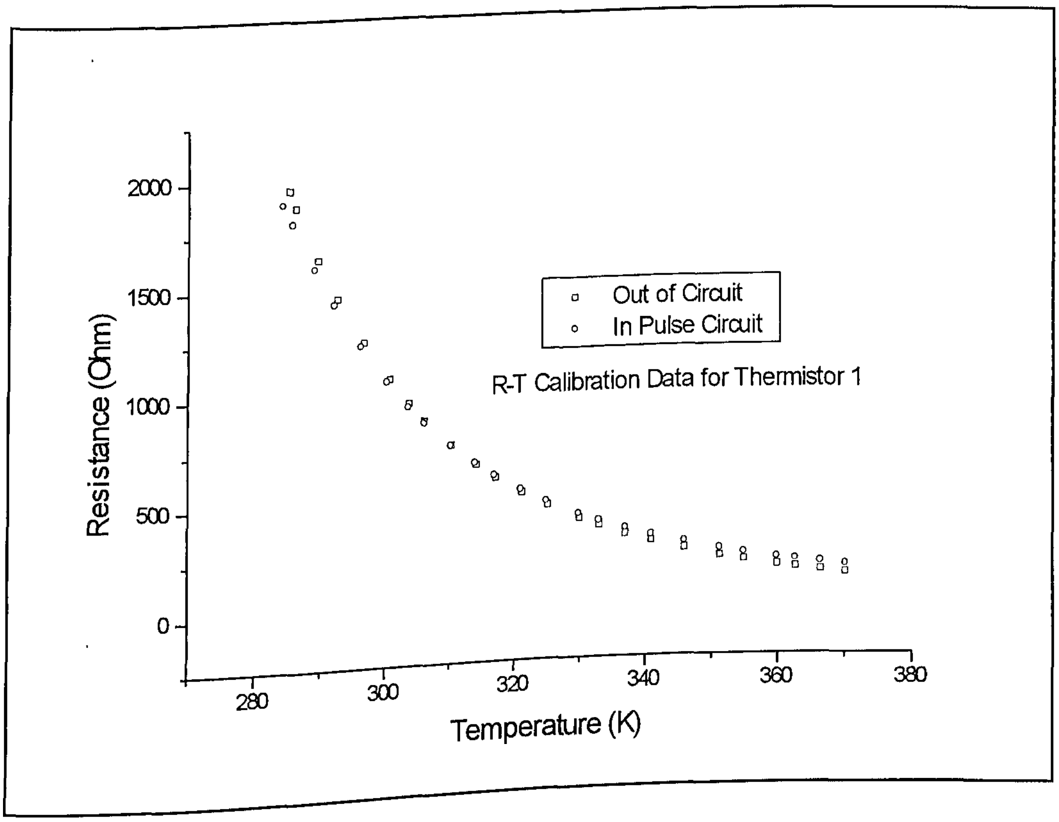

Figure (4.4) R-T calibration data for thermistor 1.

provided a maximum deviation of 1.9% from measured resistance (against 18.6% using the theoretical form of calculating the resistances with the pulse circuit output):

$$\frac{\frac{R}{R_a} - 1}{\frac{R}{R_a}} = P_2(R) \qquad (4.1)$$

where R - resistance obtained from pulse circuit output

R_a - actual resistance

1 - ideal ratio

P_2 - second degree polynomial in R

Equation (4.1) can be written as:

$$R_a = (1 - P_2(R))\,R \tag{4.2}$$

where R_a was a function basically of R, which could be calculated from the readings of probe wire voltage and current, in the circuit of heat pulse at temperature sensing mode. Doing that, the heat pulse circuit was adjusted to the R-T calibration curves obtained with zero power applied to the sensors.

Data of R-T calibration for the two sensors, as well as the two constant regression fit, are represented in figures (4.5) and (4.6):

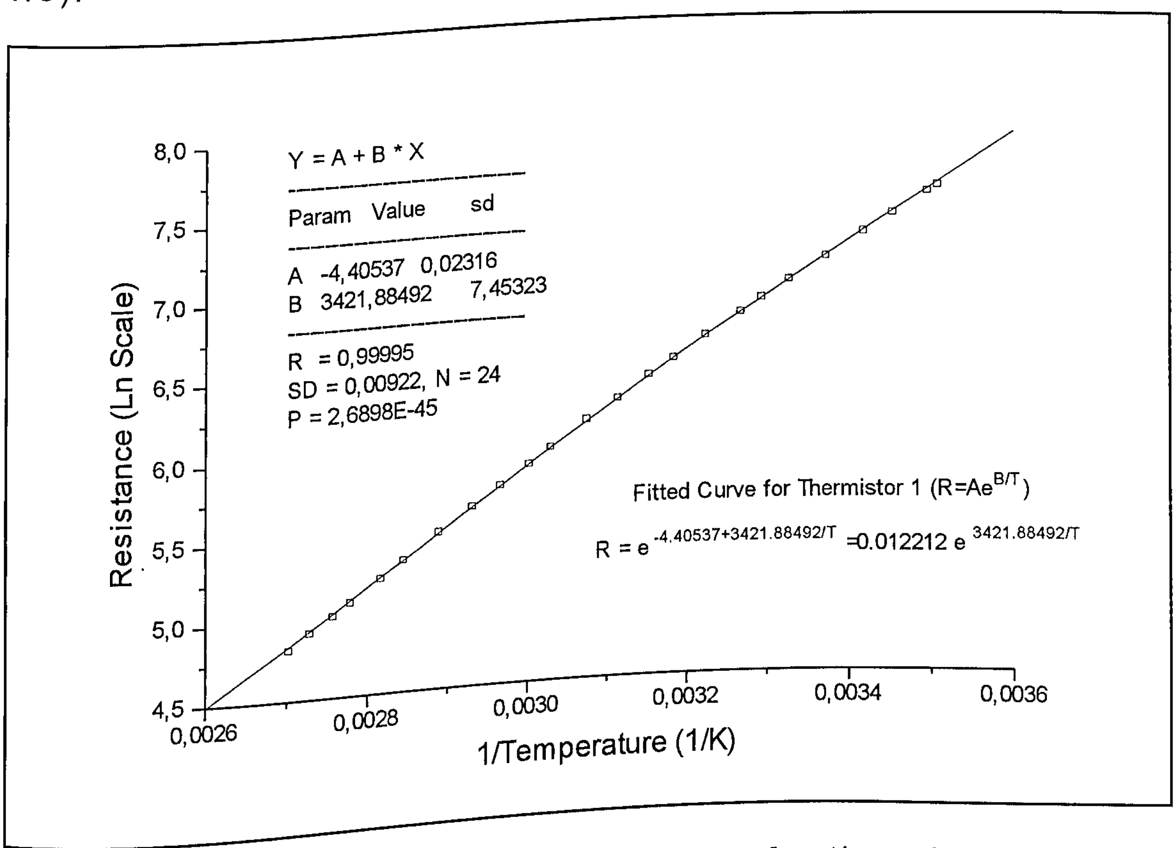

Figure (4.5) Fitted calibration curve for thermistor 1.

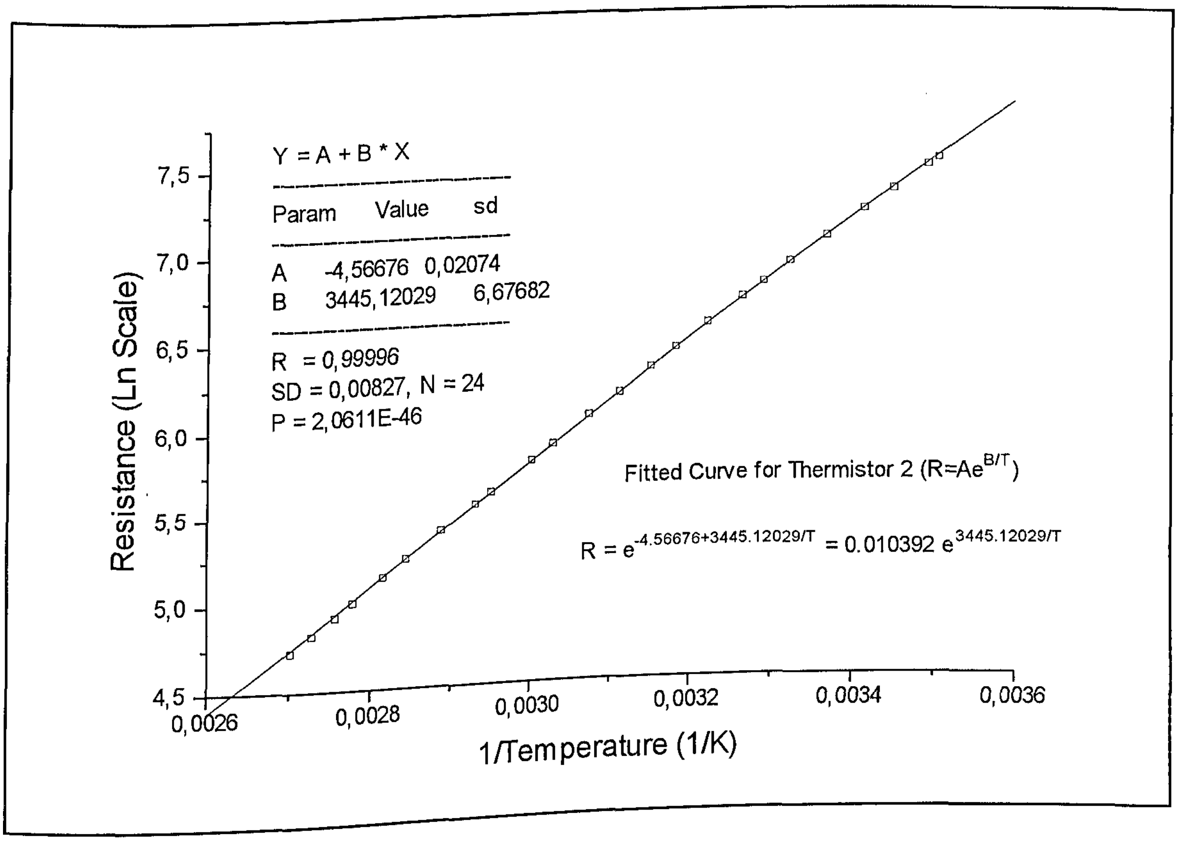

Figure (4.6) Fitted calibration curve for thermistor 2.

The R-T curves for thermistors 1 and 2 were, respectively:

$$R = 0,012212\ e^{3421,88492/T} \tag{4.3}$$

$$R = 0,010392\ e^{3445,12029/T} \tag{4.4}$$

The time constant τ was estimated for each probe, as described in chapter two, utilising the same thermostatic bath, adopting the time to achieve 63.2 percent of water temperature. Time constants in air of 22 sec for the glass probe and 10 sec for the mini probe were supplied by the manufacturer. These values were obtained experimentally in water, and estimated in air as 25 times that in water (Rasmussen, 1961).

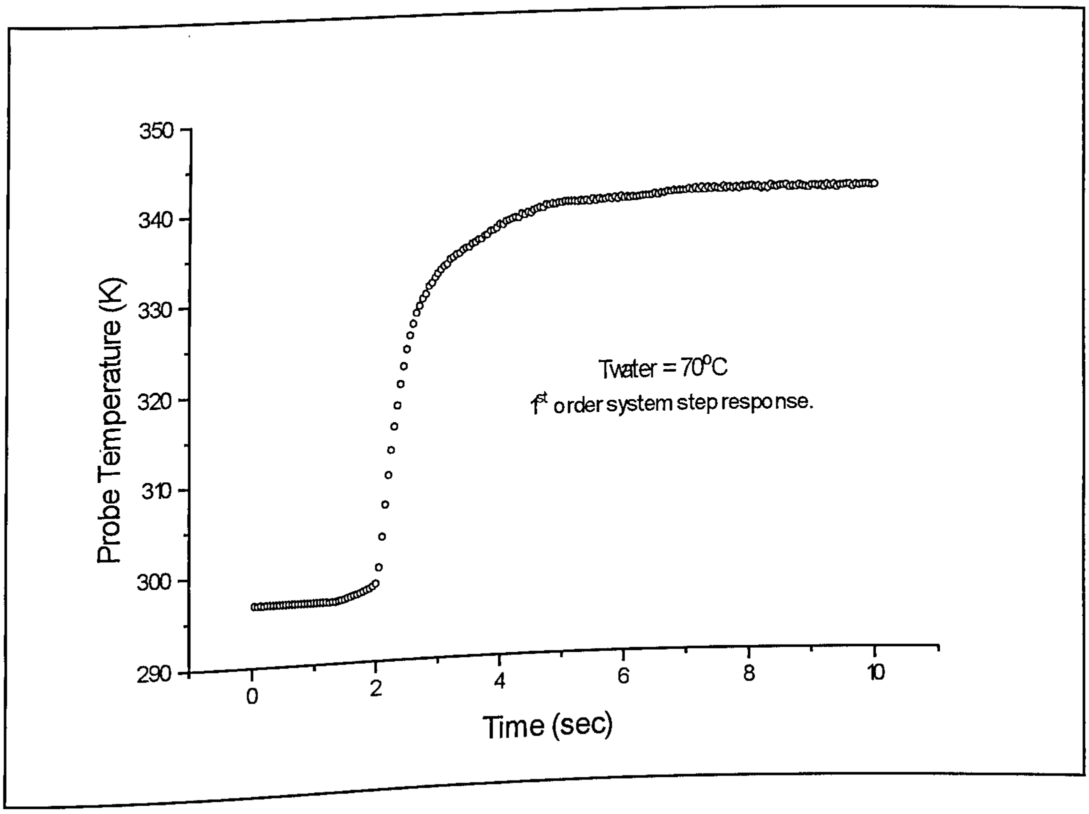

Figure (4.7) Step response in water for thermistor 1.

The procedure was repeated for bath temperatures of 60, 70 and 80°C, and the response curves prior to dipping of the thermistors into the experiment were collected at a sampling frequency of 1000 Hz by the automated data acquisition system, described in section (4.5). The estimated time constants in air were 22.5 and 7.3 sec, for the glass probe and the mini probe, respectively.

A serious problem during calibration was the contact of the probe wires with the water, which caused a large a-c level to be added to the circuit output in consequence of a capacitive effect, turning the signal impossible to be evaluated. This matter was solved by assembling the probe in a 5 mm-dia aluminium tube and sealing the gap between probe and tube with a silicon glue.

4.3 - ELECTRONIC EQUIPMENT

The following electronic equipment was used for developing the circuits, as well as for allowing their correct operation:

a) Digital multimeters accurate to 41/2 digits, which permitted adjustment of voltage and current levels for correct operation of the circuits, specially in the initial phase of building. In spite of helping, their presences in the circuits showed significant influence on the output values, which could only be eliminated with the automation of acquisition of this information, and substitution of the multimeters by the differential channels "0" and "1" of the A/D acquisition board.

b) A stable d-c power supply model TC 15-02 B (Tectrol S.A.), having two independent output tensions of 0-15V and currents of 0-2A, with possibility to be inter-connected in mode "auto", permitting to regulate the circuit feed tensions (±15V to the heat pulse circuit and 0-30V to the constant temperature circuit).

c) A square wave generator model ETB-515 (Entelbra S.A.) was utilised in the initial phase to apply the pulse, permitting to control frequency and shape of the electric pulse. The automation of the acquisition substituted this equipment by the digital output "outport O", see figure (4.15), of the board, which permitted to put the heat pulse under the control of the software.

4.4 - CALIBRATION TO AIR SPEED

The calibration to air velocities was conducted in a probe calibrator model 1125 (TSI Inc.), over a range of about 0.05 to 12 m/s.

The calibrator was connected to an air compressor (model MS-V-10/175, Schulz S.A.), and the compressed air was filtered inside the calibrator. Besides filtering, this equipment included everything that was necessary for flow control, as shown in figure (4.8):

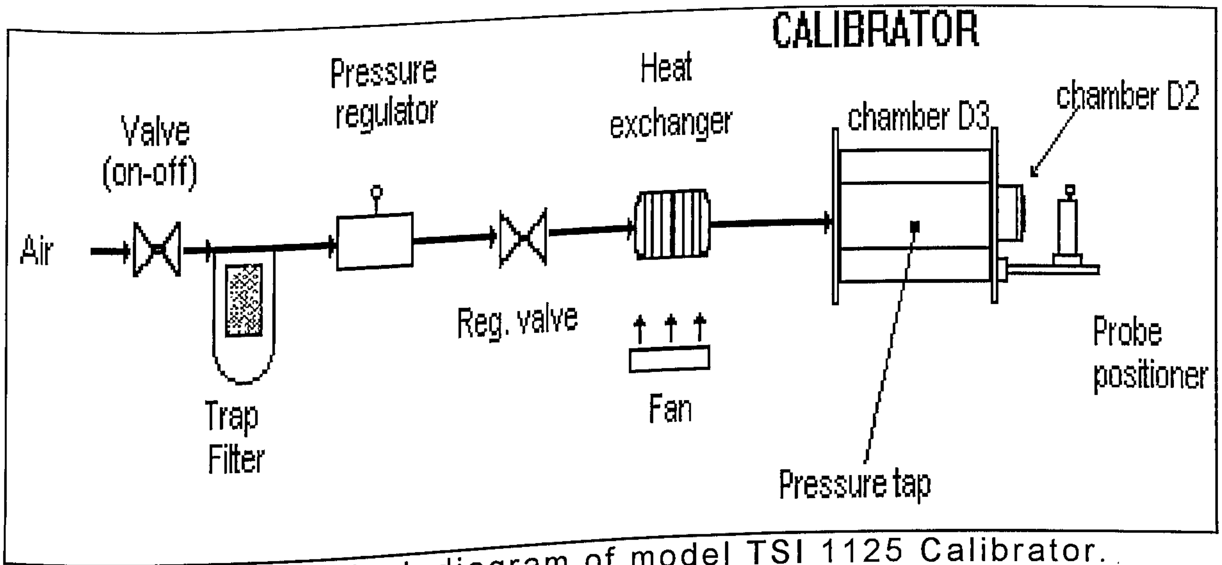

Figure (4.8) Block diagram of model TSI 1125 Calibrator.

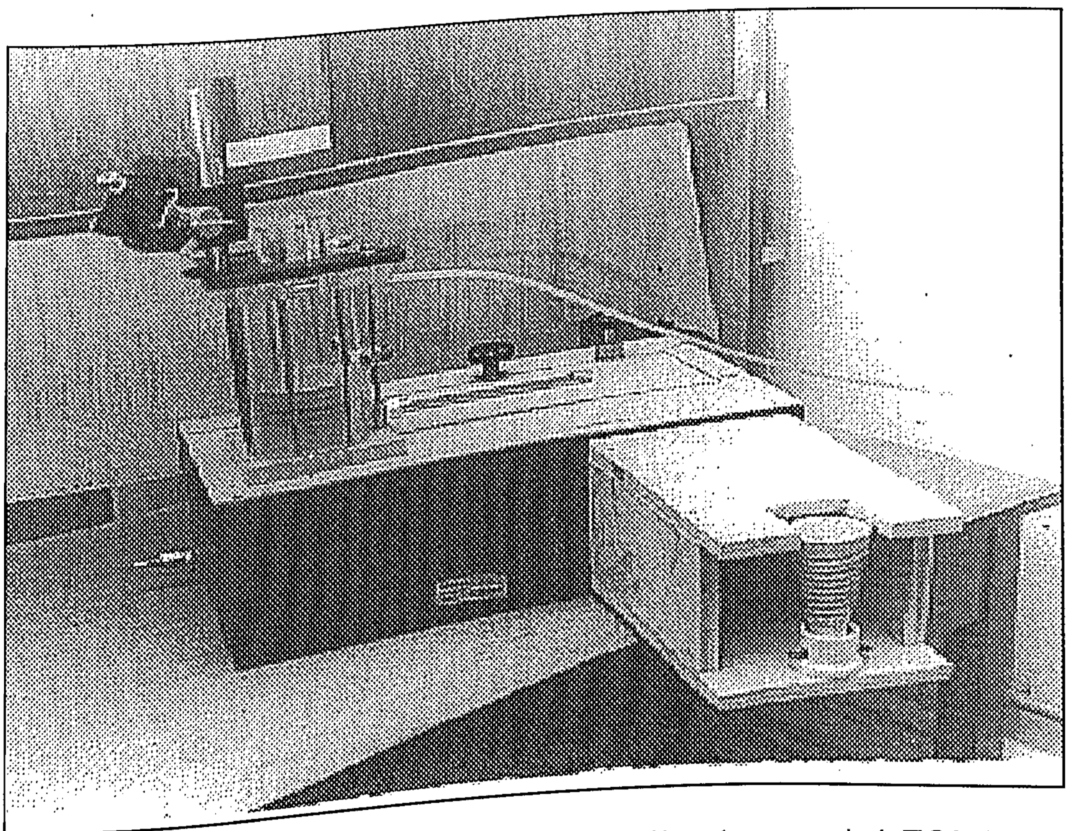

Figure (4.9) General view of probe calibrator model TSI 1125.

The chambers D2 and D3, utilised for calibration, are shown in figure (4.8), however the system also permits to use an external chamber D1 for greater velocities. The mid-range chamber D2 has an internal diameter of 16.5 mm and can be used for velocities from 0.63 to 15 m/s, while the low range chamber has an internal diameter of 71.7 mm and can be used for velocities from 0.01 to 1m/s.

Figure (4.9) shows an electrical resistance for heating the inlet air to the heat exchanger. This was done to permit an investigation of the influence of the fluid temperature on the instrument calibration. The electrical power was supplied to the resistance by connecting it in series to a variable a-c power supply. The fluid temperature was monitored with a mercury-in-glass thermometer of 2°F (1.1°C) resolution.

The air velocity was obtained by means of measuring the pressure differential across an orifice of pressure tap with water and mercury manometers. There is a relation between velocity and pressure differential (chamber pressure-atmospheric Pressure), which is provided by the manufacturer in the form of calibration sheets. As the geometries of the probes affected the free uniform flow, sheets corrected for average hot-wire geometries were used (see appendix C).

For each calculated air velocity, a correction factor for ambient conditions was applied, according to manufacturer's recommendations. The manufacturer quoted a maximum error of 8% for the chamber D2 at a velocity of 15 m/s.

Calibration was conducted for fluid temperatures of 299.82, 303.15, 306.48 and 309.82 K. The probes were placed in the chambers with help of a 5 mm-dia aluminium tube, conform figures (4.10) and (4.11):

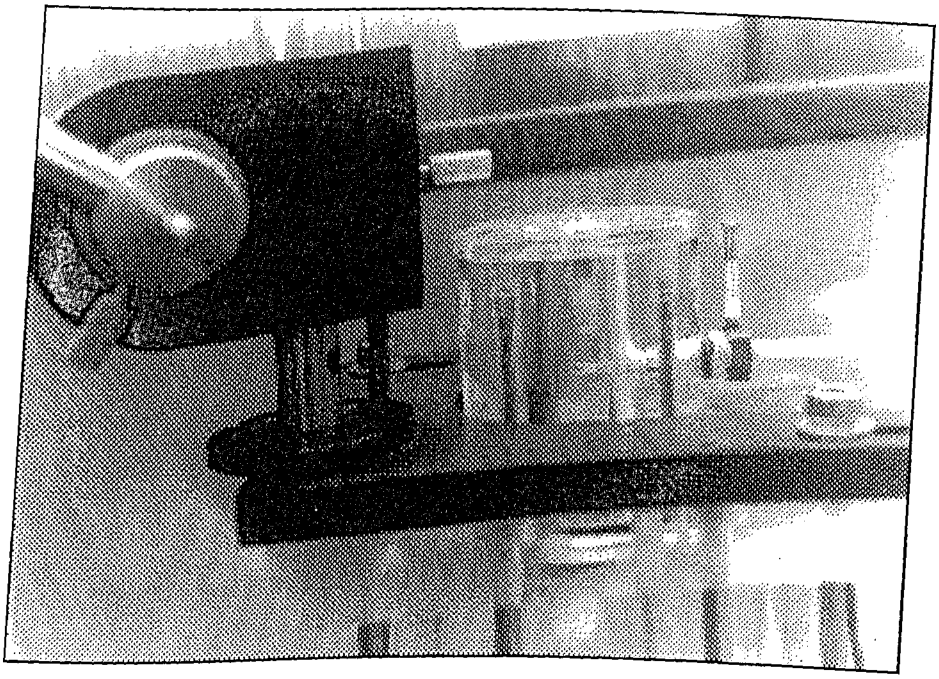

Figure (4.10) Positioning the probes into the calibrator.

Both fluid velocity and temperature were allowed reaching a steady-state condition before data were collected (15~30 min). About 50 readings over the range of 0.05-12 m/s were taken for each temperature and for each sensor, for both circuits.

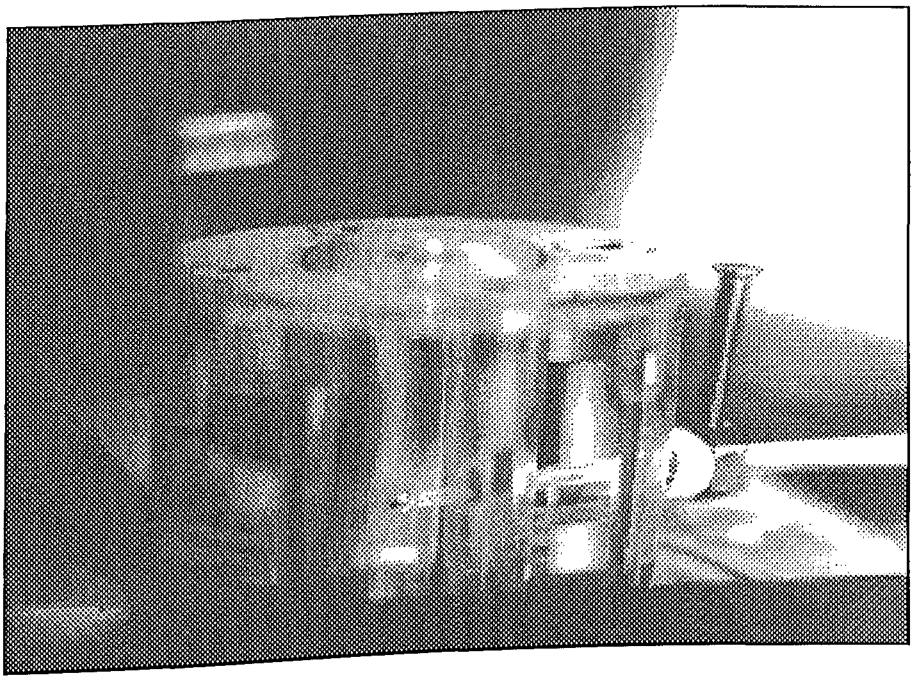

Figure (4.11) Detail of probe placement in chamber D2.

For the constant temperature circuit, the procedure involved an acquisition at a rate of 100 Hz during a period of 2 sec, after fluid steady conditions being achieved. The averaged voltage and current (and consequently the power) were correlated to air velocity and fluid temperature.

For the heat pulse circuit, an increased sampling rate of 200 Hz was selected to represent the phenomenon accurately. A cooling period of 3 sec was adopted and heating periods of 2 and 1 sec was preferred for thermistor 1 and thermistor 2, respectively. Three consecutive heating-and-cooling periods were imposed, but only the first two were considered. At the first cooling period (before any pulse application), the probe temperature was approximately the same as the fluid's, and an average of 400 readings (2 sec) were taken to obtain T_∞. The linearization, according to equation (2.18), was applied to the second cooling phase. The initial temperature T_0 was set for an initial time of t_0=1 sec. After this, the points of the two sequential seconds were handled by a subroutine (see appendix B) of the software to calculate the slope of the linearized curve and associate it to a velocity.

4.5 - DESCRIPTION OF THE DATA ACQUISITION SYSTEM

Data acquisition and control systems are used in the following applications:

a) sensing physical variables;

b) converting analogue signals into digital signals, which are computer readable;

c) processing, plotting and logging the acquired data to storage devices;

d) controlling a process.

The used data acquisition and control system was composed of a data acquisition board model DAS 1402 CyberResearch installed in a Personal Computer 386 DX40. The board was programmed in the language Borland C++ (although commercial data acquisition and analysis packages were at hand for operating the board). Therefore, the acquisition features could be controlled via software. Figure (4.12) shows the PC and data acquisition and control instrumentation.

Selection of data acquisition and control hardware should be based on the following criteria:

1st) **Cost**.

2nd) **sampling rate**, i.e., the frequency of sampling. It is necessary that the sampling rate be at least twice the highest

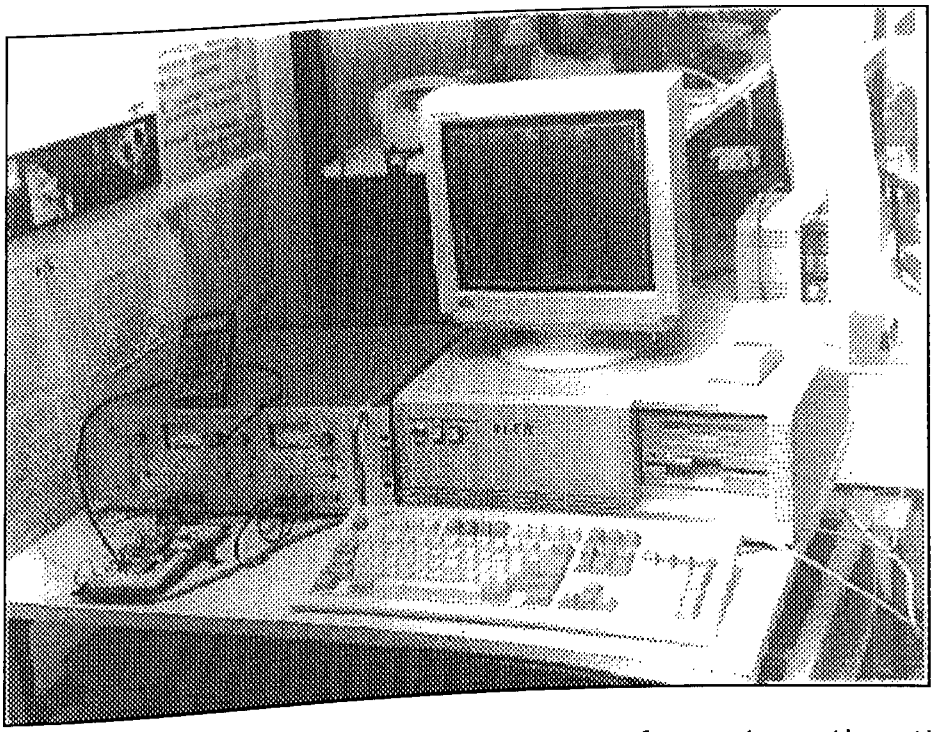

Figure (4.12) Experimental apparatus for automating the acquisition of data.

frequency of the studied phenomenon (to satisfy the Nyquest theorem). Lower sampling frequencies may modify the perceived frequency spectrum of the studied signal, known as "aliasing". On the other hand, high speed boards are more expensive.

3rd) **resolution**, i.e, the number of divisions into which the full-scale input can be divided. For instance, a n-bit resolution permits to divide the full-scale input signal into 2^{n-1} equal intervals. The board can detect only input changes greater than the ratio (full-scale/2^n), which contributes to the maximum error.

4th) **single-ended and differential inputs**. Single-ended inputs normally have a low cost, and are utilised whenever the input signals have a common external ground, which may or may not be the remote ground. Differential inputs offer greater noise immunity, and are used for measurement of several input signals with no common ground.

5th) **the presence of sample and hold circuit** allows acquisition of multiple channels at the same time.

6th) **direct memory access (DMA)** allows the maximum speed of transferring data from board to computer memory.

7th) **analog outputs (D/A)** usually are used to control experiments.

8th) **digital inputs and outputs (DIO)** are used, for instance, to generate pulse or other clock controlled signals.

The selected data acquisition board had the following characteristics:

- maximum sampling rate of 100 KHz with 12-bit resolution;
- 16 single-ended or 8 differential analog input channels;
- switch configurable for either unipolar or bipolar signals;
- channels individually programmed for gains of 1, 2, 4 or 8;

- an 8-bit register, with 4-bit to output and 4-bit to input;
- three 16-bit programmable counters. Counter 0 might utilise a 100 KHz internal clock or an external clock. Counters 1 and 2 were permanently cascaded (to obtain a 32-bit counter) and were connected to a clock of 1 MHz or 10 MHz, selected via micro-switch.

The board is described in CYRDAS 1600/1400 Series User's Guide. Figures (4.13) and (4.14) show the board installed in an accessory slot of the computer and the rear wiring assembly of the board, respectively.

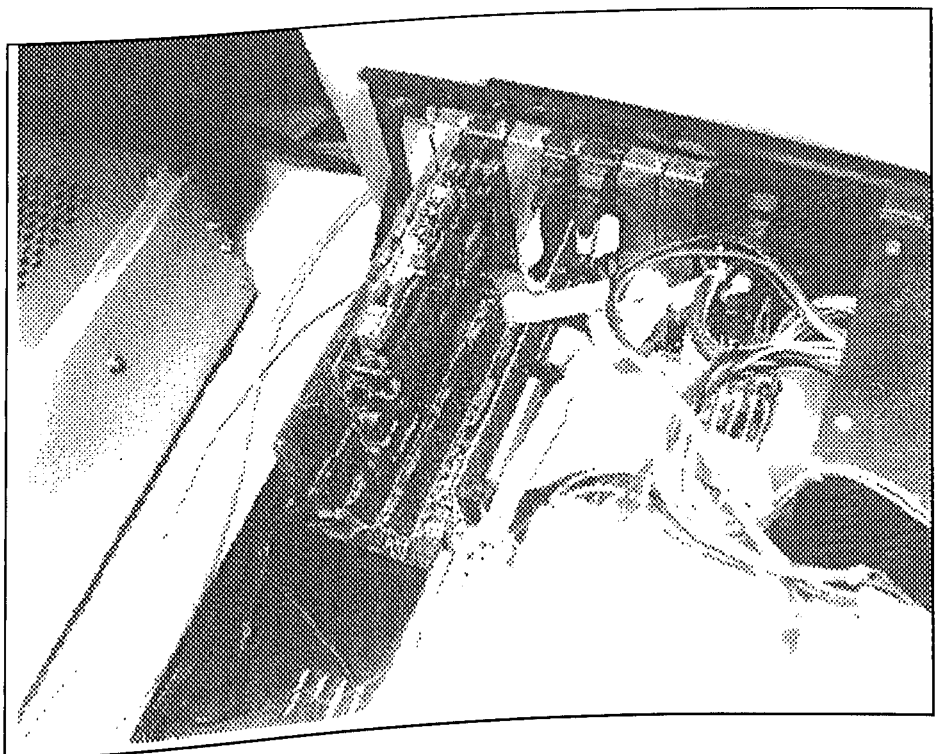

Figure (4.13) Installation of the board in the computer.

The configuration utilised for the board was 8 differential channels in unipolar mode.

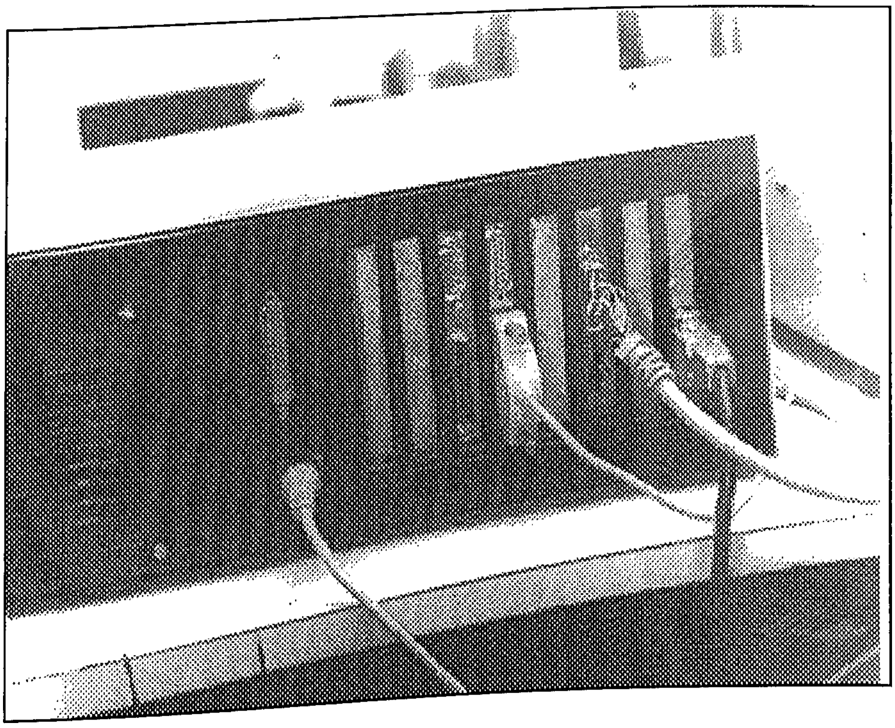

Figure (4.14) Rear wiring assembly of the board.

The board was programmed to achieve the best control of acquisition frequency, making the computer to work exclusively dedicated to the acquisition, e.g., no command could be executed during this routine. The acquired data was transferred from board to computer memory in the interval between two consecutive acquisitions. This was done by the acquisition loop routine that monitored a specific port on the board, which informed when the data was available.

The program accessed directly the register level using I/O instructions. There are 32 I/O mapped addresses, each one named according to the CYRDAS 1600/1400 Series User's Guide. Each base address has 1 byte word length, whose bits are defined by bit names. The control of board features was done by writing to a specific bit-name of a given base address.

The control of the sampling frequencies was done by means of the counter "0" connected to the internal clock of 100 KHz, which worked as a time delay, permitting to program frequencies from 2 to 50kHz (1 to 25KHz in case of using two channels) per

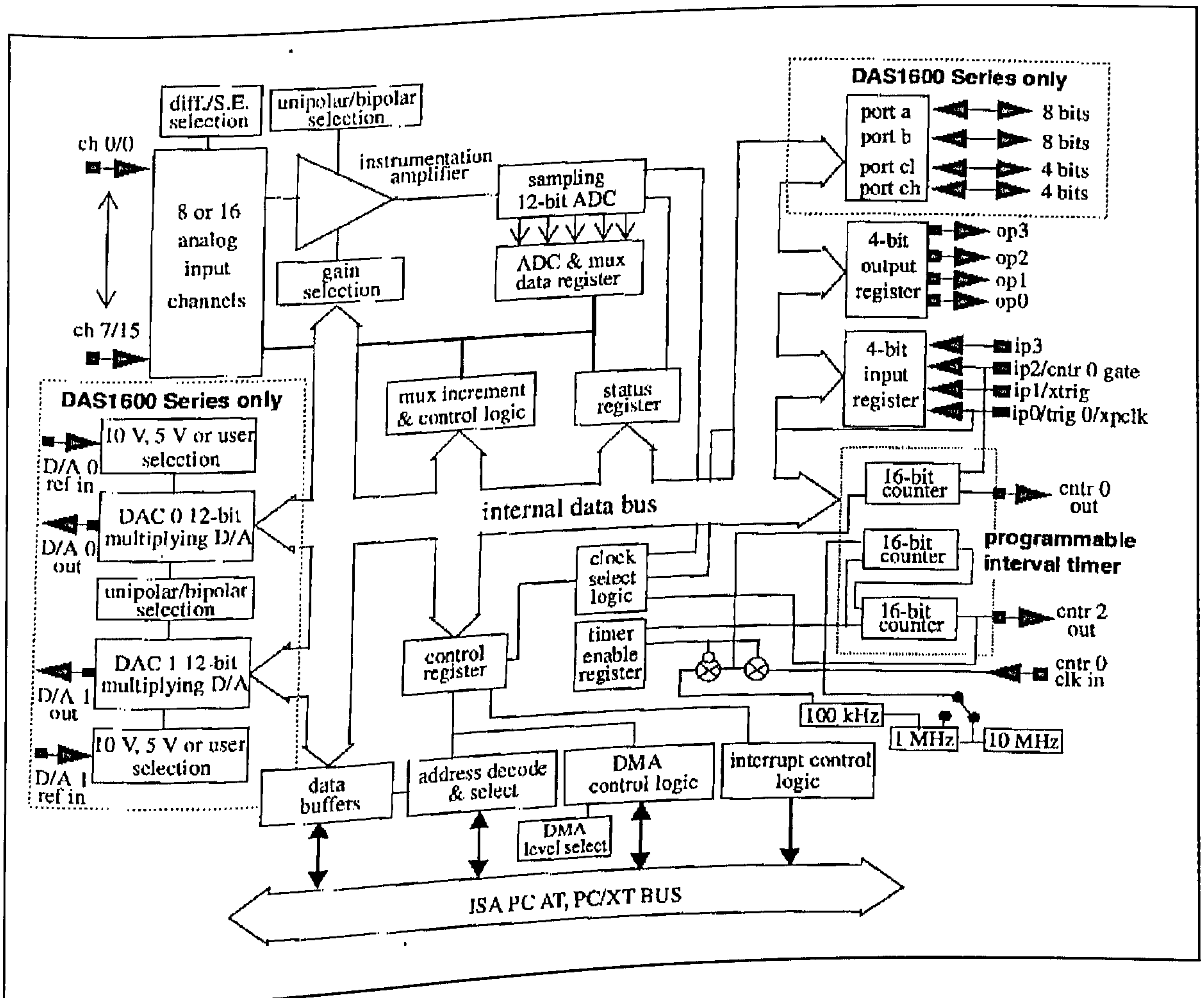

Figure (4.15) Board block diagram, from CYRDAS 1600/1400 Series User's Guide.

channel. Knowing the sampling frequency and the total process duration, the number of events to be acquired could be determined. This information was important, for instance, to program pulse application. An internal routine in the acquisition loop verified the exact moment of heating or cooling the probe, for example. The pulse was generated by writing directly to the bit OP0 (outport zero) of the output register, see figure (4.15).

The program called ONDA permits a complete control of the electronic circuits, as well as storage of data on computer memory, log them to a disk, plot on the display screen, show data in memory and analyse data. The overview-level IPO diagram for program ONDA is found in figure (4.16).

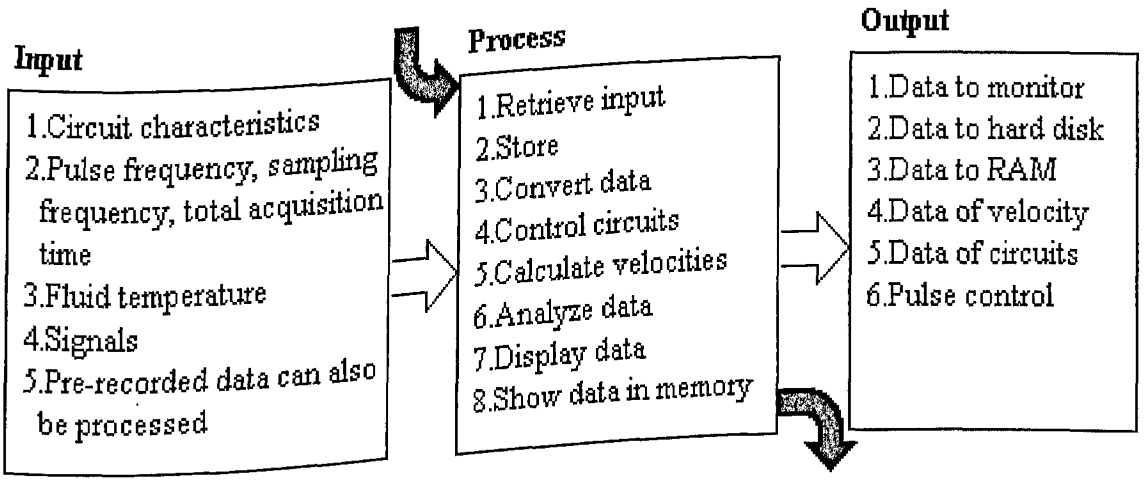

Figure (4.16) The overview-level IPO diagram for program ONDA.

CHAPTER FIVE

5 - RESULTS OF EXPERIMENTS AND DISCUSSIONS

5.1 - PERFORMANCES OF THE THERMISTOR ANEMOMETERS

On the whole, the two circuits tested with the anemometers showed a good performance, as already commented.

The constant temperature circuit maintained the probe average resistance at 593.84 Ohms (the theoretical resistance was equal to 593.00 Ohms) with 95 percent of the readings falling within ±3.88 Ohms. That means, the constancy in temperature was accurate within ±0.03 percent (according to equation (D.3)[1]). The

[1] - The statistical analysis was made with help of a graphical and statistical software Origin V3,5 and appendix D.

actual resistance was known indirectly by reading the output voltage and current (tension across a known resistance) with the acquisition system. The estimated uncertainty in this procedure was $\pm 10/2^{12}$ V for this circuit.

The heat pulse circuit showed an excellent performance in the application of the electric pulse, since the average time required to establish the final current level was around 0.03 sec, with obtainment of 99.4 percent of the final value after 0.005 sec. The estimated uncertainty in voltage readings was $\pm 2.5/2^{12}$ V for this circuit. At low power, a negligible power of about 10^{-5} W was dissipated by the probe, while about 0.1 W was delivered to the probe during the pulse period, which could not cause any damage.

5.2 - THE HEAT PULSE METHOD RESULTS

The heat pulse method, as already exposed in cited works, demonstrated to be capable of detecting fluid motion, as much in homogeneous as in porous medium. Figure (5.1) shows a family of curves obtained with application of a 0.7 s pulse in thermistor 2 for air velocities varying from 0 to 15 m/s. The results indicated that the sensor was able to determine fluid velocity using the pulse method. The adopted model was presented in chapter two, and, according to it, the slope of the normalised temperature decay could be correlated to the fluid velocity.

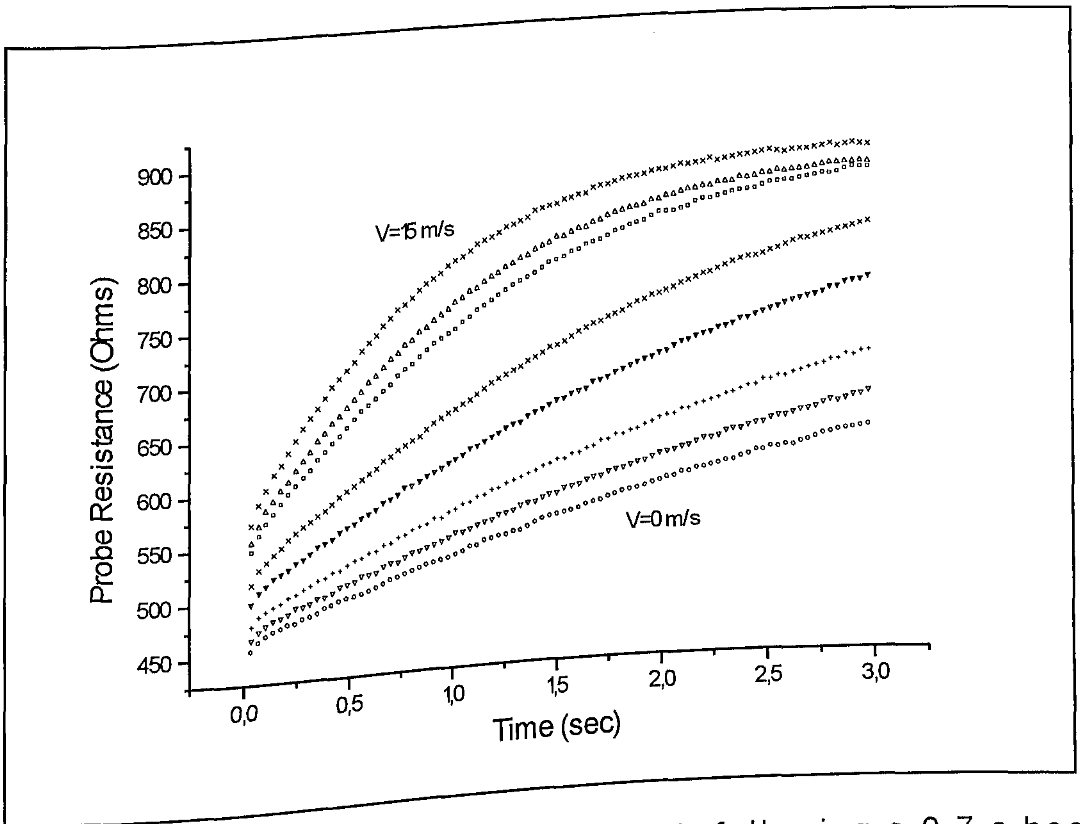

Figure (5.1) Thermistor 2 response in air following a 0.7 s heat pulse for air velocities varying from 0 to 15 m/s.

Figure (5.2) shows the normalised temperature decays for thermistor 1 and different air velocities, after a heat pulse of 2 sec, in agreement with the proposed model. Similar family of curves was obtained for thermistor 2. The effects of pulse duration and fluid initial temperature were also investigated, as explained next.

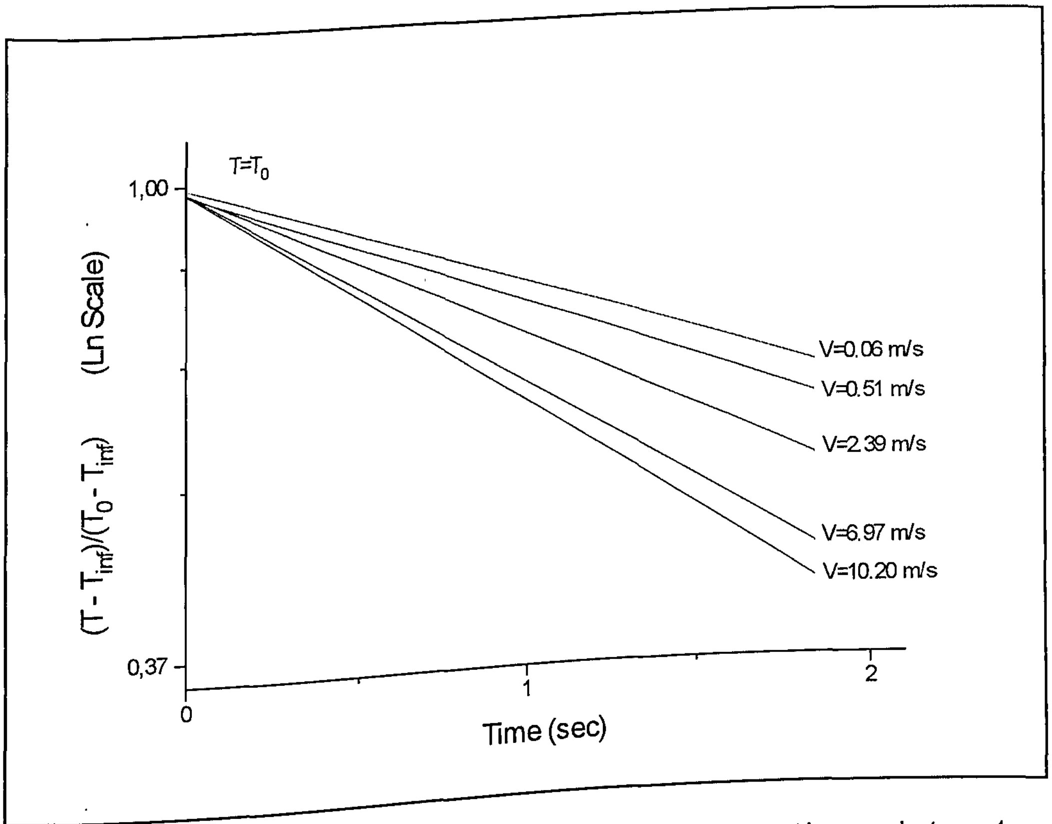

Figure (5.2) Normalised temperature decay for thesmistor 1 and different air velocities, following a 2.0 s pulse.

5.2.1 - Heat pulse duration effect:

The effect of heat pulse duration on the slope of temperature decay was studied in air, for velocities ranging from 0 to 10 m/s and heating times of 0.5, 1.0, 2.0 and 5.0 s for thermistor 1 and 0.3, 0.7, 1.0 and 1.5 s for thermistor 2. Although the slope had remained invariant within 7 percent for the former thermistor in a given velocity, see figure (5.3), the same thing was not observed for the latter, see figure (5.4), where greater variations were observed. That can be explained with equation (2.18), where initial conditions were present. Hence, the adopted calibration was in reality dependent of the pulse duration. Also, for a given velocity, a relatively short pulse did not show a very defined behaviour. On the other hand, excessive periods of heating could unnecessarily enlarge the time required for a single reading, as well as to cause disturbance in the medium around the sensor.

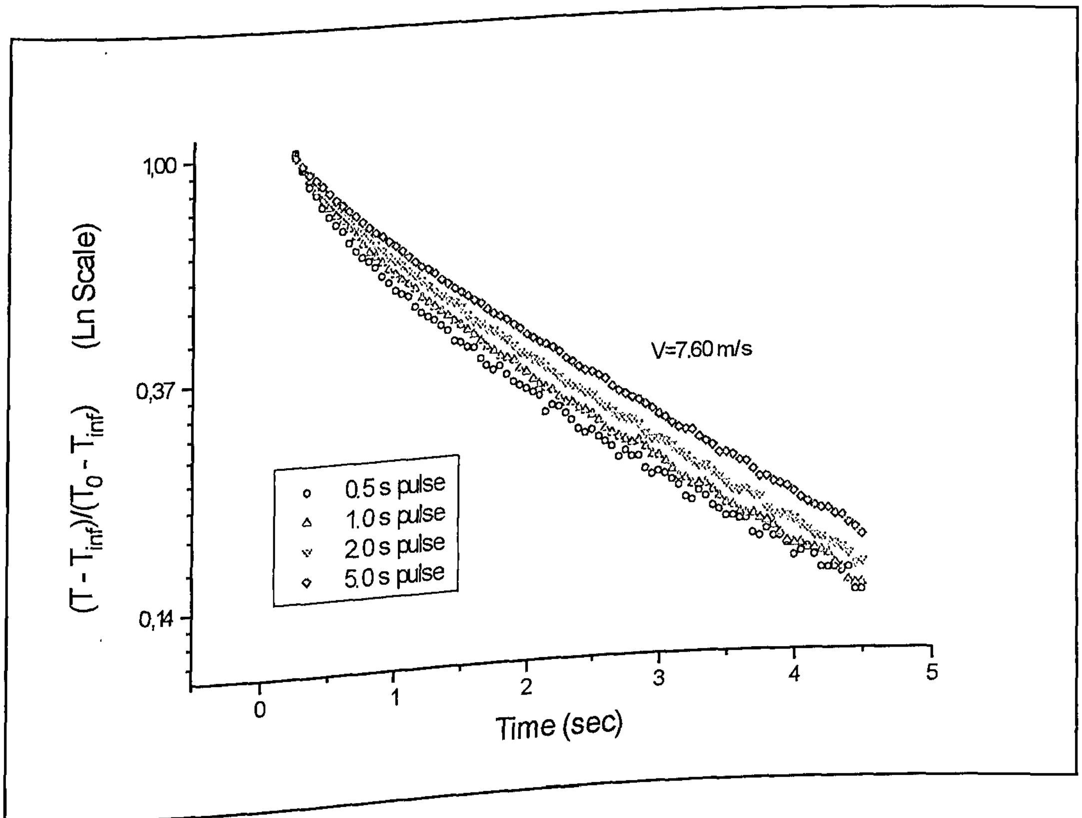

Figure (5.3) Effect of pulse duration on the slope of normalised temperature decay for thermistor 1 (V=7.60 m/s).

At all times, pulses were only admitted after the probe reached the fluid temperature. The effect of pulse magnitude was not studied.

Therefore, calibration procedures were conducted considering a 3.0 s duration for the cooling phase, and pulses of

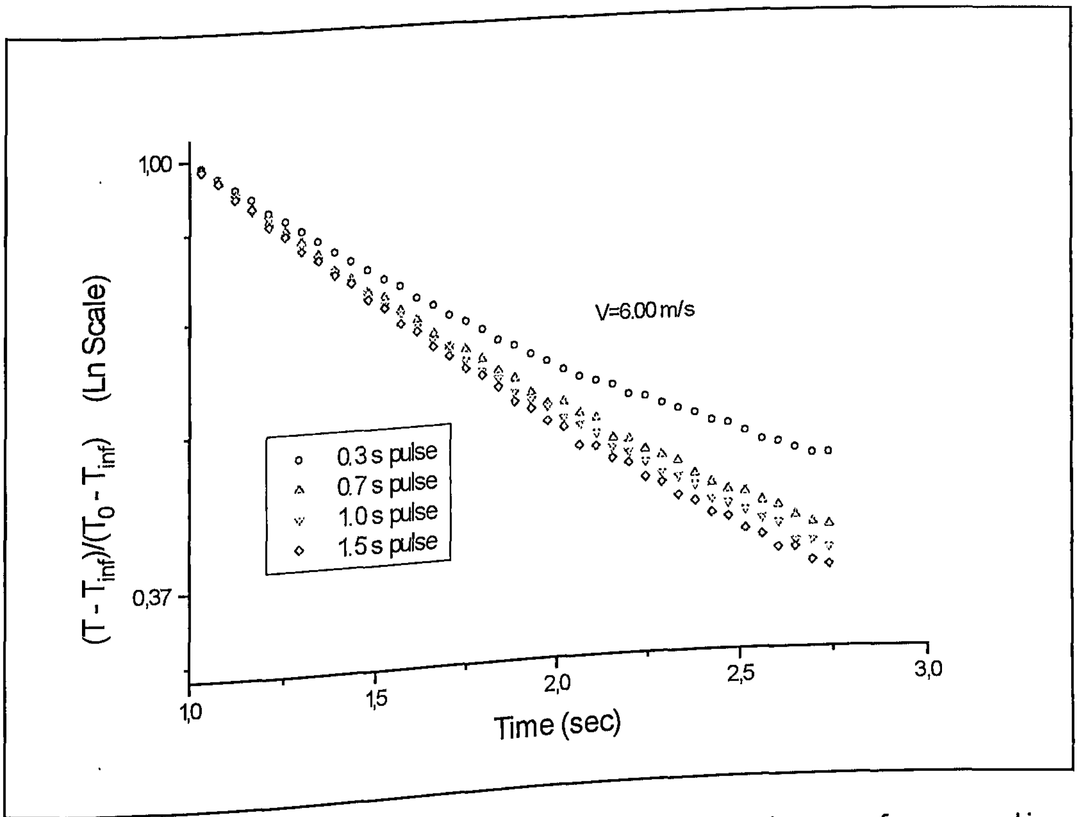

Figure (5.4) Effect of pulse duration on the slope of normalised temperature decay for thermistor 2 (V=6.00 m/s).

2.0 s and 1.0 s for thermistors 1 and 2, respectively. The process of generation of the calibration curves needed acquisition of two consecutive periods. In the first, the bulk temperature was calculated by averaging the temperature information contained in the initial 0.5 to 2.5 s. The slope of the normalised temperature decay was calculated using the second cooling period, considering t_0=1 s as the initial time and obtaining the straight line of the temperature behaviour on a semi-logarithmic plot until the third second (end of cooling phase, shown in figure (5.5)), which provided a very good least squares linear fit. The process of reapplying another pulse, e. g., a new velocity reading, was done after a period for the probe to return to the fluid bulk temperature (approximately 20 s for thermistor 1, which was of the same order as its time constant).

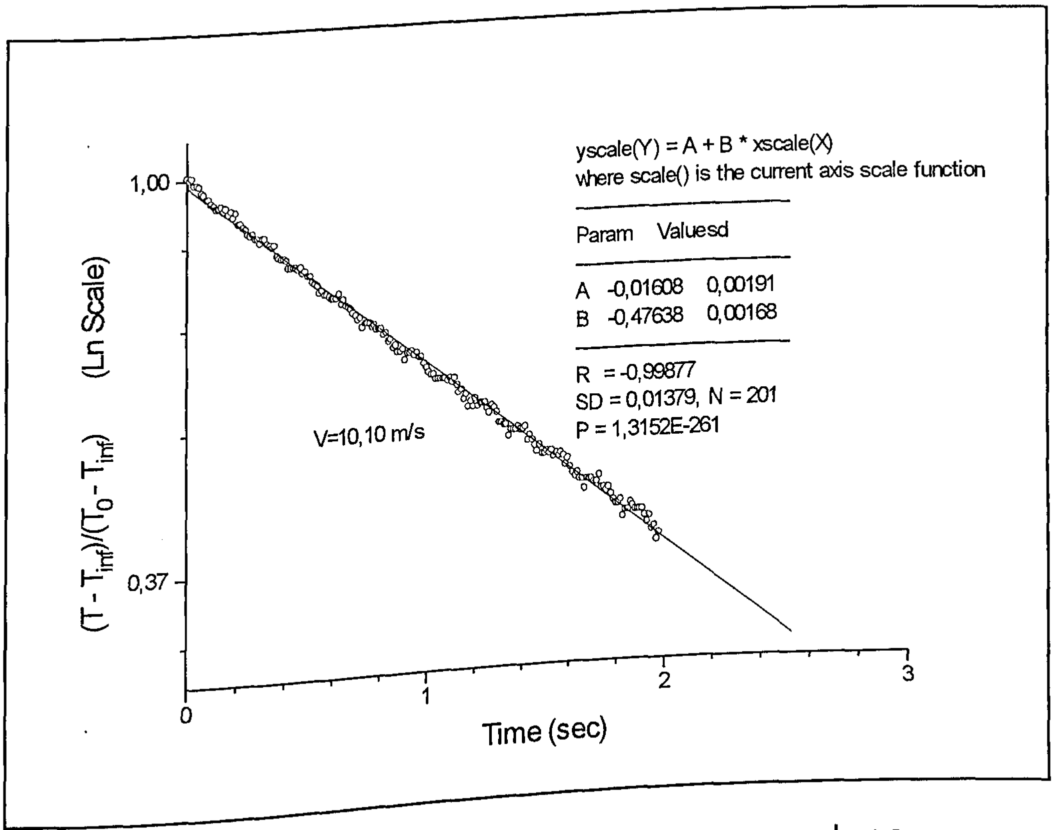

Figure (5.5) Temperature decay curve slope.

5.2.2 - Fluid bulk temperature effect:

The calibration was performed for a fluid temperature range of 299.82 to 309.82 K, as shown in figure (5.6). For this range of temperature, the normalised temperature slope varied with only ±4.3 % of full scale.

Therefore, the calibration curve for thermistor 1 was generated by gathering all curves on the same plot, figure (5.7), and fitting a second degree polynomial.

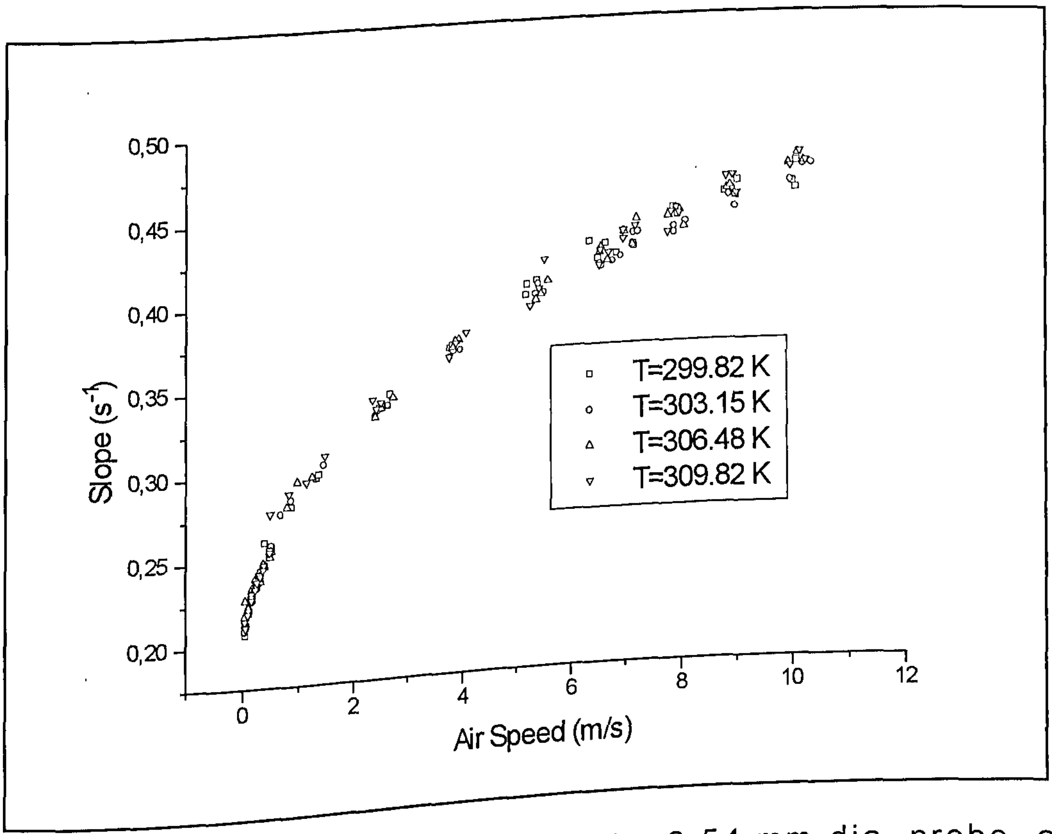

Figure (5.6) Calibration curves for the 2.54 mm-dia probe at several fluid temperatures.

The method provided an average error of 15.7 percent for the fitted curve in relation with calibration data. The explication for this fact was the use of a large range of velocity to obtain the fitted curves, where for small values of velocities, like 0.05 m/s, the error could reach a magnitude of 200 percent. For a shorter range, for example 0.1 to 12 m/s, the error was reduced to 7.56 percent, and so on. That suggests that, for a more exact calibration, it is better to use look-up tables than curve fits.

Another way is to specify small ranges of velocities for calibrating the instrument.

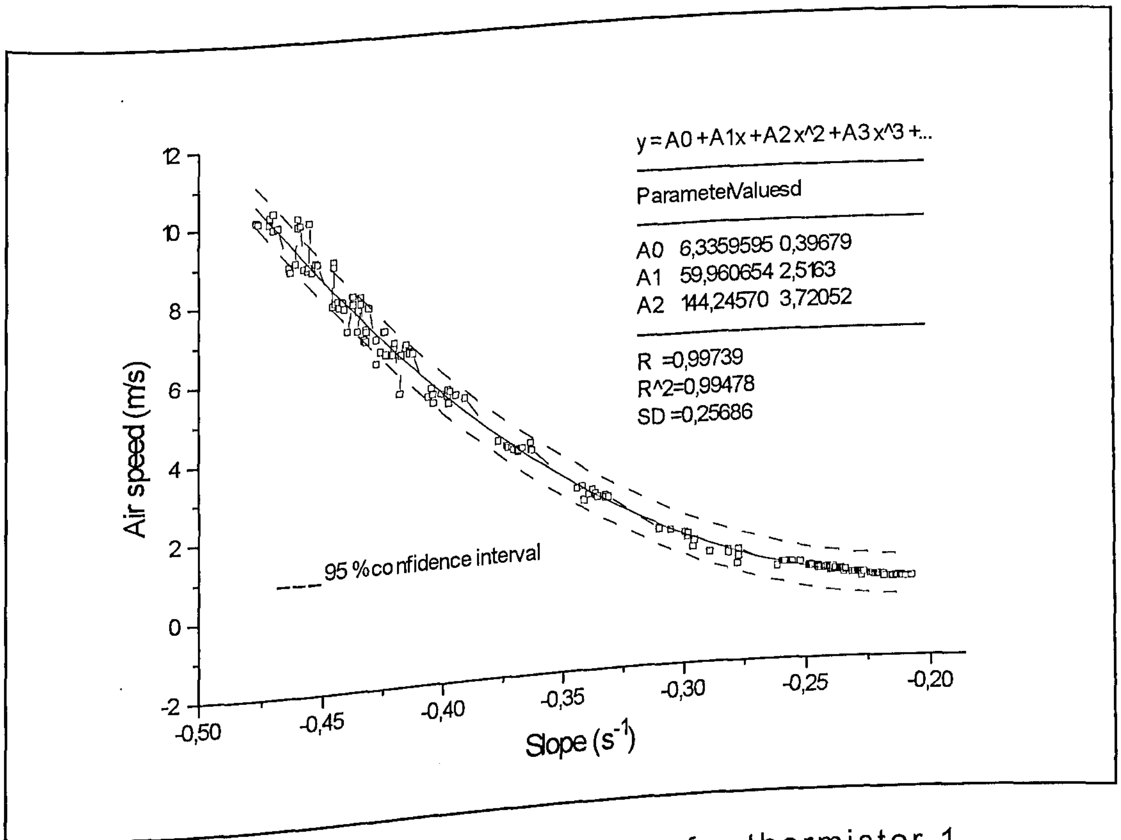

Figure (5.7) Calibration curve for thermistor 1, air velocity vs slope.

A similar curve was obtained for the other thermistor, see figure (5.8). These figures show that the thermistor 2 provides a better sensitivity to the method, i.e., for the same velocity range a greater slope range is achieved with the smallest sensor.

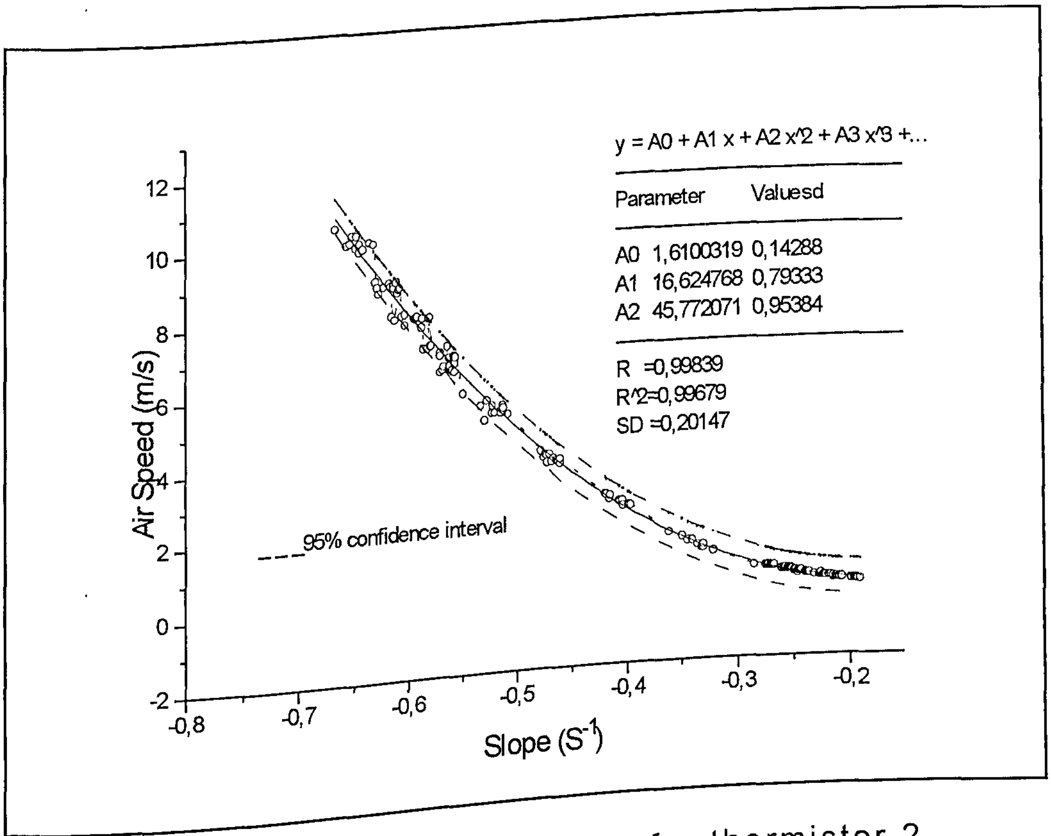

Figure (5.8) Calibration curve for thermistor 2, air velocity vs slope.

The calibration expression for thermistor 1 and 2 are respectively:

$$V = 6.33596 + 59.96065\,(S) + 144.24570\,(S)^2 \tag{5.1}$$

$$V = 1.61003 + 16.62477\,(S) + 45.77207\,(S)^2 \tag{5.2}$$

where V - air velocity (m/s)

S - slope (s^{-1})

5.3 - THE CONSTANT TEMPERATURE METHOD RESULTS

The constant temperature principle demonstrated good applicability in fluid velocity measurement, including the possibility to measure fluctuating components of velocity. Figure (5.9) shows the circuit response in terms of the output voltage vs air speed.

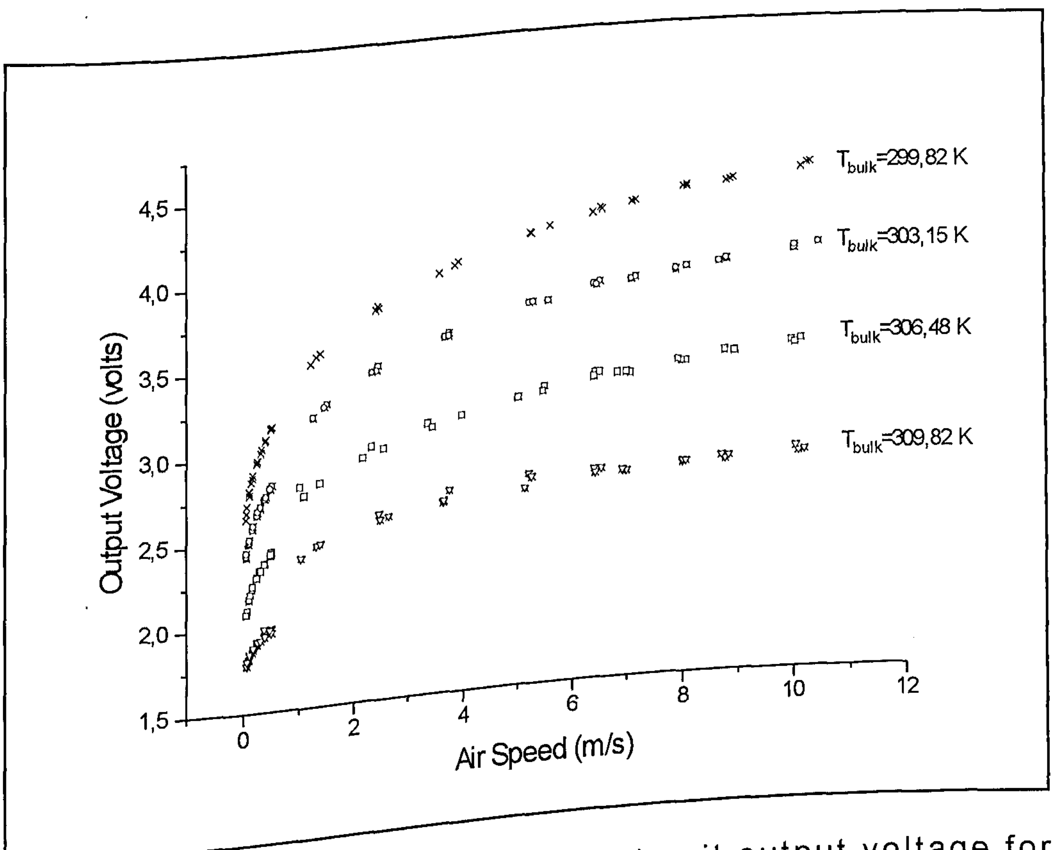

Figure (5.9) Constant temperature circuit output voltage for several air velocities and fluid temperatures - thermistor 2.

As can be seen in the above figure, the fluid temperature significantly influenced the calibration curves, and a source of error was the way in which fluid temperature was read. A characteristic of this circuit was that the probe had to be insensitive to fluid temperature, hence, the fluid temperature was read with a mercury-in-glass thermometer installed before the chambers of calibration. This caused inaccuracies in fluid bulk temperature measurements, which varied with fluid temperature

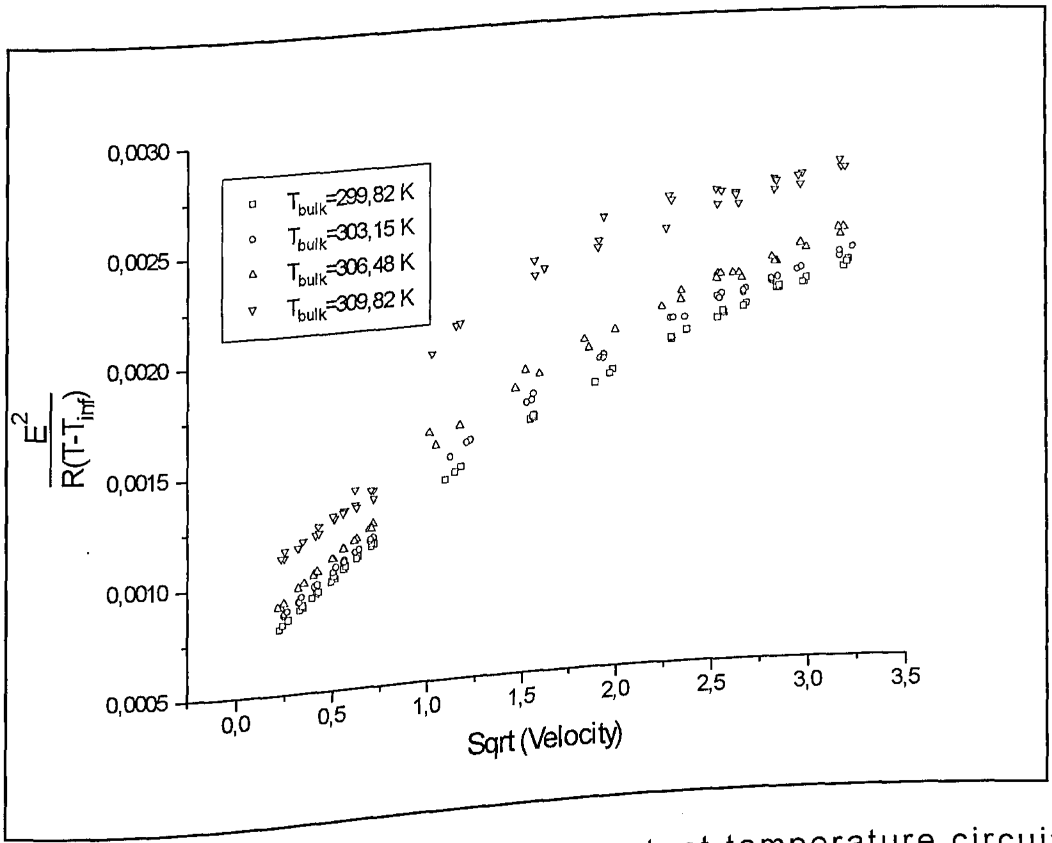

Figure (5.10) P/ΔT response of the constant temperature circuit vs sqrt (velocity) for several fluid bulk temperatures - thermistor 2.

from 0.2 percent at 299.82 K to 0.5 percent at 309.82 K. The constant temperature anemometer showed to be strongly affected by those inaccuracies.

Figure (5.10) summarises equation (2.28), with a plot of $E^2/(R\ (T-T_{inf}))$ vs sqrt(V) for several fluid temperatures.

Separated plots of each response curve permitted to fit the regression parameters required by the model:

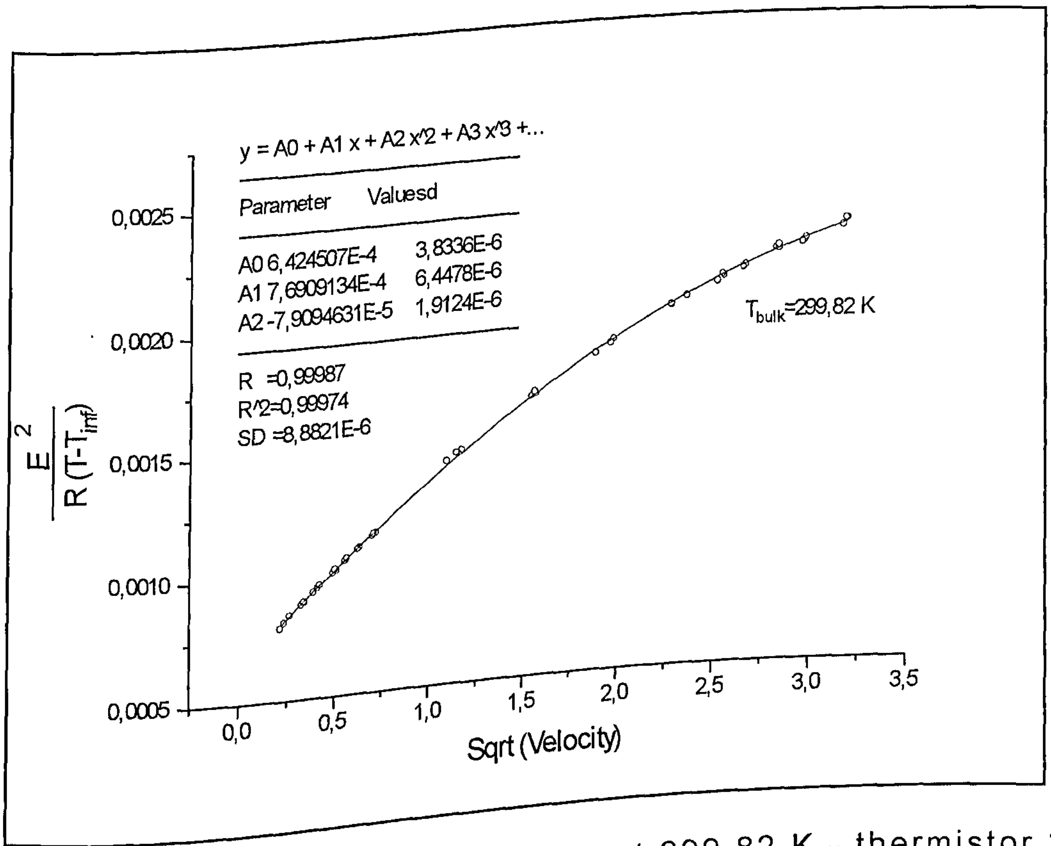

Figure (5.11) P/ΔT vs sqrt (velocity) at 299.82 K - thermistor 2.

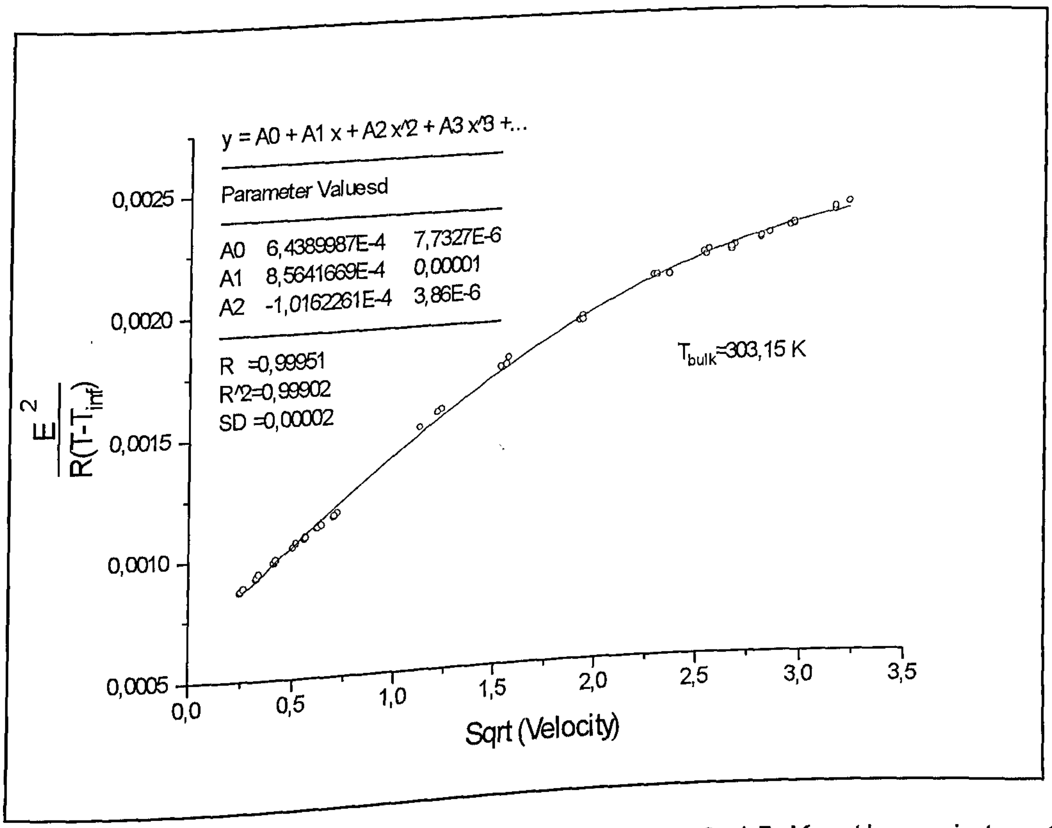

Figure (5.12) P/ΔT vs sqrt (velocity) at 303.15 K - thermistor 2.

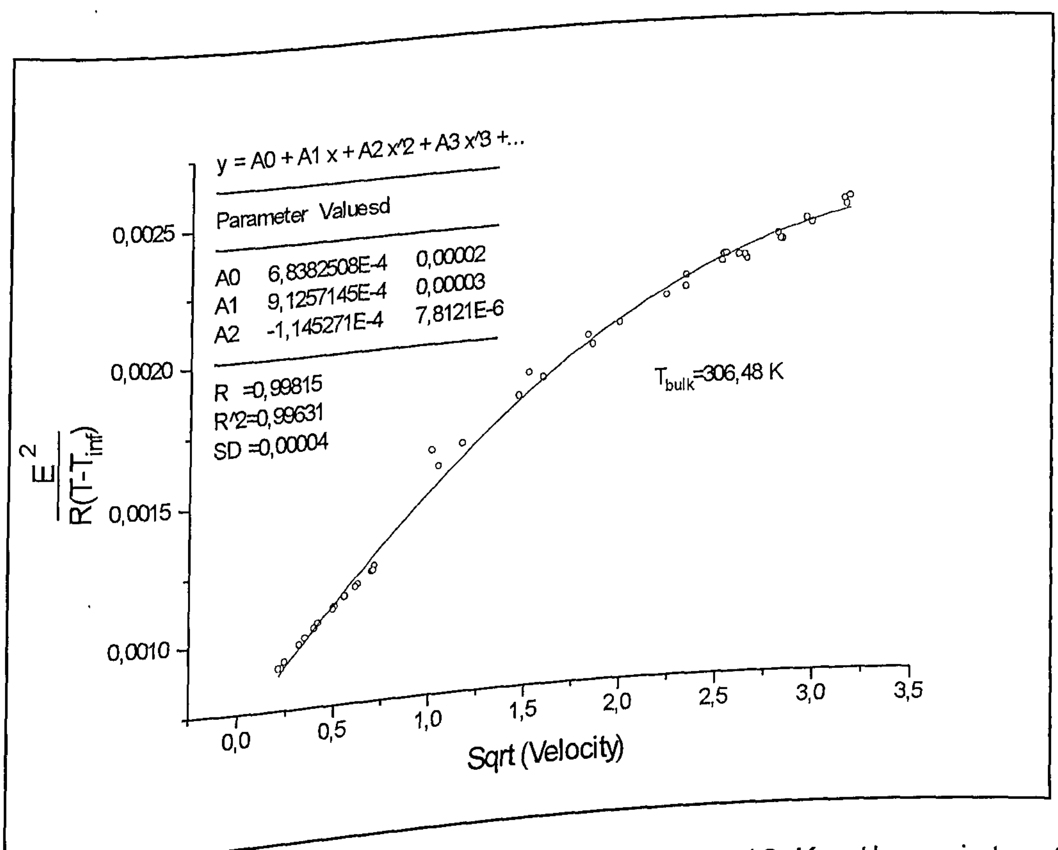

Figure (5.13) P/ΔT vs sqrt (velocity) at 306.48 K - thermistor 2.

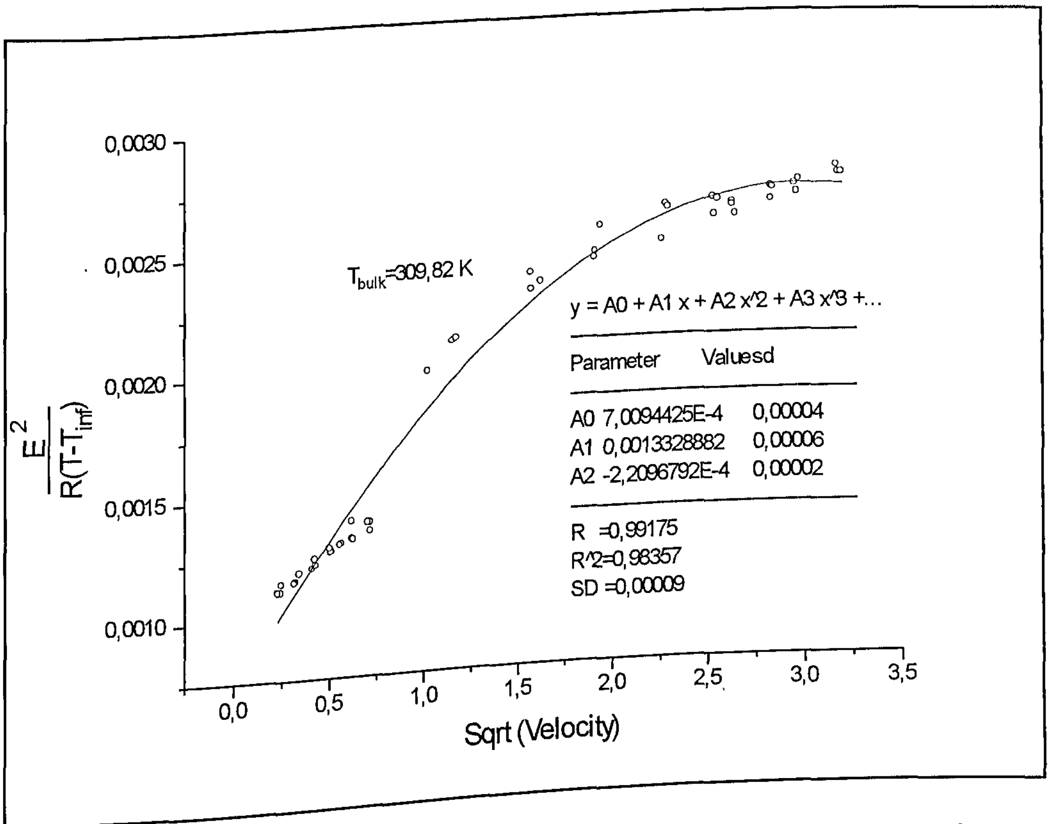

Figure (5.14) P/ΔT vs sqrt (velocity) at 309.82 K - thermistor 2.

From these plots, four sets of a, b and c[2] were obtained as a function of fluid temperature. In order to establish the dependence of that parameters on bulk temperature, a plot of each parameter vs fluid temperature was made and a second degree polynomial was fitted, according to equation (2.29).

[2] - The figures (5.11) to (5.14) mention A_0, A_1 and A_2, respectively, i.e., $a=A_0$, $b=A_1$, and $c=A_2$.

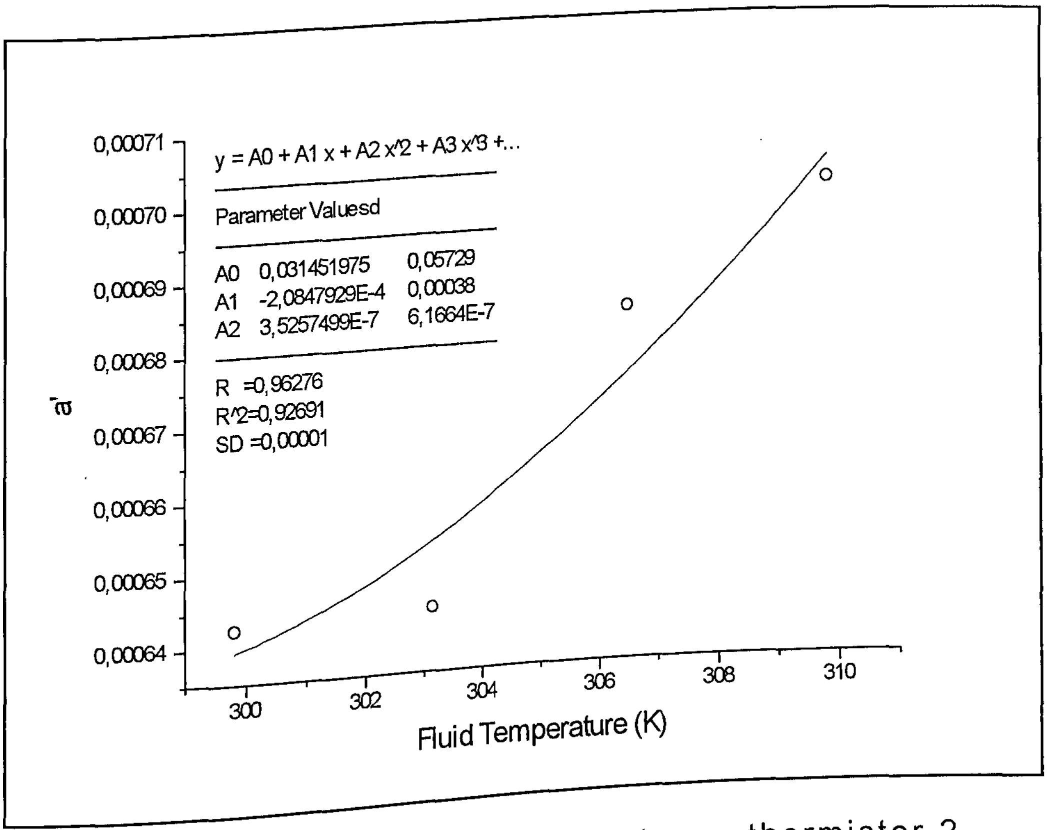

Figure (5.15) a' vs fluid temperature - thermistor 2.

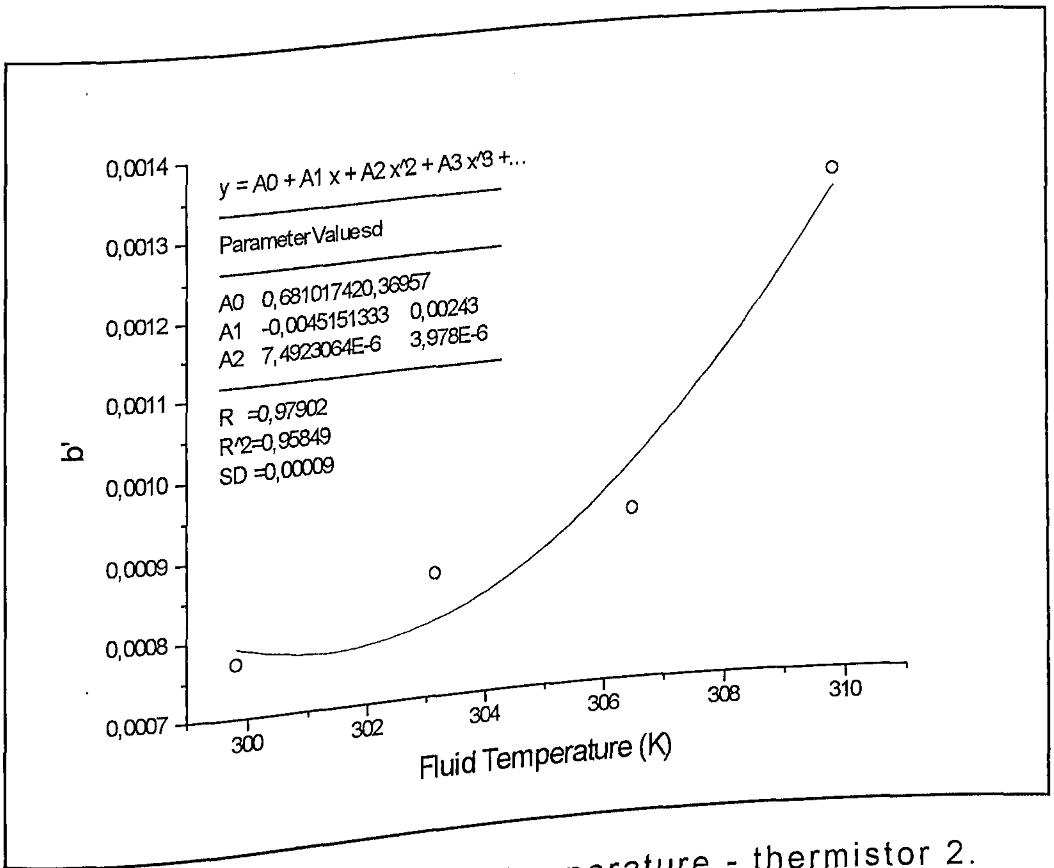

Figure (5.16) b' vs fluid temperature - thermistor 2.

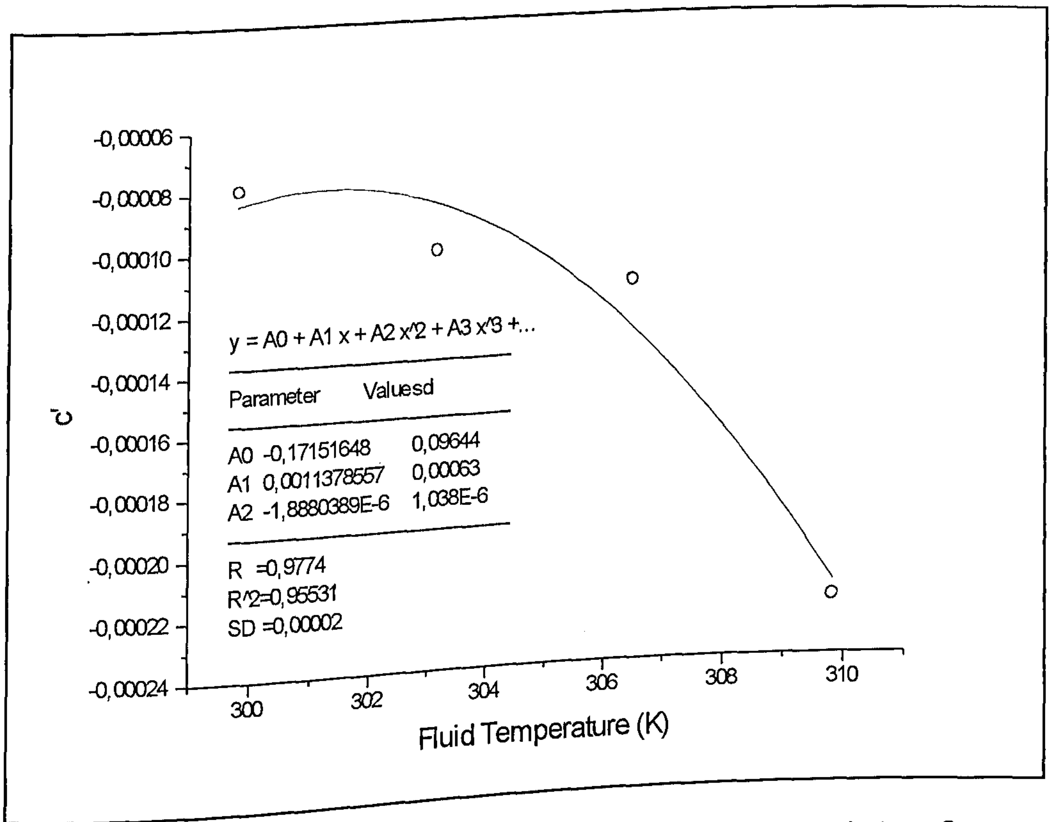

Figure (5.17) c' vs fluid temperature - thermistor 2.

With $a'=a'(T_\infty)$, $b'=b'(T_\infty)$ and $c'=c'(T_\infty)$, the fluid temperature and the output voltage, expression (2.28) gave the fluid velocity. As mentioned before, an inconvenience in this procedure was that the fluid temperature had to be sensed by another probe, which might or might not be incorporated into the circuit. In the present work, temperature values were read with the mercury thermometer, during calibration, and with other thermistor during applications, were introduced to the model via keyboard. An example on how the model fitted the calibration data is shown in figure (5.18), for a fluid temperature of 299.82 K:

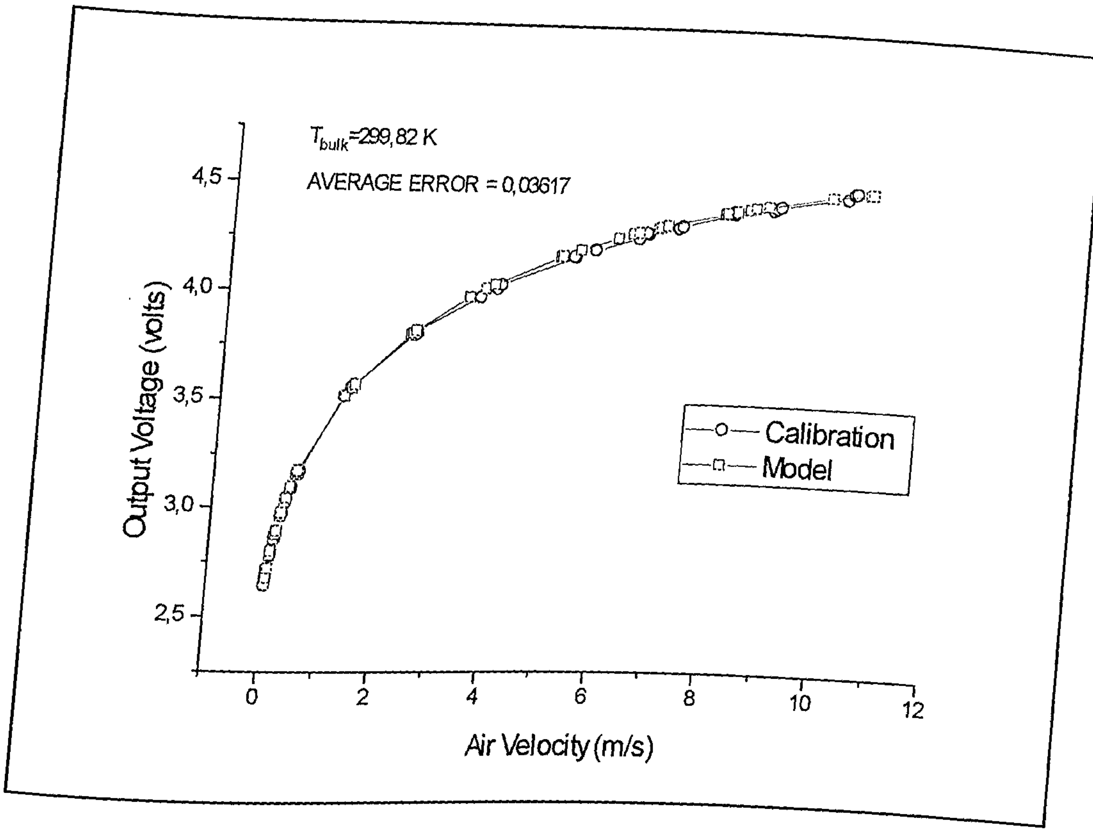

Figure (5.18) Fitted calibration curve for constant temperature circuit at Tbulk=299.82 K - thermistor 2.

The average percental errors for different fluid temperatures were 3.617 at 299.82 K, 8.944 at 303.15 K, 11.977 at 306.48 K and 23.295 at 309.82 K for thermistor 2. The same trend was observed for thermistor 1.

The increase in average errors with fluid temperature were attributed mainly to the occurrence of dispersion in the data for the two higher calibration temperatures, as can be seen in figures (5.13) and (5.14), due to smaller differences between temperatures of fluid and probe operation, which called for lower power to be delivered to the probe. At high fluid temperatures, the probe worked with great sensitivities to fluid temperature and velocity variations, therefore, catching all fluctuation in temperature.

Furthermore, the same commentary about velocity range, as for the heat pulse anemometer, is needed here.

Figures (5.19) (5.21) show a', b' and c' as a function of fluid temperature, for the 2.54 mm-dia probe.

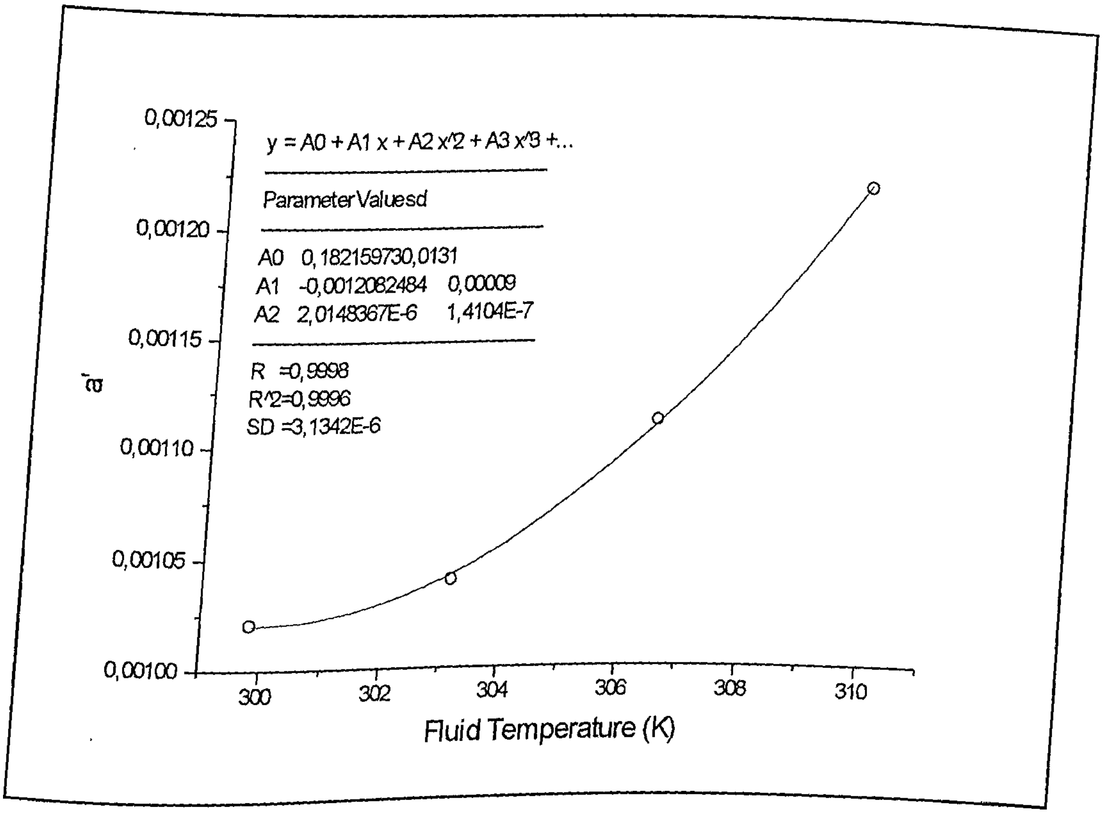

Figure (5.19) a' vs fluid temperature - thermistor 1.

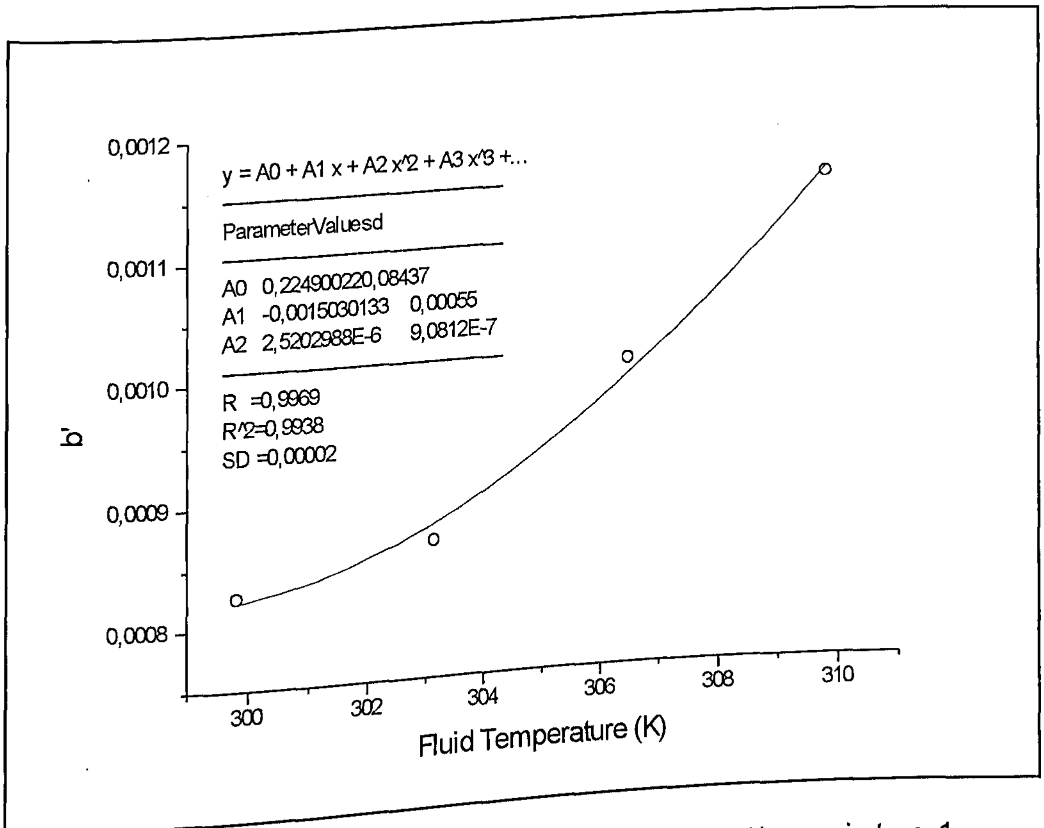

Figure (5.20) b' vs fluid temperature - thermistor 1.

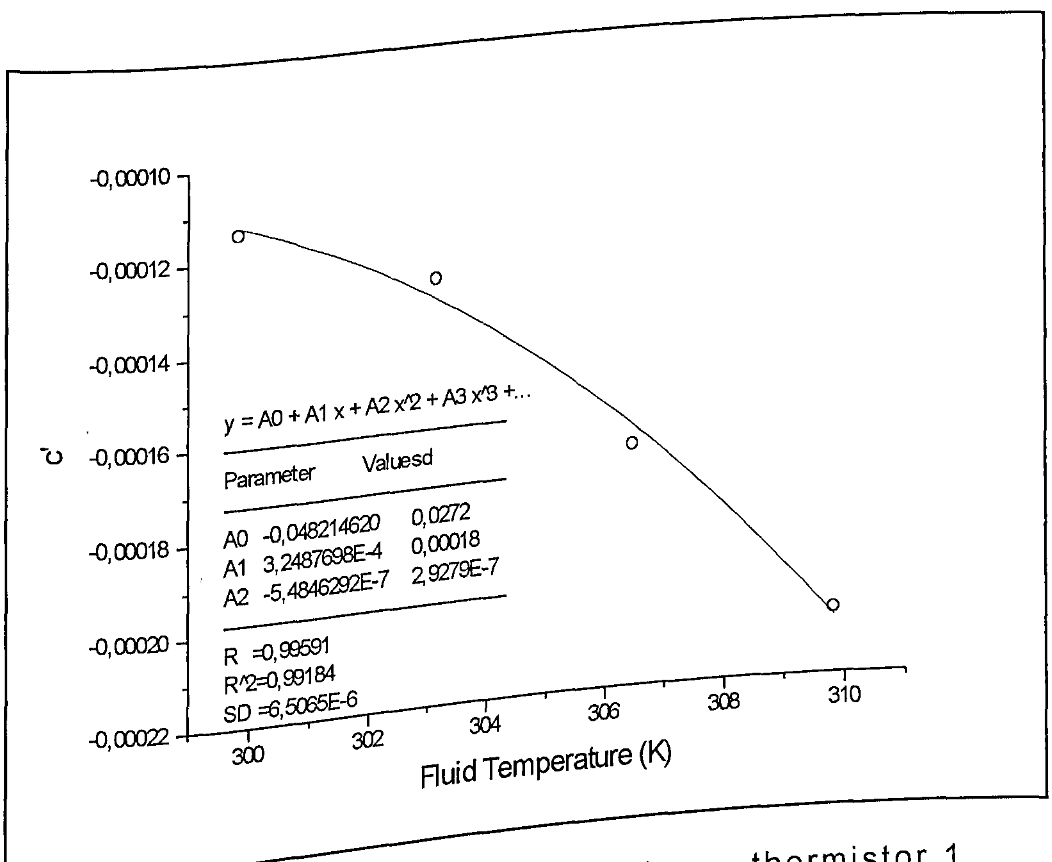

Figure (5.21) c' vs fluid temperature - thermistor 1.

The adjusted calibration parameters for thermistor 1 and 2 are respectively:

$$\begin{cases} a'_1 = 0.1822 - 0.0012\,T_f + 2.0148\times10^{-6}\,T_f^2 \\ b'_1 = 0.2249 - 0.0015\,T_f + 2.5203\times10^{-6}\,T_f^2 \\ c'_1 = -0.0482 + 3.2488\times10^{-4}\,T_f - 5.4846\times10^{-7}\,T_f^2 \end{cases} \qquad (5.3.a)$$

$$\begin{cases} a'_2 = 0.0315 - 0.0002\,T_f + 3.5257\times10^{-7}\,T_f^2 \\ b'_2 = 0.6810 - 0.0045\,T_f + 7.4923\times10^{-6}\,T_f^2 \\ c'_2 = -0.1715 + 0.0011\,T_f - 1.8880\times10^{-6}\,T_f^2 \end{cases} \qquad (5.3.b)$$

CHAPTER SIX

6 - APPLICATIONS

Once calibrated, the instruments were evaluated by a wind tunnel experiment, where suitability for Reynolds numbers up to 32,000 (based on the test section average width (a+b)/2, see figure(6.1)) was verified.

The experiment comprised of the determination of a velocity profile of the test section with each anemometer, for subsequent comparison with Pitot tube result (detailed in appendix E). Thermistor 2 was utilised with the constant temperature anemometer, and thermistor 1 was tested with the heat pulse anemometer.

The tunnel material was acrylic, and its cross section dimensions were a=65.4 mm x b=64.3 mm, conform figure (6.1). The transducers were introduced into the tunnel through an orifice situated in the middle of the upper surface. In order to collect pairs of data (vertical distance, y, vs air velocity, V) the aluminium tube (see chapter four) used to introduce the sensor into the tunnel was fixed to a beam calliper, which allowed to vary the position of measurement in y-direction. The same was done for the Pitot tube, figure (6.2).

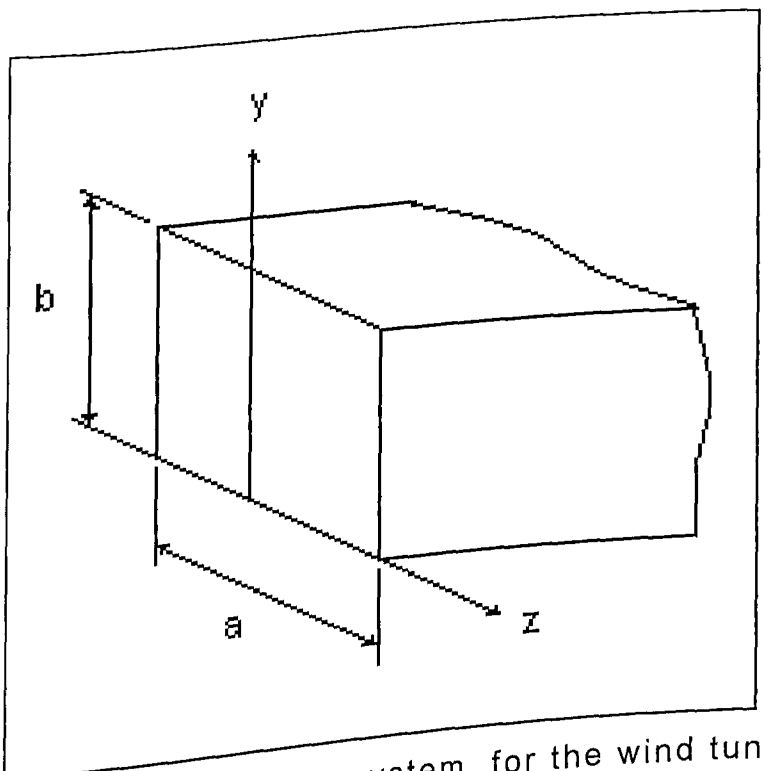

Figure (6.1) Coordinate system for the wind tunnel.
(not to scale)

From first measurements, it was inferred that the aluminium stem caused flow turbulence which induced serious disturbance on the velocity profile. That led to a procedure of bending the stem at a right angle to the test cross section, that is, parallel to the stream lines, similar to a Pitot tube shape.

Fluid temperature measurement, with the constant temperature anemometer, was monitored with a similar 1.52 mm-dia thermistor placed 5 cm downstream from the velocity transducer. The temperature was calculated from the probe resistance, measured with a multimeter, and entered the program via keyboard.

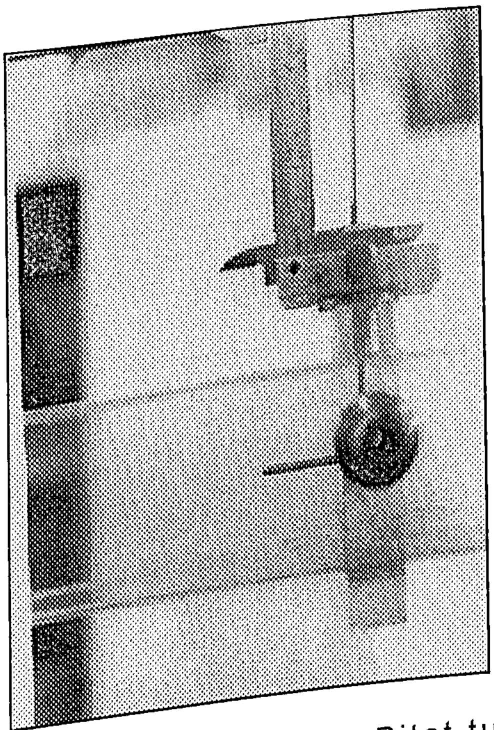

Figure (6.2) View of the Pitot tube installed in the wind tunnel.

The first readings were taken with the distance between transducer and tunnel wall equal to the transducer radius, about 20 points over the vertical distance y were considered. Three sets of velocity profiles were determined with each anemometer. Figure (6.3) shows the average results with all three methods.

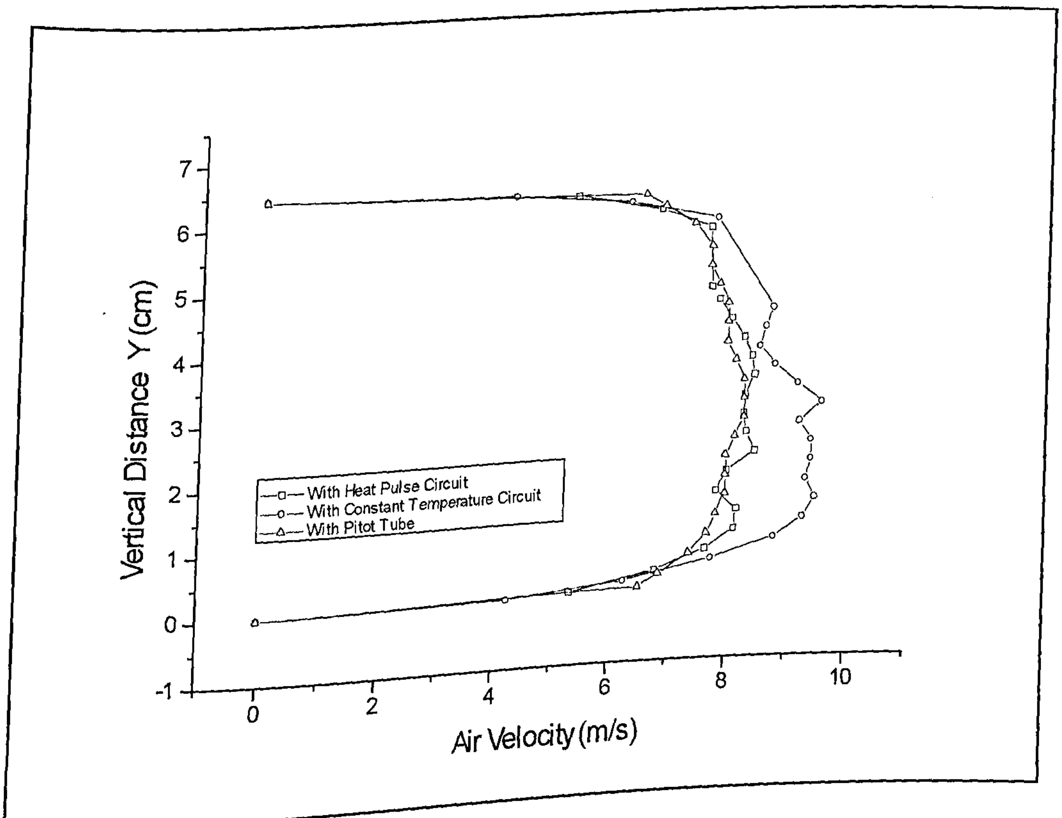

Figure (6.3) Air velocity profile in the wind tunnel (Re=32,000).

As can be observed in figure (6.3), the flow was not laminar. A division of core region and boundary layer can be observed. Therefore, the form adopted to compare the performance of each developed anemometer with the Pitot's was an average error calculated in relation to the mean velocity acquired out of the boundary layer region, starting from the fifth measure. The relative error detected for the heat pulse anemometer was of 2.2 %, which lay within the uncertainty of the Pitot tube measurements (estimated in 3.5 %), and was in conformity with the expected result as the calibration showed good accuracy for this range of velocity. The relative error for the constant temperature anemometer, calculated in 14.3 %, had explication in the already commented causes, and could be faced as a limitation of the method, which needed better calibration conditions and a fluid temperature compensation (information of temperature either by the same probe or other one) present in the circuit. Besides, the test temperature was around 306 K, which proved influencing the measures, as the probe operated with great sensitivity to temperature variation.

In spite of the above, both anemometers showed satisfactory responses and possibilities of being applied in measurement of average velocities in fluids. The constant temperature anemometer also promised to work with fluctuating levels of velocities (that cannot be seen in figure (6.3)).

CHAPTER SEVEN

7 - CONCLUSIONS AND RECOMMENDATIONS

The development of two different thermistor anemometers resulted in a good understanding of the sensor applicability in fluid velocity measurements. Two circuits were constructed and tested, the heat pulse and the constant temperature. Both showed great suitability for mean velocity measurements.

The automation of data acquisition was essential for the success of the investigation. Thanks to the control of the heat pulse duration, as well as data analysis at cooling phases, the transient anemometer enable velocity measurement. Also, the automation permitted a precise description of probe operation, by acquiring at real time the information of circuit response.

The proposed techniques and calibration models were valid and could be applied to velocity measurements. However, calibration conditions had to be controlled, mainly for the constant temperature method, in order to achieve reliable measurements. The deviations were also attributed to the great range of velocity, which was about 10^{-2} to 10 m/s. Another possible cause of error, not yet considered, could be heat conduction through the probe glass "neck".

The heat pulse anemometer made use of the transient behaviour of the thermistor during the cooling period after a pulse application. The experimental results were in agreement with the theory. Also, the range of fluid temperature used for calibration (299.82 to 309.82 K) did not affect the mean velocity measurements.

The results of the pulse duration tests showed significant effect on calibration, and, hence, the same calibration conditions were suggested to be used in applications of the instrument.

Although relatively accurate, the method presented the inconvenience of being inadequate to measure fluctuating components of velocity, because it needed a finite time to operate. At this stage, no commentary can be done about repulsing, that is, application of a new pulse before probe temperature returning to the steady state flow fluid temperature.

The constant temperature anemometer, although more susceptible to fluid temperature variations, was sensitive for average as well as varying velocity. The average errors of this circuit were a consequence of uncertainties about procedure conditions, and were expected to be eliminated with a well controlled temperature and flow conditions. In addition, an increase in the temperature of operation (probe temperature) could help to reduce sensitivity to temperature variations.

It can be concluded that the characteristics of stability, mechanical resistance and sensitivity to temperature variations made the thermistor a very good velocity sensor, when under the control of one of the proposed methods, with applications in a many laboratory experiments, engineering and industry.

The heat pulse anemometer can be used for measurements in the range of velocities from 0.05 m/s to 12 m/s. The average instrument error is about 15.5%, with 95% certainty.

The constant temperature anemometer has been tested in the same range of velocities mentioned above. The average instrument errors vary with fluid temperature from about 3.5% at 299.82 K to about 23.5% at 309.82 K, again with 95% certainty.

With future developments, there is scope for improvement of these performances.

Recommendations for future works are:

(a) For the constant temperature anemometer:

- improvement of the circuit, for reading fluid temperature;
- selection of a higher probe operation temperature;
- further investigation for turbulent flow measurements.

(b) For the heat pulse anemometer:

- development of a general calibration curve;
- development of a more complex mathematical model which includes the effects of heat conduction through probe "neck" and actual probe geometry;
- adaptation of the model for applications in porous media.

REFERENCES

[1] Arpaci, V. S., **Conduction Heat Transfer**, Addison-Wesley Publishing Company, Massachusetts, 1966, 550p.

[2] Bailey, J. L., et al., **Evaluation of the Performance Characteristics of a Thermal Transient Anemometer**, Experiments in Fluids, 15, 1993, pp. 10-16.

[3] Carslaw, H. S., and Jaeger, J. C., **Conduction of Heat in Solids**, Second Edition, Oxford University Press, Oxford, Great Britain, 1959, 510p.

[4] Chen,Y. T.,et al., **Measurement of Velocities in Packed Beds**, National Heat Transfer Conference, Heat Transfer Measurements, Analysis, and Flow Visualization, HTD-Vol. 112, 1989, pp. 47-54.

[5] CyberResearch, Inc., **Cyrdas 1600/1400/1200 Series User's Guide**, United States, 1994.

[6] Doebelin, E. O., **Measurement Systems**, McGraw-Hill Kogakusha, Tokyo, Japan, 1976, 772p.

[7] Draper, N. R., and Smith, H., **Applied Regression Analysis**, Second Ed., John Wiley & Sons, New York, USA, 1980, 709p.

[8] Goldstein, J. R., **Fluid Mechanics Measurements**, Hemisphere Publishing Corporation, United States, 1983, 630p.

[9] Gomide, R. L., **A Transient Heat Probe Sensor For Measuring Transpiration In The Stem of Woody Plants**, PhD Dissertation, The University of Arizona, U.S., 1990, 166p.

[10] Holman, J. P., **Experimental Methods for Engineers**, Third Edition. McGraw-Hill, Tokyo, Japan, 1978, 493p.

[11] Jordan, K. A., **System Response**. In: Instrumentation and Measurement for Environmental Sciences; Mitchell, B. W., Ed. St. Joseph, Michigan, American Society of Agricultural Engineers; 2nd Edition, pp. 11.01-11.09, 1983.

[12] Kaliyugavaradan, S., et alii., **A New Compensation Scheme for Thermistors and its Implementation for Response Linearization Over a Wide Temperature Range**, IEEE Transactions on Instrumentation and Measurement, Vol 42 N5, 1993, pp. 952-956.

[13] Michaelides, E. E., and Feng, Z., **Heat Transfer From a Rigid Sphere in a Nonuniform Flow and Temperature Field**, J. Heat and Mass Transfer, Vol. (37) N 14, 1994, pp. 2069-2076.

[14] Moffat, R. J., **Describing the Uncertainties in Experimental Results**, Experimental Thermal and Fluid Science, 1988, pp. 1:3-17.

[15] Morss, A. G., **Measurements of Temperature Fluctuations in Liquid Sodium Using Fast-Response Thermocouples**, Experimental Thermal and Fluid Science, 1988, pp. 1:127-133.

[16] Pinchak, A. C., and Petras, E. G., **CMOS Microprocessor Based Dual-Bridge Thermistor System for Measurement of Intragravel Water Flow**, Case Western Reserve University, Cleveland, Ohio, 1979, pp. 637-648.

[17] Preobrazhensky, V., **Measurements & Instrumentation in Heat Engineering**, Vol. 2, Translated from the Russian by Boris Kuznetzov, Mir Publishers, Moscow, 1980, 342p.

[18] Rasmussen, R. A., **Application of Thermistors to Measurements in Moving Fluids**, The Review of Scientific Instruments, Vol 33 N 1,1962, pp. 38-42.

[19] Sobrinho, M. D., and Maciel, G. F., **Medição de Velocidades Pontuais em Àgua por Meio de Transferência de Calor, Utilizando Sonda Térmica NTC**, 3th North-Northeastern Congress of Mechanical Engineering, Belem, PA, Brazil, 1994, pp. 311-314.

[20] Spiegel, M. R., **Probabilidade e estatistica**, Translated to Portuguese by Alfredo A. de Faria, McGraw-Hill, São Paulo, Brazil, 1978, 517p.

[21] Stephenson, G., **Uma Introdução às Equações Diferenciais Parciais**, Translated to Portuguese by: Paulo Teixeira. Edgard Blücher, Ed. da Universidade de São Paulo, São Paulo, 1975, 122p.

[22] Yovanovich, M. M., **General Expression for Forced Convection Heat and Mass Transfer from Isopotential Spheroids**, AIAA 26th Aerospace Sciences Meeting, Nevada, 1988, 11p.

APPENDIX A

A NEW FOUR CONSTANT FIT FOR R-T CHARACTERISTIC OF A THERMISTOR

The four-constant equation (2.3) suggested by Kaliyugavaradan *et al.* (1993) was solved by a successive approximation method, according to the procedure presented by those authors. A computational routine producing the four parameters was written in QuickBasic V4.0. The program asks for four pairs of resistance in Ohms and temperature in K (the temperatures in increasing order and nearly equally spaced in the range), and verifies the convergence conditions. A listing of the program, called PARAM.BAS, follows:

```
CLS
'PROGRAM FOR DETERMINING THE R-T PARAMETERS OF A THERMISTOR
'
PRINT "YOUR CURVE WILL BE FITTED ASSUMING A FOUR-CONSTANT"
PRINT "EQUATION GIVEN BY="
PRINT "1/(Ri-P1)=P2+(1/P3)EXP(-P4/Ti)"
PRINT "ENTER FOUR PAIRS OF R-T"
DIM R(4),T(4)
FOR I=1 TO 4
      LOCATE 5+I,5: PRINT "R";I;: INPUT R(I)
      LOCATE 5+I,30: PRINT "T";I;: INPUT T(I)
NEXT I
X1=0: Y1=0
X=R(3)/R(4): Y=0
N=0
KI=(T(2)*(T(4)-T(3)))/(T(4)*(T(3)-T(2)))
```

```
        K2=(T(3)*(T(2)-T(1)))/(T(1)*(T(3)-T(2)))
        D1X=K1*(R(2)/R(3))^K1*((R(2)-R(3))*(R(4))^2/(R(2)*R(3)*   (R(3)-
R(4)))
        D2X=(R(2)/R(3))^K2*((R(3)*(R(2)-R(1))+K2*R(1)*(R(2)-R(3))*
(R(4))^2/((R(3)*R(4))*R(3)*(R(1))^2)
        D1Y=(R(2)/R(3))^K1*(R(4)-R(3)+K1*(R(2)-R(3)))/(R(1)-R(2))
        D2Y=K2*(R(2)/R(3))^K2*(R(2)*(R(2)-R(3)))/(R(1)*(R(1)-R(2)))
        C1=ABS(D1X)+ABS(D2X)
        C2=ABS(D1Y)+ABS(D2Y)
        IF C1>1 OR C2>1 THEN GOTO 100
        'CONVERGENCE CRITERIA
        DO UNTIL ABS (X1-X)<.00001# AND ABS(Y1-Y)<.00001#
                X1=X: Y1=Y
                N=N+1
                A=((X*(R(2)-R(4))+R(3)-R(2))*(Y*(R(1)-R(3))+R(3)-
R(2))/(X*Y*(R(1)-R(2))*(R(3)-R(4))))^K1
                F1=(Y*(R(1)-R(3))+R(3)-R(2))/(Y*(R(1)-R(4))+R(4)-R(2))*A
                B=((X*(R(2)-R(4))+R(3)-R(2))*(Y*(R(1)-R(3))+R(3)-
R(2))/(X*Y*(R(1)-R(2))*(R(3)-R(4))))^K2
                F2=(X*(R(2)-R(4))+R(3)-R(2))/(X*(R(1)-R(4))+R(3)-R(1))*B
                X=F1: Y=F2
        LOOP
        P1=(R(4)*X-R(3))/(X-1)
        P2=(Y-1)/(P1-R(2)+R(1)*Y-P1*Y)
        M=(1/(R(3)+P1)-P2)/(1/(R(1)+P1)-P2)
        P4=LOG(M)/(T(3)-T(1))*(T(3)*T(1))
        P3=EXP(-P4/T(1))/(1/(R(1)+P1)-P2)
        PRINT X,Y,"NUMBER OF ITERATIONS=";N
        PRINT "P1=";P1, "P2=";P2, "P3=";P3, "P4=";P4
        GOTO 110
100     PRINT "CONVERGENCE CONDITIONS WERE NOT SATISFIED"
        PRINT "|DXF1|+|DXF2|= ";C1, "|DYF1|+|DYF2|= ";C2
110     END
```

APPENDIX B

LINEAR INTERPOLATION BY THE LEAST SQUARES METHOD

Graphical analysis of experimental data are essential to a better understanding of physical phenomena. In some cases, theoretical knowledge calls for representation of the graphical data by an analytical function, for instance an e-power, polynomial or a straight line.

An often used method to fit a straight line to data is the method of least squares. The method minimizes the sum of squares of the distances between data and the straight line. A detailed description of the method is given by for instance Draper and Smith (1980) and Holman (1978). According to those authors, if (X1,Y1), (X2,Y2),..., (Xn,Yn) represent a set of n observations, therefore, the slope ($S \equiv \frac{dY}{dX}$) of the straight line is:

$$S = \frac{\sum XiYi - [(\sum Xi)(\sum Yi)]/n}{\sum Xi^2 - (\sum Xi)^2/n} \qquad (B.1)$$

and I, the intercept at X=0 of the line, is:

$$I = \frac{(\Sigma Yi)(\Sigma Xi^2) - (\Sigma XiYi)(\Sigma Xi)}{n\Sigma Xi^2 - (\Sigma Xi)^2} \qquad (B.2)$$

where all summations are from i=1 to n.

APPENDIX C

CALIBRATION SHEETS FOR
CALIBRATOR'S CHAMBERS D2 AND D3

Calibration sheets corrected for average hot-hire geometries were given by calibrator's manufacturer, for standard atmospheric conditions:

ρ (density) = 1.2 Kg/m^3

T (temperature) = 293 K

P (pressure) = 1 atm (760 mmHg)

Chamber D2		Chamber D3	
delta P mmHg	velocity m/s	delta P mmHg	velocity m/s
0.560	0.630	0.077	0.01
0.913	0.80	0.119	0.0125
1.44	1.00	0.170	0.015
2.27	1.25	0.300	0.020
3.30	1.50	0.464	0.025
5.94	2.00	0.664	0.030
24.5	4.00	1.17	0.040
38.6	5.00	1.81	0.050
62.0	6.30	2.85	0.063
101.0	8.00	4.55	0.080
159.0	10.0	7.05	0.10
251.0	12.5	10.9	0.125
365.0	15.0	15.6	0.15
		27.4	0.20
		42.5	0.25
		60.8	0.30
		107.0	0.40

		166.0	0.50
		261.0	0.63
		417.0	0.8
		646.0	1.0

Table (C.1) Calibrator's calibration sheets.

Curves were fitted for both chambers, shown in figures (C.1.a) and (C.1.b)

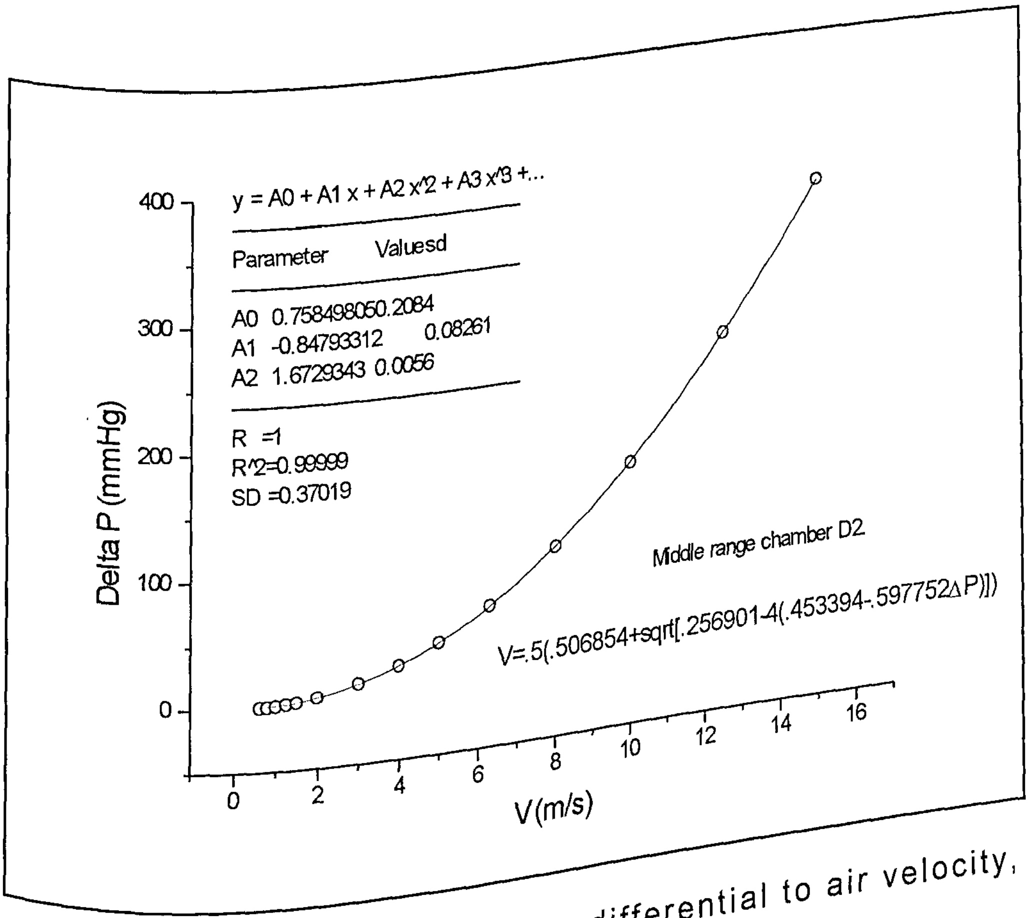

Figure (C.1.a) Relation of pressure differential to air velocity, for the TSI calibrator (chamber D2).

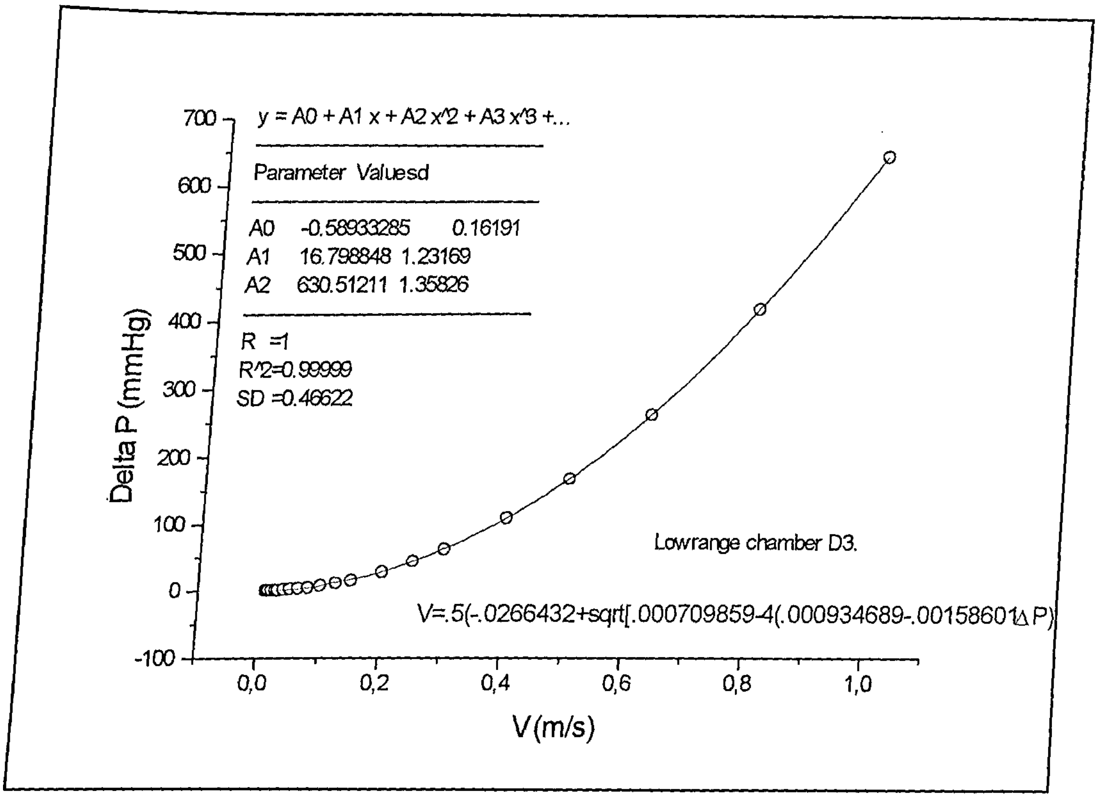

Figure (C.1.b) Relation of pressure differential to air velocity, for the TSI calibrator (chamber D3).

A factor of 1/13.6 was used to convert pressure readings from mmH2O to mmHg. A correction factor for varying ambient conditions is given by:

$$K = \sqrt{\left(\frac{293}{273+T}\right)\left(\frac{P}{760}\right)} \qquad (C.1)$$

where K - correction factor

T - atmospheric temperature (°C)

P - atmospheric pressure (mmHg)

Some important properties of dry air at atmospheric pressure of 1 atm and temperature of 30 °C are listed below:

ρ (density)	1.165×10^{-3}	g/cm^3
μ (viscosity)	1.86×10^{-4}	g/cm s
ν (kinematic viscosity)	0.160	cm^2/s
K (thermal conductivity)	2.6×10^{-4}	W/cm K
Pr (Prandtl number)	0.71	

Table (C.2) Properties of dry air at T=30 °C and P=1atm.

APPENDIX D

EXPERIMENTAL UNCERTAINTIES

An important question a researcher needs to ask himself is about the validity of his data. This question will remain unanswered unless he performs an error analysis on his experimental results. According to Holman (1978), it may be a simple verbal assessment of the results, or may take the form of complex mathematical analysis of errors (see also Moffat (1988), Doebelin (1976) and Spiegel (1978)).

This section was written in an attempt to clarify the error analysis used in this work.

Helpful definitions are:

a) Error - the difference between the true value and the measured value, used for calibrating an instrument. In other situations it is more difficult to talk about error in measurements, and the term uncertainty is used.

b) Uncertainty - possible value of the error, that is, the interval around the experimental value within which the true value can be encountered.

c) Readability - characteristic of analog output instruments, which also depends on the observer, reading the scale.

d) Resolution - minimum input value that causes a detected change in output.

e) Accuracy - is the measure of how well an observation can be repeated.

f) Confidence interval - interval around a mean value within which 95 percent (customarily) of the data lie. Frequently reported as $\pm 2\sigma$ (two times the standard deviation) for single sample analysis, and $tS_{(N)}/\sqrt{N}$ for multiple sample experiments, where t is the applicable Student's t for N samples and 0,95 confidence level (which are tabulated in some of the cited literature), and $S_{(N)}$ is the standard deviation of the set of N samples.

g) Single-sample analysis - when a small number of independent data points are taken at each point tested. An acquisition system, acquiring data at a frequency of 50 Khz, for instance, can be assumed to be performing a single-sample acquisition, if the autocorrelation time of the signal (inverse of Nyquest frequency) is smaller compared to the period of sampling (20 μs for the example).

h) Multiple-sample analysis - when a large number of independent data points are taken at each point tested.

i) Average calibration curve - is taken as a curve that best fits the scattered data, based on a given criterion (usually the least squares).

j) Coefficient of correlation (r^2) - measures the goodness of a straight line fit. It varies from 0 to 1, where 0 means no correlation at all and 1 means a perfect correlation.

k) Chauvenet's critereon - specifies the maximum acceptable deviation (Yi-Ym) in relation to standard deviation (σ), which can be applied to eliminate dubious data points. The criterion may be applied only one time, and lists of ratios $(Yi-Ym)_{max}/\sigma$ are available in cited references.

Helpful mathematical definitions are:

Arithmetic mean:

$$Xm = \frac{1}{n}\sum_{i=1}^{n} Xi \qquad (D.1)$$

where Xi denotes each of the n readings.

Standard deviation:

$$\sigma = \left[\frac{1}{n}\sum_{i=1}^{n}(Xi - Xm)^2\right]^{1/2} \qquad (D.2)$$

and σ^2 is called the variance.

Uncertainty in dependent variable:

$$\delta R = \left[\sum_{i=1}^{n}\left(\frac{\partial R}{\partial Xi}\delta Xi\right)^2\right]^{1/2} \qquad (D.3)$$

where R is dependent on variables Xi (i=1 to n).

Coefficient of correlation:

$$r^2 = \frac{\Sigma(Yest - Ym)^2}{\Sigma(Y - Ym)^2} \qquad (D.4)$$

where Yest is the estimated value of Y, correspondent to a given X, and Ym is the arithmetic mean of Y.

APPENDIX E

PITOT-TUBE OPERATION

A Pitot-tube is used to measure velocity by determining the difference between stagnation (total) and static pressure (P_t-P_s). The velocity is related to the differential pressure (dynamic pressure) through the Bernoulli's theorem (incompressible case only, i.e. M~<0.3, where M is the undisturbed Mach number):

$$P_t - P_s = \rho V^2 / 2 \tag{E.1}$$

where ρ is the fluid density, and V is the fluid velocity. Hence, the velocity is:

$$V = \sqrt{\frac{2\Delta P}{\rho}} \tag{E.2}$$

where $\Delta P = P_t - P_s$ is the differential pressure.

The total pressure is measured by one tapping facing the stream, and the static pressure is measured by several taps made in the lateral wall of the tube, see figure (E.1). The used Pitot tube has an outer diameter of 3 mm.

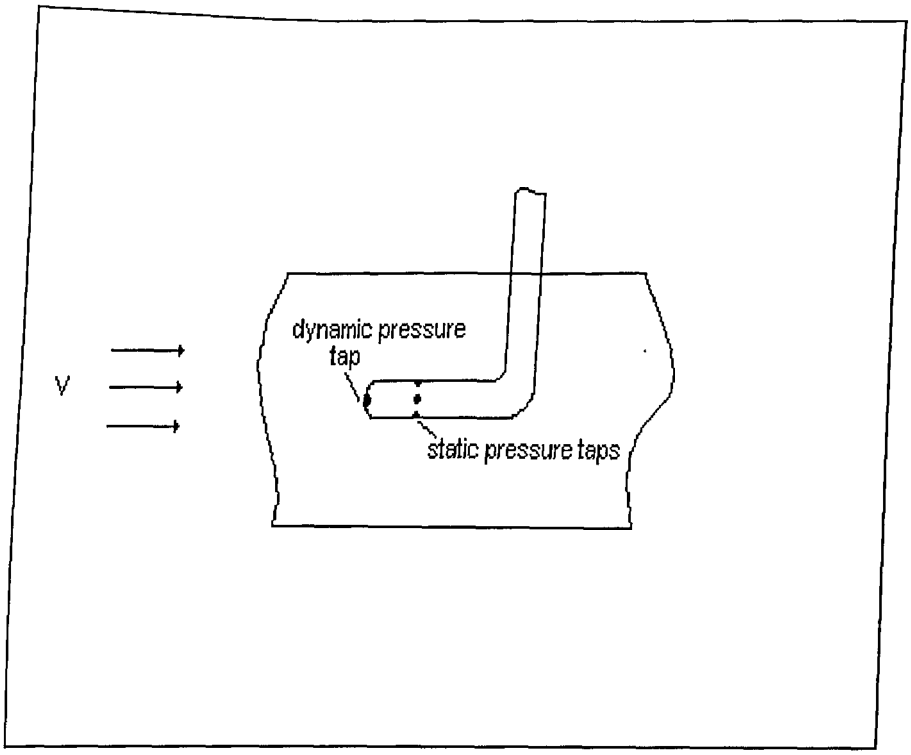

Figure (E.1) Measurement of differential pressure by Pitot tube.

The differential pressure can be measured by a liquid column manometer connected to the output tubes. The used manometer was an inclined-tube manometer, having water as the manometric fluid, and an angle α of 14,1°. For this type of manometer, there is a correction factor for the difference in height of columns (h1+h2) and the length in the inclined tube (h), as can be seen in the figure (E.2).

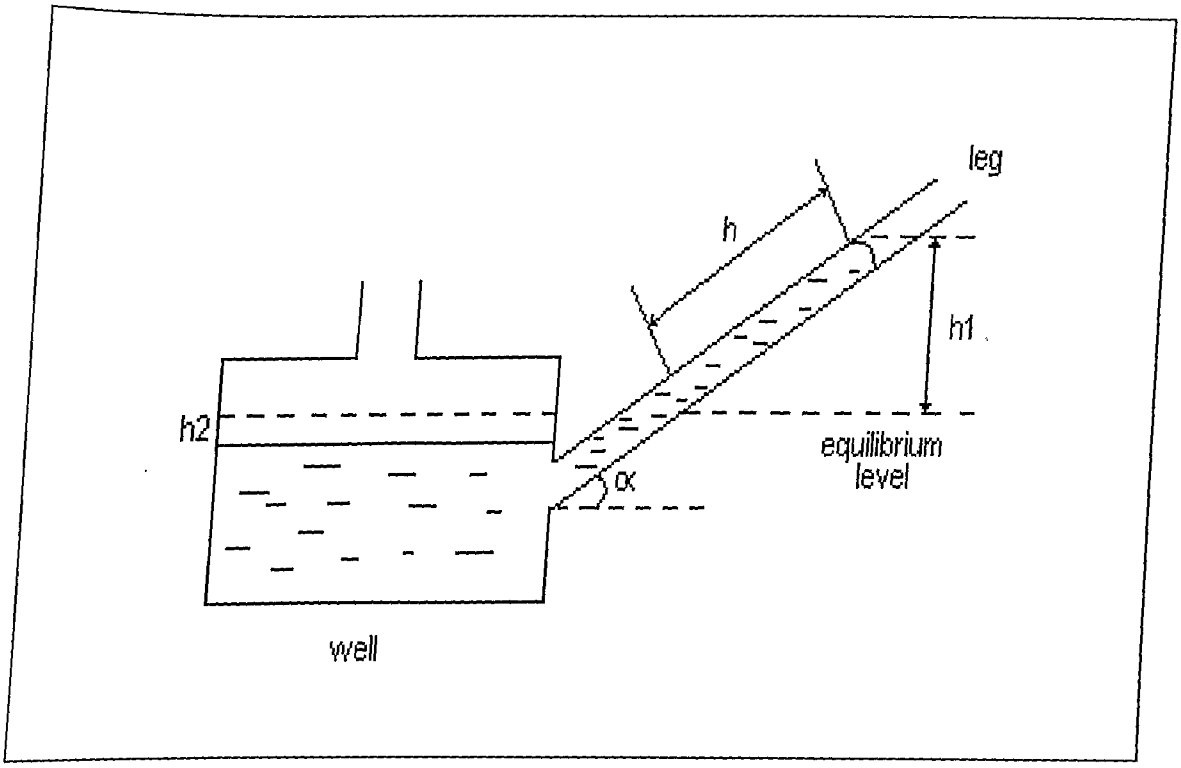

Figure (E.2) Inclined tube manometer.

Hence, the actual height (see Preobrazhensky (1980)) $\Delta h = h1 + h2$ can be derived easily from geometrical considerations:

$$\Delta h = h \sin\alpha \left(1 + \frac{d^2}{D^2}\right) \tag{E.3}$$

where d and D are the internal diameters of the leg and the well, respectively.

Knowing the differential pressure, in terms of Δh, the pressure differential ΔP in equation (APF.2) can be obtained by the equation:

$$\Delta P = \rho_w g \Delta h \tag{E.4}$$

where ρ_w is the density of the water, and g is the acceleration due to gravity.